References

Arico A. S. et al., “Nanostructured materials for advanced energy conversion and storage devices”, Nat. Mater., 4, 366-377, 2005.

Arai H., Kunisaki T., Shimizu Y., Seiyama T.,”Electrical properties of calcia doped ceria with oxygen ion conduction”, Solid State Ionics, 20, 241-248, 1986.

Abrantes J.C.C., Coll D.P., Nunez P., Frdae J.R., “Electronic transport in $Ce_{0.8}Sm_{0.2}O_{1.9}$ ceramics under reducing conditions”, Electrochem. Acta, 48, 2761-2766, 2003.

Badwal S., “Zirconia-based solid electrolytes: microstructure, stability and ionic conductivity”, Solid State Ionics, 52, 23-32, 1992.

Basu S., Devi P. S., Maiti H. S. “Synthesis and properties of nano-crystalline ceria powders”, J. Mater. Res., 19, 3162-3171, 2004.

Benamira M. et al., “Gadolinium doped ceria mixed with alkali carbonates for solid oxide fuel cell applications: I A thermal, structural and morphological insight”, J. of Power Sources, 196, 5546-5554, 2011.

Bouwmeester H.J.M., Burggraaf A.J., in: A. Burggraaf, L. Cot (Eds.), Fundamentals of Inorganic Membrane Science and Technology, Elsevier, Amsterdam, 1996, p. 435.

Bradley J., Slater P.R., Ishihara T., Irvine J.T.S., Electrochemical Society Proceedings, 2003-07, SOFC VII, 2003, pp. 315–323.

Brook R., Kilner J., “A study of oxygen ion conductivity in doped non-stoichiometric oxides”, Solid State Ionics, 6, 237-252, 1982.

Balazas G., Robert S., “AC impedance studies of rare earth oxide doped ceria”, Solid State Ionics, 76, 155–162, 1995.

Butler V., Catlow C.R.A., Fender B.E.F., Harding J.H., “Dopant ion radius and ionic conductivity in cerium oxide”, Solid State Ionics, 8, 109-113, 1983.

Bhoga S.S., Singh K., “Li_2CO_3–ABO_3 (A = Li, K, Ba and B = Nb, Ti) composite solid electrolyte systems”, Solid State Ionics, 111, 85–92, 1998.

Blumenthal R.N., Pinz B.A., “Nature of the electrical conduction transients observed in CeO_2 and Ca-doped CeO_2”, J. Appl. Phys., 38, 2376-2378, 1967.

Blumenthal R.N., Garnier J.E., “The electrical conductivity and thermodynamic behavior of SrO-doped nonstoichiometric cerium dioxide”, J. Solid State Chem., 16 21-34, 1976.

Banerjee S., Devi S., “Understanding the effect of calcium on the properties of ceria prepared by a mixed fuel process”, Solid State Ionics, 179, 661-669, 2008.

Catlow C.R.A., “Transport in doped fluorite oxides”, Solid State Ionics, 12, 67-73, 1984.

Chen Y., Fung Z., Electrochemical Society Proceedings, 2003-07, SOFC VII, 2003, pp. 339–348.

Cho P.S. et al., “Effect of CaO concentration on enhancement of grain-boundary conduction in gadolinia-doped ceria”, J. Power Sources 183, 518-523, 2008.

Cho P.S. et al., “Grain-Boundary Conduction in Gadolinia-Doped Ceria: The Effect of SrO Addition”, J. Electrochem. Soc. 156, B339-B344, 2009.

Cho Y.H. et al., “Enhancement of grain boundary conduction in gadolinia doped ceria by the scavenging of highly resistive siliceous phase”, Acta Mater., 55, 4807-4815, 2007.

Cioatera N., Parvulescu V., Rolle A., Vannier R. N., “Effect of strontium addition on europium-doped ceria properties”, Solid State Ionics, 180, 681-687, 2009.

Cullity B. D., in: M. Cohen (Eds.), Elements of X-ray Diffraction Wesley Publishing Company Inc., London, England, (1959) p. 179.

Chen T.P., Wright J.D., Krist K., in: U. Stimming, S.C. Singhal, H. Tagawa, W. Lehnert (Eds.), SOFC V, The Electrochemical Society, Pennington, NJ, 1997, p. 69, PV 97-40.

Cho et al., “Improvement of grain boundary condition in gadolinia doped ceria by the addition of CaO, Electrochem. Solid State Lett., 9, A399-A402, 2006.

Christie G. M., Berkel F.P.F., “Microstructure-ionic conductivity relationships in ceria-gadolinia electrolytes”, Solid State Ionics, 83, 17-27, 1996.

Chen M. et al., “Ceria-carbonate composite for low temperature solid oxide fuel cell: Sintering aid and composite effect”, Int J of Hydrogen Energy, 39, 12309-12316, 2014.

Chen J., Wang C., Zhang J., “Samarium doped ceria-$(Li/Na)_2CO_3$ composite electrolyte and its electrochemical properties in low temperature solid oxide fuel cell”, J. of Power Sources, 195, 4695-4699, 2010.

Di J. et al., “Samarium doped ceria-$(Li/Na)CO_3$ composite electrolyte and its electrochemical properties in low temperature solid oxide fuel cell”, J. Power Sources, 195, 4695-4699, 2010.

Dixon M. et al., “Electrical resistivity of stabilized zirconia at elevated temperatures”, J. Electrochem. Soc., 110, 276-280, 1983.

Djurado E., Boulch F., Dessemond L., Electrochemical Society Proceedings, 2003-07, SOFC VII, (2003), 160.

Doshi R. et al., "Development of solid oxide fuel cells that operate at 500 °C", J. Electrochem. Soc., 146, 1273-1278, 1999.

Dudek M., "Ceramic oxide electrolytes based on CeO_2 preparation, properties and possibility of application to electrochemical devices", J Eur Ceram Soc., 28, 965–971, 2008.

Delnick F.M., Guidoti R.A., "Ionic conduction in porous media", J. Electrochem. Soc., 137, 11-16, 1990.

Etsell T. H., Flengas S. N., "Electrical properties of solid oxide electrolytes", Chem. Rev., 70, 339-376, 1970.

Fabor J. et al., "Ionic conductivity of calcia, yttria, and rare earth-doped cerium dioxide", J. Electrochem. Soc., 126, 264, 1979.

Fan L. et al., "Potential low temperature application and hybrid ionic conducting property of ceria carbonate composite electrolytes for solid oxide fuel cells", Int. J. Hydrogen Energy, 36, 9987-9993, 2011.

Fan L. et al., "Recent development of ceria based nanocomposite materials for low temperature ceramic fuel cell and electrolyte free fuel cell", Journal of Power Sources, 234, 154-174, 2013.

Faro et al., "Intermediate temperature solid oxide fuel cell electrolytes", J. of the Indian Institute of Science, 89, 363-380, 2009.

Feng M., Goodenough J. B., “A superior oxide ion electrolyte”, Eur. J. Solid State Inorg. Chem., T31, 663-672, 1994.

Feng B., Wang C. Y., Zhu B., “Catalysts and performances for direct methanol low-temperature (300 to 600 ° C) solid oxide fuel cells”, Electrochem. Solid State Lett., 9, A80-A81, 2006.

Fu Q.X. et al., “Intermediate temperature fuel cells based on doped ceria LiCl-$SrCl_2$ composite electrolyte”, J. Power Sources, 104, 73-78, 2002.

Fu Y.P., Chen S.H., Huang J., “Preparation and characterization of $Ce_{0.8}M_{0.2}O_{2-\delta}$ (M = Y, Gd, Sm, Nd, La) solid electrolyte materials for solid oxide fuel cells”, Int. J. Hydrogen Energy, 35, 745–752, 2010.

Fan L. et al., “Proton and oxygen ion conductivity of doped ceria-carbonate composite by modified Wagner polarization”, Int. J. Electrochem Sci., 7, 8420– 8435, 2012.

Fergus W.J., “Electrolytes for solid oxide fuel cells”, J. Power Sources, 162, 30-40, 2006.

Gao Z. et al., “Preparation and characterization of $Sm_{0.2}Ce_{0.8}O_{1.9}/Na_2CO_3$ nanocomposite electrolyte for low-temperature solid oxide fuel cells”, Int. J. Hydrogen Energy, 36, 3984-3988, 2011.

Gerhardt R. et al., “The grain boundary conductivity effect in ceria doped with trivalent cations. Part-II-Microstructure and microanalysis”, J. Am. Ceraam. Soc., 69 647-651, 1986.

Godickemeier, M., Sasaki, K., Gauckler, L. J. Proceedings of the Second European Solid Oxide Fuel Cell Forum, ed. Thorstensen, B. (1996) 717.

Goodenough J. B. et al., “Oxide-ion conduction in $Ba_2In_2O_5$ and $Ba_3In_2MO_8$ (M = Ce, Hf, or Zr)”, Solid State Ionics, 44, 21-31, 1990.

Goodenough J., “Ceramic technology: Oxide ion conductors by design”, Nature, 404, 821-823, 2000.

Herle V. et al., “Lanthanide co-doping of solid electrolytes: AC conductivity behavior”, J. Eur. Ceram. Soc., 19, 837-841, 1999.

Hodge I. M., Ingram M. D., West A. R., “Impedance and modulus spectroscopy of polycrystalline solid electrolytes”, J. of Electroanal Chem., 74, 125-143, 1976.

Hohnke D.K., “Ionic conductivity of $Zr_{1-x}In_{2x}O_{2-x}$”, J. Phys. Chem. Solids, 41, 777-784, 1980.

Holland T.J.B., Redfern S.A.T., “Unit cell refinement from powder diffraction data; the use of regression diagnostics”, Mineralogical Magazine, 61, 65-77, 1997.

Holtappels P., Poulsen F.W., Mogensen M., “Electrical conductivities and chemical stabilities of mixed conducting pyrochlores for SOFC applications”, Solid State Ionics, 135, 675-679, 2000.

http:/www4.nau.edu.

http//www.altenergymag.com.

http//www.wikipedia.com.

http://www.osakagas.co.jp/fuel cell/sofc/img.

http:// www.netzsch-thermal-analysis.com.

http:// www.fei.com/products/sem/nova-nanose.

Hu J. D. et al., “Dual phase electrolytes for advanced fuel cells”, J. Power Sources, 154, 106-114, 2006.

Huang J. B. et al., “Development of novel low temperature SOFCs with co-ionic conducting SDC carbonate composite electrolyte”, Electrochem. Commun., 9, 2601–2605, 2007.

Huang J. et al., “A high performance ceramic fuel cell with samarium doped ceria-carbonate composite electrolyte at low temperature”, Electrochem. Commun., 8, 785-789, 2006.

Huang J. et al., “Effects of salt composition on the electrical properties of samaria-doped ceria/carbonate composite electrolytes for low-temperature SOFCs”, Int. J. Hydrogen Energy, 35, 4270-4275, 2010.

Huang K. et al., “Superior perovskite oxide-Ion conductor; strontium and magnesium doped $LaGaO_3$: III, performance tests of single ceramic fuel cells”, J. Am. Ceram. Soc., 81, 2581-2585, 1998.

Holtappels P., Poulsen F.W., Mogensen M., “Electrical conductivities and chemical stabilities of mixed conducting pyrocholres for SOFC application”, Solid State Ionics 135, 675-679, 2000.

Hong S. J., Virkar A V, “Lattice parameters and densities of rare earth oxide doped ceria electrolytes”, J. Am. Ceram. Soc. 78, 433-439, 1995.

Huang J., Mao Z., Yang L., Peng R., “SDC-carbonate composite electrolyte for low temperature SOFCs”, Electrochem Solid-State Lett., 8, A437-A440, 2005.

Huang J., Mao Z., Liu Z., Wang C., “Performance of fuel cell with proton conducting ceria based composite electrolyte and nickel based electrode”, J. Power Sources, 175, 238-243, 2008.

Hacker V. and Kordesh K. 2003. Ammonia Crackers. In Handbook of Fuel Cells, Eds. Vieltasch W. et al., J. Wiley & Sons, Chichester, U.K., Vol. 3, 121-127.

Inaba H., Tagawa H., "Ceria based electrolytes", Solid State Ionics, 83, 1-16, 1996.

Ishihara T. et al., "Doped $LaGaO_3$ perovskite type oxide as a new oxide ionic conductor", J. Am. Chem. Soc., 116, 3801-3803, 1994.

Ishihara T., Tabuchi J., Ishikawa S., Yan J., Enoki M., Matsumoto H., "Recent progress in $LaGaO_3$ based solid electrolyte for intermediate temperature SOFCs", Solid State Ionics, 177, 1949-1953, 2006.

Jacobson A. J., "Materials for solid oxide fuel cells", Chem. Mater., 22, 660-674, 2010.

Jia L. et al., "A direct carbon fuel cell with molten carbonate/doped ceria composite electrolyte", J. Power Sources, 195, 5581-5586, 2010.

Jiang N. et al., "A higher conductivity Bi_2O_3-based electrolyte", Solid State Ionics, 150, 347-353, 2002.

Johansen H.A., Cleary J.G., "High temperature electrical conductivity in the systems CaO - ZrO_2 and CaO - HfO_2", J. Electrochem. Soc., 111, 100-103, 1964.

Jung D. W. et al., "Effect of total dopant concentration and dopant ratio on the conductivity of $(DyO_{1.5})_x$-$(WO_3)_y$-$(BiO_{1.5})_{1-x-y}$", Acta Mater., 58, 355-363, 2010.

Junior J. M. S. et al., "Raman and rietveld structure characterization of sintered alkaline earth doped ceria", Materials Chemistry and Physics, 135, 957-964, 2012.

Kajitani M. et al., “Effect of Al doping on crystal structure and electrical conduction properties of $LaGa_{0.9}Mg_{0.1}O_{2.95}$ perovskite compound”, Solid State Ionics, 178, 355-358, 2007.

Kharton V.V., Naumovich E.N., Vecher A.A., “Research on the electrochemistry of oxygen ion conductors in the former Soviet Union- I. ZrO_2-based ceramic materials”, J. Solid State Electrochem., 3, 61-81, 1999.

Kharton V.V., Naumovich E.N., Yaremchenko A.A., Marques F.M.B., “Research on the electrochemistry of oxygen ion conductors in the former Soviet Union-IV. Bismuth oxide-based ceramics”, J. Solid State Electrochem., 5, 160-187, 2001.

Kilner J. A., “Fast anion transport in solids”, Solid State Ionics, 8, 201-207, 1983.

Kim D.J., “Lattice parameters, ionic conductivities, and solubility limits in fluorite structure MO_2 oxide [M = Hf^{4+}, Zr^{4+}, Ce^{4+}, Th^{4+}, U^{4+}] solid solutions”, J. Am. Ceram. Soc., 72, 1415-1421, 1989.

Kim et al., “Direct oxidation of liquid fuels in a solid oxide fuel cell”, J. Electrochem. Soc., 148, A693-A695, 2001.

Kim J. W. et al., “Polarization effects in intermediate temperature, anode-supported solid oxide fuel cells”, J. Electrochem. Soc., 146, 69-78, 1999.

Kim J., Yoo H., “Partial electronic conductivity and electrolytic domain of $La_{0.9}Sr_{0.1}Ga_{0.8}Mg_{0.2}O_{3-\delta}$”, Solid State Ionics, 140, 105-113, 2001.

Kim N. et al., “Effect of co-dopant addition on properties of gadolinium doped ceria”, J. Power Sources, 90, 139-143, 2000.

Kordesch K.V., Oliveira C. T., in Ullmann’s Encyclopedia of Industrial Chemistry, (Ed.:W. Gerhartz), Weinheim, VCH, Vol. A 12 1990, pp. 83–95.

Kuharuangrong S., “Ionic conductivity of Sm, Gd, Dy and Er-doped ceria”, J. Power Sources, 171, 506-510, 2007.

Kharton V.V., Marques F.M.B., Atkinson A., “Transport properties of solid oxide electrolyte ceramics: a brief review”, Solid State Ionics, 174, 135-149, 2004.

Kharton V.V. et al., “Ceria based materials for solid oxide fuel cells”, J. Mater. Sci., 36, 1105-1117, 2001.

Lai W., Haile S.M., “Impedance spectroscopy as a tool for chemical and electrochemical analysis of mixed conductors: A case study of ceria”, J. Am. Ceram. Soc., 88, 2979–2997, 2005.

Lapa C.M. et al., “Synthesis and characterization of composite electrolytes based on samarium doped ceria Na/Li carbonates”, Int. J. Hydrogen Energy, 35, 2953-2957, 2010.

Lee J. H. et al., “Electrical conductivity and defect structure of yttria-doped ceria-stabilized zirconia”, Solid State Ionics, 144, 175-184, 2001.

Li C. et al., “Electrolytic domain boundary between ionic and electronic conduction of doped ceria”, J. Mater. Sci. Technol., 14, 451-456, 1998.

Li X., Xiao G., Huang K., “Effective ionic conductivity of a novel intermediate temperature oxide ion and carbonate ion conductor”, J. Electrochem. Soc., 158, B225-B232, 2011.

Liu W. et al., “Ceria (Sm^{3+}, Nd^{3+})/carbonates composite electrolytes with high electrical conductivity at low temperature”, Compos. Sci. Technol., 70, 181-185, 2010.

Liu X.R., Zhu B., Xu J.R., Sun J.C., Mao Z., “Sulphate-ceria composite ceramics for energy environmental co-generation technology”, Key Eng. Mater., 280-283, 425-430, 2004.

Lubke S., Wiemhofer D., “Electronic conductivity of Gd-doped ceria with additional Pr-doping”, Solid State Ionics, 117, 229-243, 1999.

Li S., Wang X.D., Zhu B., “Novel ceramic fuel cell using non ceria based composites as electrolyte”, Electrochem Commun., 9, 2861-2866, 2007.

Ma Y. et al., “Thermal stability study of SDC/Na_2CO_3 nanocomposite electrolyte for low temperature SOFCs”, Int. J. Hydrogen Energy, 35, 2580-2585, 2010.

Matraszek et al., “Phase diagram study in the La_2O_3-Ga_2O_3-MgO-SrO system in air”, Solid State Ionics, 166, 343-350, 2004.

Minh N. Q., Takahashi T, in Science and Technology of Ceramic Fuel Cells, Elsevier Science, Amsterdam, The Netherlands, 1995.

Minh N.Q., “Ceramic fuel cells”, J. of Am. Ceram. Soc., 76, 563-588, 1993.

Minh N.Q., in: S.C. Singhal, M. Dokiya (Eds.), Proc. 6th Int. Symp. Solid Oxide Fuel Cells (SOFC-VI), The Electrochemical Society, Pennington, NJ, 1999, p. 127.

Minh Q. et al., “Solid oxide fuel cell technology—features and applications”, Solid State Ionics, 174, 271–277, 2004.

Mori T., Drennan J., Lee J.H., Li J.G., Ikegami T., “Oxide ion conductivity and microstructure of Sm or La doped CeO_2 based system”, Solid State Ionics, 154, 461-466, 2002.

Murray et al., “A direct-methane fuel cell with a ceria-based anode”, Nature, 400, 649-651, 1999.

Mogensen M., Sammes N.M., Tompsett G.A., “Physical, chemical and electrochemical properties of pure and doped ceria”, Solid State Ionics, 129, 63-94, 2000.

Mizuhata M., Bleke A. B., Watanabe H., Harada Y., Deki S., “Effect of ϒ-$LiAlO_2$ powder on ionic conductivity of co-existing single alkali carbonates”, Electrochimica Acta, 53, 71–78, 2007.

Minervini L, Zacate M.O., Grimes R.W., “Defect cluster formation in M_2O_3-doped CeO_2”, Solid State Ionics, 116,339-349, 1999.

Mizuhata M., Haranda Y., Ju G., Bienvenu A., Deki S., “Physicochemical properties of molten alkali metal carbonates coexisting with inorganic powder”, J. Electrochem. Soc., 151, E179–E185, 2004.

Minervini L., Zacate M.O., Grimes R.W., “Defect cluster formation in M_2O_3-doped CeO_2”, Solid State Ionics, 116, 339-349, 1999.

Omar S., Wachsman E., Nino J., “A co-doping approach towards enhanced ionic conductivity in fluorite based electrolytes”, Solid State Ionics, 177, 3199-3203, 2006.

Pal U. B., Singhal S.C., “Electrochemical vapor deposition of yttria stabilized zirconia films”, J. Electrochem. Soc., 137, 2937-2941, 1990.

Park S.Y. et al., “Improved of grain boundary conduction in SiO_2-doped GDC by BaO addition”, J. Electrochem. Soc., 156, B891-B896, 2009.

Perfilyev M. V. et al., High-Temperature Electrolysis of Gases, Nauka, Moscow, 1988.

Prokhorov Y., Electrochemical Society Proceedings, 2005- 07, SOFC IX, (2005), 998.

Parkash O., Singh N., Singh N., Kumar D., "Prepararion and characterization of ceria co-doped with Ca and Mg", Solid State Ionics, 212, 100-105, 2012.

Rajesh K. et al., "A novel approach based on impedance spectroscopy for measurement of magnetic permeability of ceramics" Indian Journal of Engineering & Materials Sciences, 6, 34-42, 1999.

Ramesh S., Reddy V., "Electrical properties of co-doped ceria electrolyte $Ce_{0.80-x}Gd_{0.20}Sr_xO_{2-\delta}$ ($0 \leq x \leq 0.10$)", Acta Physica Polonica, A115, 909-913, 2009.

Raza R., Wang X., Ma Y., Zhu B., "Study on calcium and samarium co-doped ceria based nanocomposite electrolytes", J. Power Sources, 195, 6491-6495, 2010.

Rickert H., Electrochemistry of solids- An introduction. Springer-Verlag, Berlin, 1982.

Sakai N. et al., "Significant effect of water on surface reaction and related electrochemical properties of mixed conducting oxides", Solid State Ionics, 175, 387-391, 2004.

Sammes N. et al., "Bismuth based oxide electrolytes-structure and ionic conductivity", J. Eur. Ceram. Soc., 19, 1801-1826, 1999.

Sha X. et al., "Study on La and Y co-doped ceria-based electrolyte materials", J. Alloys Compd., 28, 59-64, 2007.

Schober T. and Ringel H., “Proton conducting ceramics: Recent advances”, Ionics, 10, 391, 2004.

Sha X.Q. et al., “Preparation and properties of rare earth co-doped $Ce_{0.8}Sm_{0.2-x}Y_xO_{1.9}$ electrolyte materials for SOFC”, J. Alloys and Compd., 424, 315-321, 2006.

Shannon R.D., Prewitt C.T., “Effective ionic radii in oxides and fluorides”, Acta Cryst., B25, 925-946, 1969.

Shimonosono T. et al., “Electronic conductivity of La-doped ceria ceramics”, J. Am. Ceram. Soc., 88, 2114–2120, 2005.

Shuk P. et al., “Oxide ion conducting solid electrolytes based on Bi_2O_3”, Solid State Ionics, 89, 179-196, 1996.

Singhal S.C., “Advances in solid oxide fuel cell technology”, Solid State Ionics, 135, 305-313, 2000.

Singhal S.C., “Science and technology of solid oxide fuel cell techonology”, Mater. Res. Soc. Bull., 25, 16-21, 2000.

Singhal S.C., “Solid oxide fuel cells for stationary, mobile, and military applications”, Solid State Ionics, 152-153, 405-410, 2002.

Song S.A. et al., “Enhancement of cell performance using a gadolinium strontium cobaltite coated cathode in molten carbonate fuel cell”, J. Power Sources, 196, 9900-9905, 2011.

Steele B.C.H., “Appraisal of Ce_{1-y} $Gd_yO_{2-\delta}$ electrolytes for IT-SOFC operation at 500 °C”, Solid State Ionics, 129, 95-110, 2000.

Steele B.C.H., in: High Conductivity Solid Ionic Conductors, ed. Takahashi T. (World Scientific, Singapore, 1989).

Stevenson J.W. et al., "Effect of A-site cation nonstoichiometry on the properties of doped lanthanum gallate", Solid State Ionics, 113–115, 571-583, 1998.

Stevenson J.W. et al., "Processing and electrical properties of alkaline earth-doped lanthanum gallate", J. Electrochem. Soc., 144, 3613–3620, 1997.

Stimming U., Singhal S.C., Tagawa H., Lehnert W., The Electrochem. Soc., eds. Proc. of SOFC VIII; 2002.

Strickler D.W., Carlson W.G., "Ionic conductivity of cubic solid solutions in the system CaO-Y_2O_3-ZrO_2", J. Am. Ceram. Soc., 47, 122-127, 1964.

Suda E. et al., "Sintering characteristics, electrical conductivity and thermal properties of La-doepd ceria powders", J. Alloys Compd., 408–412, 1161–1164, 2006.

Steele B.C.H., "Material science and engineering: The enabling technology for the commercialization of fuel cell systems", J. Mater. Sci., 36, 1053-1068, 2001.

Singh N.K., Singh P., Singh M.K., Kumar D., Parkash O., "Auto-combustion synthesis and properties of $Ce_{0.85}Gd_{0.15}O_{1.925}$ for intermediate temperature solid oxide fuel cells electrolyte", Solid State Ionics, 192, 431-434, 2011.

Schober T., "Composites of ceramic high-temperature proton conductors with inorganic compounds", Electrochem Solid State Lett., 8, A199-A200, 2005.

Shiqiang H. et al., "A brief review of the ionic conductivity enhancement for selected oxide electrolytes", Journal of Power Sources, 172, 493-502, 2007.

Singh N.K., Singh P., Kumar D., Parkash O., “Electrical conductivity of undoped, singly doped and co-doped ceria”, Ionics, 18, 127-134, 2012.

Singh N., Singh N.K., Kumar D., Parkash O., “Effect of co-doping of Mg and La on conductivity of ceria”, J. of Alloys & Compounds, 519: 129-135, 2012.

Shannon R.D., “Revised effective ionic radii and systematic studies of interatomic distances in halides and chalcogenides”, Acta Crystallogr, A 32, 751-767, 1976.

Stauffer D. Introduction to percolation theory, Taylor and Francis, Philadelphia, PA, 1985.

Shing O., Ping T., Hin T., “Mechanochemical synthesis and characterization of calcium doped ceria oxide ion conductor”, Material Science and Engineering, 17, doi: 10.1088/1757-899X/17/1/012017, 2011.

Steele B., Heinzel A., “Materials for fuel-cell technologies” Nature, 414, 345-352, 2001.

Takahashi T. et al., “High oxide ion conduction in sintered oxides of the system Bi_2O_3-Y_2O_3”, J. Appl. Electrochem., 5, 187-195, 1975.

Tang Z., Lin Q., Mellander B. E., Zhu B., “SDC–Li/Na carbonate composite and nanocomposite electrolytes”, Int. J. Hydrogen Energy, 35, 2970-2975, 2010.

Tao J.T., Irvine S., Kilner J. A., “An efficient solid oxide fuel cell based upon single phase pervoskite”, Adv. Mater., 17, 1734, 2005.

Tuller H.L., in: Tuller H., Schoonman J., I. Riess (Eds.), Oxygen Ion and Mixed Conductors and their Technological Applications, Kluwer (NATO ASI series), Dordrecht, 2000, p. 245-270.

Trejo E.R., Benitez R., Reynoso S., Rosas M., “Nanoparticles and nano-grain sized Y-doped CeO_2 ceramics”, J. Electrochem. Soc., 154, A258-A262, 2007.

Tadokoro S.K., Muccillo E.N.S., “Effect of Y and Dy co-doping on electrical conductivity of ceria ceramics”, J. Eur Ceram Soc., 27, 4261–4264, 2007.

Tian C., Chan S.W., “Ionic conductivities, sintering temperatures and microstructures of bulk ceramics CeO_2 doped with Y_2O_3”, Solid State Ionics, 134, 89–102, 2000.

Tsung H.Y., Chen C.C., “Ionic conductivity investigation in samarium and strontium co-doped ceria system”, Phys. Scr., T 129, 303-307, 2007.

Tianshu Z., Hing P., Huang H., Kilner J., “Ionic conductivity in the CeO_2–Gd_2O_3 system ($0.05 \leq Gd/Ce \leq 0.4$) prepared by oxalate co-precipitation”, Solid State Ionics, 148, 567-573, 2002.

Vegard L., Dale H., “Tests on mixed crystals and alloys”, Z Kristallogr, 67,148-162, 1928.

Wade J.L. et al., “Composite electrolyte membranes for high temperature CO_2 separation”, J. Membr. Sci., 369, 20-29, 2011.

Wade J.L., West A.C., Lackner K.S., 213th ECS Meeting Abstracts, vol. 1, 2008, p. 390.

Wang F.Y., Chen S., Wang Q., Yu S., Cheng S., “Study on Gd and Mg co-doped ceria electrolyte for intermediate temperature solid oxide fuel cells”, Catal. Today, 97, 189-194, 2004.

Wang X., Ma Y., Li S., Kashyout A. H., Zhu B., Muhammed M., "Novel core shell SDC/amorphous Na_2CO_3 nanocomposite electrolyte for low temperature SOFCs"J. Power Sources, 196, 2754-2758, 2011.

Wang X., Ma Y., Raza R., Muhammed M., Zhu B., "Novel core shell SDC/amorphous Na_2CO_3 nanocomposite electrolyte for low temperature SOFCs", Electrochem. Commun., 10, 1617-1620, 2008.

Wasiucionek M. et al., "EXAFS/XANES studies of the local structure of amorphous ionic and electronic-ionic conductors", Materials Science-Poland, 24, 182-187, 2006.

Wolf Vielstich et al. Hand book of fuel cells vol.1 Wiley.

Wang D.Y., Norwick A.S., "Dielectric relaxation from a network of charged defects in dilute CeO_2:Y_2O_3solid solutions", Solid State Ionics, 5, 551-555, 1981.

Wang F.Y., Wan B.Z., Cheng S., "Study on Gd^{3+} and Sm^{3+} co-doped ceria-based electrolytes", J. Solid State Electrochem., 9, 168-173, 2005.

Guo X., Maier J., "Grain boundary blocking effect in zirconia: a schottky barrier analysis", J. Electrochem. Soc., 148, E121-E126, 2001.

Xia C. et al., "Intermediate temperature fuel cell with a doped ceria carbonate composite electrolyte", J. Power Sources, 195, 3149-3154, 2010.

Xia C. et al., "A high performance composite ionic conducting electrolyte for intermediate temperature fuel cell and evidence for ternary ionic conduction", J Power Sources, 188, 156-162, 2009.

Yahiro H. et al., "Electrical properties and microstructure in the system ceria alkaline earth oxide", J. Mater. Sci., 23, 1036-1041, 1988.

Yamamura H. et al., “Multiple doping effect on the electrical conductivity in the $(Ce_{1-x-y}La_xM_y)O_{2-\delta}$ (M=Ca, Sr) system”, Electrochem. Commun., 68, 455-459, 2000.

Yeh et al., “Ionic conductivity investigation in samarium and strontium co-doped ceria system”, Phys. Scr., T129, 303-307, 2007.

Yaremchenko A.A. et al., “Oxygen ionic transport in Bi_2O_3-based oxides: II. The Bi_2O_3–ZrO_2–Y_2O_3 and Bi_2O_3–Nb_2O_5–Ho_2O_3 solid solutions”, J. Solid State Electrochem., 2, 308-314, 1998.

Yamamoto O., “Solid oxide fuel cells: fundamental aspects and prospects”, Electrochim. Acta, 45, 2423-2435, 2000.

Yashiro K. et al., “Electrical properties and defect structure of niobia-doped ceria”, Solid State Ionics, 175, 341–344, 2004.

Yasuda et al., “Electrical conductivity and mechanical properties of alumina dispersed doped lanthanum gallates”, Solid State Ionics, 135, 381-388, 2000.

Yeh T.H. et al., “Mechanical and electrical properties of ZrO_2 (3Y) doped with $RENbO_4$ (RE = Yb, Er, Y, Dy, YNd, Sm, Nd)”, J. Phys. IV France, 128, 213-219, 2005.

Yang Z., Weil K.S., Paxton D.M., Stevenson J.W, “Selection and evaluation of heat-resistant alloys for SOFC interconnect applications”, J. Electrochem. Soc. 150, 1188-1201, 2003.

Ying et al., “Enhanced ionic conductivity in calcium doped ceria carbonate electrolyte: A composite effect”, Int. J. of Hydrogen Energy, 37, 19401-19406, 2012.

Yahiro H., Eguchi K., Arai H., “AC conductivity and conductivity relaxation studies in the CeO_2-Y_2O_3 system”, Solid State Ionics, 21, 49-53, 1986.

Yamashita K., Ramanujachary K.V., Greenblatt M., “Hydrothermal synthesis and low temperature conduction properties of substituted ceria ceramics”, Solid State Ionics, 81, 53-60, 1995.

Zha S.W. et al., “Effect of Gd (Sm) doping on properties of ceria electrolyte for solid oxide fuel cells”, J. Power Sources, 115, 44-48, 2003.

Zhang L. et al., “A high performance intermediate temperature fuel cell based on thick oxide carbonate electrolyte”, J. Power Sources, 194, 967-971, 2009.

Zhao et al., “Validation of H^+/O^{2-} conduction in doped ceria-carbonate composite material using an electrochemical pumping method”, Int. J. of hydrogen energy, 37, 11378-11382, 2012.

Zhao et al., “Oxide ion and proton conduction in doped ceria-carbonate composite materials”, Int. J. of Hydrogen Energy, 38, 1553-1559, 2013.

Zheng Y. et al., “Effect of Sm and Mg co-doping on the properties of ceria based electrolyte materials for IT-SOFCs”, Material Research Bull., 44, 775-779, 2009.

Zheng Y., Yueming S., Haitao G., Gao L., Chen H., Guo L., “La and Ca co-doped ceria-based electrolyte materials for IT-SOFCs”, Material Research Bulletin, 44, 1717-1721, 2009A.

Zheng Y. et al., “The effect of Sr on the properties of Y-doped ceria electrolyte for IT-SOFCs”, J. Alloys and Compd., 486, 586-589, 2009B.

Zhi J. et al., American Ceramic Soc. Bulletin, 85, 9501-9502, 2006.

Zhu B., Mellander B.E., in S. C. Singhal and M. Dokiya (Eds.), Solid Oxide Fuel Cells-VI (The Electrochemical Society, Inc.), Pennington, NJ, (1999) 244.

Zhu B. et al., “Calcium doped ceria based materials for cost effective intermediate temperature solid oxide fuel cells”, Solid State Sciences, 5, 1127-1125, 2003.

Zhu B. et al., “Innovative low temperature SOFCs and advanced materials”, J. Power Sources, 118, 47-53, 2003.

Zhu B. et al., “Novel hybrid conductors based on doped ceria and BCY20 for IT-SOFC application”, Electrochem. Commun., 6, 378-383, 2004.

Zhu B. et al., “Theoretical approach on ceria based two phase electrolytes for low temperature (300-600 °C) solid oxide fuel cells”, Electrochem. Commun., 10, 302-305, 2008.

Zhu B. et al., “Electrolysis studies based on ceria-based composites”, Electrochem. Commun., 8, 495-498, 2006.

Zhu B., “Advantages of intermediate temperature solid oxide fuel cells for tractionary application”, J. Power Sources 93, 82-86, 2001.

Zhu B., “Next generation fuel cells R & D”, Int. J. Energy Res., 30, 895-903, 2006.

Zhu B., “Proton and oxygen ion mixed conducting ceramic composites and fuel cells”, Solid State Ionics, 145, 371, 2001.

Zhu B., “Studies on dual phase ceria based composites in electrochemistry”, J. Electrochem. Sci., 1, 383-402, 2006.

Zhu B., Mat M.D., “Studies on dual phase ceria based composites in electrochemistry”, Int. J. Electrochem. Sci., 1, 383-402, 2006.

Zhu B., Mellander B.E., “Proton conduction in nitrate-based oxides and related ceramics at intermediate temperatures”, Solid State Ionics, 70-71, 285-290, 1994.

Zhu W.Z., Deevi S.C., “A review on the status of anode materials for solid oxide fuel cells”, Materials Science and Engineering, A362, 228–239, 2003.

Zizelman J., Botti J., Tachtler J., Strobl W., “New plastics and the automobile”, Automotive Engineering International, (2000, September) 14.

Zhu B., Liu X.R., Zhu Z.G., Ljungberg R., “Solid oxide fuel cell (SOFC) using industrial grade mixed rare-earth oxide electrolytes”, Int. J. Hydrogen Energy, 33, 3385–3392, 2008.

Zhao Y.C. et al., “Quantifying multiionic conduction through doped ceria-carbonate composite electrolyte by a current-interruption technique and product analysis”, Int. J. Hydrogen Energy, 37, 8556-8561, 2012.

Zhu B. et al., “Innovative solid carbonate–ceria composite electrolyte fuel cell”, Electrochem. Commun., 3, 566-571, 2001.

Zhu B., “Functional ceria salt composite materials for advanced IT-SOFC applications”, J. Power Sources, 114, 1-9, 2003.

Zhu B., “Nanocomposites for advanced fuel cell technology”, J. Nanosci. Nanotechnol., 11, 8873-8879, 2011.

Outcomes of the Thesis

(a) In the International Peer Reviewed Journals

1. **Nandini Jaiswal**, Shail Upadhyay, Devendra Kumar, Om Parkash, Ionic conductivity investigation in lanthanum (La) and strontium (Sr) co-doped ceria system, **J. of Power Sources** 222 (2013) 230-236**.**
2. **Nandini Jaiswal**, Shail Upadhyay, Devendra Kumar, Om Parkash, Effect of Mg and Sr co-doping on the electrical properties of ceria-based electrolyte materials for intermediate temperature solid oxide fuel cells, **J. of Alloys & Compound**, 577 (2013) 456-462.
3. **Nandini Jaiswal**, Shail Upadhyay, Devendra Kumar, Om Parkash, Ceria co-doped with calcium (Ca) and strontium (Sr): a potential candidate as a solid electrolyte for intermediate temperature solid oxide fuel cells, **Ionics** 20 (1) (2014) 45-54.
4. **Nandini Jaiswal**, Shail Upadhyay, Devendra Kumar, Om Parkash, Sm^{3+} and Sr^{2+} co-doped ceria prepared by citrate-nitrate auto-combustion method, **Int. J. of Hydrogen Energy**, 39 (1) (2014) 543-551**.**
5. **Nandini Jaiswal**, Shail Upadhyay, Devendra Kumar, Om Parkash, Preparation and characterization of $Ce_{0.85}La_{0.15-x}Sr_xO_{\{2-(0.075+x/2)\}}$ solid electrolytes for intermediate temperature solid oxide fuel cells, **Ionics** (2014) (DOI) 10.1007/s11581-014-1190.
6. **Nandini Jaiswal**, Shail Upadhyay, Devendra Kumar, Om Parkash, Ceria (La3+, Sr2+)/carbonates nanocomposite electrolytes with high electrical conductivity for low temperature SOFCs, **Int. J. Appl. Ceram. Technol**, 1–8 (2014) DOI:10.1111/ijac.12327.
7. **Nandini Jaiswal**, Shail Upadhyay, Devendra Kumar, Om Parkash, Ionic conduction in Mg^{2+} and Sr^{2+} co-doped ceria/carbonates nanocomposite electrolytes, **Int. J. of Hydrogen Energy**, 40, (2015) 3313-3320.

8. **Nandini Jaiswal**, Shail Upadhyay, Devendra Kumar, Om Parkash, Enhanced ionic conductivity in La^{3+} and Sr^{2+} co-doped ceria: carbonate nanocomposite, **Ionics**, (2015). DOI: 10.1007/s11581-015-1386-2.

(b) In National/International Conferences

1. **Nandini Jaiswal**, Shail Upadhyay, Devendra Kumar, Om Parkash Paper presented **at Advanced NanoTech Dubai 2015** to be held at **Dubai** 16-18 march, 2015.

Journal of Power Sources 222 (2013) 230–236

Contents lists available at SciVerse ScienceDirect

Journal of Power Sources

journal homepage: www.elsevier.com/locate/jpowsour

Ionic conductivity investigation in lanthanum (La) and strontium (Sr) co-doped ceria system

Nandini Jaiswal [a], Shail Upadhyay [b], Devendra Kumar [a], Om Parkash [a,*]

[a] Department of Ceramic Engineering, Indian Institute of Technology (Banaras Hindu University), Varanasi 221005, India
[b] Department of Applied Physics, Indian Institute of Technology (Banaras Hindu University), Varanasi 221005, India

HIGHLIGHTS

- The system $Ce_{1-x-y}La_xSr_yO_{2-\{x/2+y\}}$ has been investigated for the first time.
- In present study, number of oxygen vacancies is kept constant in all composition.
- Composition $Ce_{0.89}La_{0.07}Sr_{0.04}O_{1.925}$ has maximum conductivity more than highest conductivity reported in SDC and GDC at 600 °C.
- It is much less costly than that of SDC and GDC.
- This makes CL7S4 is a potential candidate as a solid electrolyte for ITSOFCs.

ARTICLE INFO

Article history:
Received 18 June 2012
Received in revised form
29 August 2012
Accepted 31 August 2012
Available online 10 September 2012

Keywords:
Doped ceria
Combustion synthesis
Co-doping effect
Impedance analysis
Electrical conductivity

ABSTRACT

Effect of strontium doping on ionic conductivity of lanthanum-doped ceria has been investigated. Distribution and average radius of oxygen vacancies formed from divalent and trivalent dopant cations in co-doped system has been calculated using hard-sphere model. Phase identification, microstructure and ionic conductivities of samples have been studied by X-ray diffraction (XRD), scanning electron microscopy (SEM), and AC impedance spectroscopy, respectively. X-ray diffraction reveals that all the samples are single phase with cubic fluorite-type structure. Dense ceramics with density ~95% of the theoretical density have been obtained without using any sintering aid. The results show that the samples co-doped with La and Sr exhibit higher ionic conductivity and lower activation energy than those of ceria doped with La only in the intermediate temperature range. The highest ionic conductivity has been observed for $Ce_{0.89}La_{0.07}Sr_{0.04}O_{1.925}$ in the samples investigated (4.01×10^{-3} S cm^{-1}) at 500 °C, which is 20 times as high as that of $Ce_{0.85}La_{0.15}O_{1.925}$. Concept of average oxygen vacancy radius has been found to be a useful in calculating the lattice parameter in this system.

1. Introduction

Solid oxide fuel cells (SOFCs) are considered as an alternative electric power generation systems due to high energy conversion efficiency, fuel flexibility and operation directly on natural gas [1–5]. Application of SOFCs is, however, still limited because of high cost of component materials. The SOFC-based generators can be commercially viable only if their production cost drops [2,3]. This can be done through development of new materials as solid electrolytes because these are the key components of electrochemical cells [5]. Solid electrolytes should have numerous requirements, such as high oxide ion conductivity, negligible electronic conduction and thermodynamically stability over a wide range of temperature and oxygen partial pressure. Doped ceria is a well known material in modern ceramics because of its high oxide ionic conductivity for the fabrication of fuel cells and oxygen sensors [6].

An increase of oxygen vacancies in ceria enhances the ionic conductivity. The vacancies are not, however, free; these are associated with dopant cations leading to decrease in ionic conductivity beyond a particular concentration. For example, 20 mol% of rare earth dopants produce sufficient concentration of oxygen vacancies in samarium doped ceria, $Ce_{0.80}Sm_{0.20}O_{1.90}$ (SDC) [2] and gadolinium doped ceria $Ce_{0.80}Gd_{0.20}O_{1.90}$ (GDC) systems [3]. If the content of the trivalent dopant exceeds 20 mol %, then the ionic conductivity decreases due to defect association and/or clustering of oxygen vacancies. Ionic radius of the dopant also affects the ionic conductivity. If the difference in the ionic

* Corresponding author. Tel.: +91 542 6701791; fax: +91 542 2368428.
E-mail address: oprakash.cer@itbhu.ac.in (O. Parkash).

0378-7753/$ – see front matter © 2012 Elsevier B.V. All rights reserved.
http://dx.doi.org/10.1016/j.jpowsour.2012.08.095

radius of the dopant and host ion (Ce^{4+}) is large, then large strain is induced in the lattice and the ionic conductivity decreases. Compatibility of ionic radius of the dopant and the host cation is very critical in achieving the desired lattice match and, thereby, the properties. Moreover, the lattice binding energy of dopant should be low. Thus, taking into consideration these critical factors, enhancement of the ionic conductivity has been achieved by suitable dopants.

Co-doping has been reported as a novel method to increase the ionic conductivity of ceria [4,5,7–15]. The results reported on co-doped and singly doped ceria are however, controversial in nature. For example, Herle et al. [16] found that co-doped ceria with 3,5 or 10 dopants show higher ionic conductivity than the best singly doped materials whereas Yoshida et al. [17,18] did not find additive effect of La^{3+} and Y^{3+} co-doping on the ionic conductivity of ceria. $Ce_{0.80}Gd_{0.2-x}Pr_xO_{1.9}$ [19], $Ce_{0.80}Gd_{0.2-x}Sm_xO_{1.9}$ [20] and $Ce_{0.85}Gd_{0.1}Mg_{0.05}O_{1.9}$ [21] electrolytes provide evidence for enhancement of the ionic conductivity due to co-doing. It is found that ionic conductivity of a co-doped system is sometimes more while other times less than that of a singly doped ceria. Systematic research has been done on samarium and strontium co-doped ceria by Yeh and Chou [22] who found that $Ce_{0.78}Sm_{0.20}Sr_{0.02}O_{1.88}$ has the highest ionic conductivity (6.1×10^{-2} S-cm^{-1}) at 800 °C. These authors ascribed the enhancement in the conductivity to the increase in number of oxygen vacancies, decrease in the association enthalpy and increase in radii of oxygen vacancies which widen the channels for easy movement of oxygen ions.

In the present investigations, effect of double substitution of La^{3+} and Sr^{2+} on the electrical properties of ceria has been studied. Nanocrystalline $Ce_{0.85}La_{0.15}O_{1.925}$ (CLO15), $Ce_{0.87}La_{0.11}Sr_{0.02}O_{1.925}$ (CL11S2), $Ce_{0.89}La_{0.07}Sr_{0.04}O_{1.925}$ (CL7S4), and $Ce_{0.91}La_{0.03}Sr_{0.06}O_{1.925}$ (CL3S6) having same number of total oxygen vacancies have been prepared using citrate-nitrate auto-combustion method. A significant improvement of the electrical conductivity is observed by co-doping ceria with lanthanum and strontium.

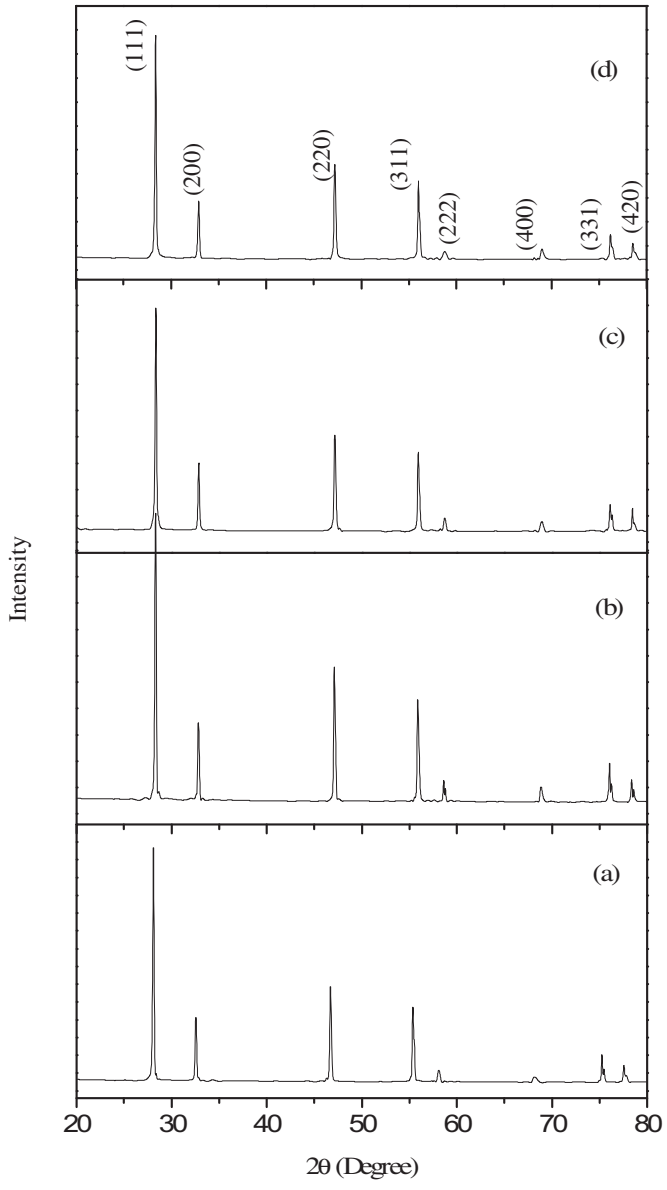

Fig. 1. Powder X-ray diffraction patterns of various compositions (a) CLO15, (b) CL11S2, (c) CL7S4, (d) CL3S6 sintered at 1350 °C.

2. Experimental

A series of samples having general formula $Ce_{1-x-y}La_xSr_yO_{2-\{x/2+y\}}$ where $\{(x = 0.15, y = 0), (x = 0.11, y = 0.02), (x = 0.07, y = 0.04)$ and $(x = 0.03, y = 0.06)\}$ were synthesized by citrate–nitrate auto-combustion method. Starting chemicals used for the synthesis of powders were ammonium ceric nitrate (purity 99%), lanthanum oxide, strontium nitrate, and citric acid. Reaction solution consisted of Ce-nitrate, La-nitrate, Sr-nitrate (purity 99.5%), and citric acid (purity>99%), in the ratio depending on the final composition. Citrate to nitrate molar ratio in the solution was kept constant as 0.3 [23]. The solution was concentrated on a hot plate at 200 °C until excess free water evaporated and the final spontaneous ignition occurred. Within a few seconds, the combustion reaction completed with yellow porous ash filling the container. During the ignition, the container was covered with a fine-mesh sieve to prevent the ash from flying out of the container. The as-collected ash was calcined at 800 °C in air for 4 h. The calcined powders were uniaxially dry-pressed into pellets (about 15 mm in diameter and 1.5 mm thick) without any binder by applying 50 kN load into a cylindrical shape. The pellets were sintered at 1350 °C for 4 h.

Crystal structure was determined using a Rigaku high resolution powder X-ray diffractometer employing Cu $K_{\alpha 1}$ radiation and Ni-filter at room temperature. Data were collected in the Bragg angle range of $20° \leq 2\theta \leq 80°$. The crystallite size, D was estimated using Scherrer's formula

$$D = \frac{0.9\lambda}{\beta \cos\theta} \quad (1)$$

where β is the full width at half maxima (FWHM) excluding instrumental broadening, λ is the wave length of X-ray diffraction and θ is the Bragg angle. β is taken for the strongest Bragg's peak corresponding to (111) reflection for all the samples. Lattice parameters were calculated using 'Cell' software. Density of sintered pellets was determined by Archimedes method and expressed as percentage of the theoretical values determined from the cubic lattice parameter and molecular weight of sample. Sintered pellets were polished using emery papers of grade 1/0, 2/0, 3/0, and 4/0 (Sia, Switzerland) followed by polishing on a velvet cloth with diamond paste of grade1/4-OS-475 (HIFIN). Then these were etched thermally at 1250 °C. Micrographs were taken with the help of a scanning electron microscope (INSPECT 50 FEI').

Electrical conductivity of the materials was measured using sintered pellets. Silver paste was used as electrodes on both the surfaces of each pellet. Impedance was measured using a Novocontrol Alpha-A High Performance Frequency Analyzer with an

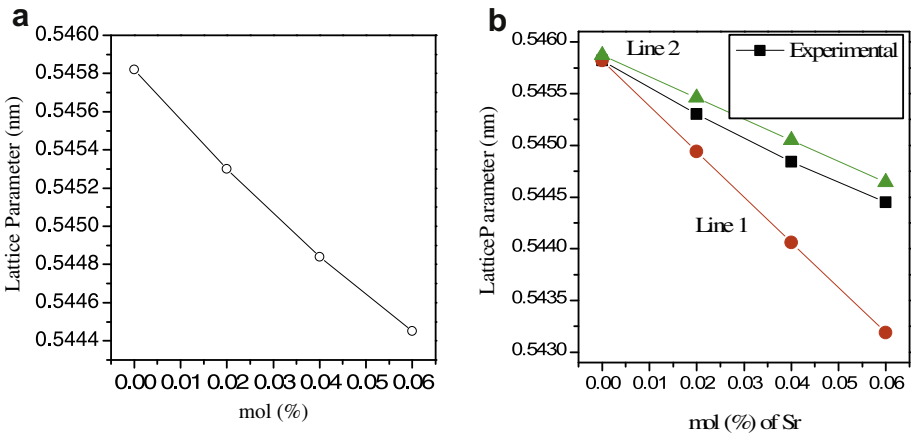

Fig. 2. (a) Variation of lattice parameter as a function of the dopant concentration for the system $Ce_{1-x-y}La_xSr_yO_{2-\{x/2+y\}}$. (b) Calculated results and experimental data for the lattice parameter of lanthanum and strontium co-doped ceria systems as a function of Sr content.

applied voltage of 20 mV. The measurements were made in air in the temperature range 200–500 °C at different frequencies in the range 1 Hz to 1 MHz.

3. Results and discussion

Powder X-ray diffraction of as-prepared ash shows the formation of a single phase solid solution having fluorite structure similar to CeO_2, suggesting that Ce ions are in the 4+ state in the as-prepared ash. If the Ce ions were present in the +3 state in the precursor, one would expect the formation of Ce_2O_3 instead of CeO_2. XRD patterns for the calcined powders are similar to those obtained after sintering except that the diffraction lines become sharper as shown in Fig. 1. This is due to grain growth occurring during sintering. Fig. 1 also shows that the 2θ values of co-doped ceria shifts slightly towards lower angles with Sr content. Diffraction patterns were indexed on the basis of fluorite structure similar to CeO_2 using JCPDS file no. 43-1002. The lattice constant was determined using "Cell" software.

Lattice constant increases from 5.4019 ± 0.0016 Å [24] to 5.4582 ± 0.0005 Å on addition of La to CeO_2. This can be attributed to the volume expansion of lattice due to larger ionic radius of La^{3+} (1.16 Å) in comparison to Ce^{4+} (0.97 Å). The bond length of the ceria matrix (Ce–O/Ce-cations) increases on addition of lanthanum since its lattice binding energy with oxygen ion is lower than the ceria matrix [22]. Doping of La^{3+} in ceria lattice will also induce a strain in the lattice as the material is elastically deformed. Lattice constant decreased linearly with increasing concentration of Sr^{2+}as shown in Fig. 2(a). This is due to decrease in the total concentration of dopants, i.e. for each mol% of Sr^{2+}, 2 mol% of La^{3+} decreases. Average crystallite size, D, of powders, calculated by Scherrer's formula from the X-ray line broadening is between 53 and 69 nm (Table 1). Pellets sintered at 1350 °C have density more than 95% of the theoretical values (Table 1).

Table 1
Crystallite size, lattice parameter and % theoretical density of compositions of the system $Ce_{1-x-y}La_xSr_yO_{2-\{x/2+y\}}$.

S.No.	Compositions	Crystallite size of sintered powder (nm)	Lattice parameter (Å)	% of theoretical density
1.	$Ce_{0.85}La_{0.15}O_{1.925}$	53	5.4582 ± 0.0005	98.3
2.	$Ce_{0.87}La_{0.11}Sr_{0.02}O_{1.925}$	58	5.4530 ± 0.0003	97.7
3.	$Ce_{0.89}La_{0.07}Sr_{0.04}O_{1.925}$	57	5.4484 ± 0.0005	95.0
4.	$Ce_{0.91}La_{0.03}Sr_{0.06}O_{1.925}$	69	5.4445 ± 0.0011	94.3

The lattice parameters of lanthanum and strontium co-doped ceria system ($Ce_{1-x-y}La_xSr_yO_{2-\{x/2+y\}}$) were calculated by hard sphere model [25]. The equation of $Ce_{1-x-y}La_xSr_yO_{2-\{x/2+y\}}$ system can be written as:

$$xLaO_{1.5} + ySrO + (1-x-y)CeO_2 = xLa'_{Ce} + ySr''_{Ce} + \left(\frac{x}{2}+y\right)V_{\ddot{O}} + (1-x-y)Ce_{Ce} + [2-(x/2+y)]O_o \quad (2)$$

where the species are written in accordance with Kroger Vink notation of defects. Lattice parameter of an ideal fluorite structure can be calculated using Eq. (3):

$$a = \frac{4}{\sqrt{3}}(r_{anion} + r_{cation}) \quad (3)$$

where r_{anion} and r_{cation} are radii of the dopant cations and anions, respectively. The radii of cation and anion can be calculated using the following Eqs. (4) and (5):

$$r_{cation} = xr_{La} + yr_{Sr} + (1-x-y)r_{Ce} \quad (4)$$

$$r_{anion} = \left(\frac{2-\left(\frac{x}{2}+y\right)}{2}\right)r_o + \left(\frac{\frac{x}{2}+y}{2}\right)r_{V_{\ddot{o}}} \quad (5)$$

where r_{Ce}, r_{Sr}, r_{La}, $r_{V_{\ddot{o}}}$ and r_o are radii of Ce^{4+}, dopant cations, oxygen vacancy and oxygen ion, respectively.

From the above equations, lattice parameter of lanthanum and strontium co-doped ceria system can be written as:

$$a = \frac{4}{\sqrt{3}}(r_{anion} + r_{cation}) = \frac{4}{\sqrt{3}}\left[xr_{La} + yr_{Sr} + (1-x-y)r_{Ce} + \left(\frac{2-\left\{\frac{x}{2}+y\right\}}{2}\right)r_o + \left(\frac{x}{4}r_{V_{\ddot{O}_t}} + 0.5yr_{V_{\ddot{O}_d}}\right)\right] \quad (6)$$

By using $r_{Ce} = 0.97$ Å, and $r_o = 1.4$ Å, lattice parameter of CeO_2 is found to be 5.473 Å. Since the actual lattice parameter of pure ceria is 5.414 Å from JCPDS files, a multiplication factor of 5.414/

5.473 = 0.9892 was taken in all of the above equations [26]. Hence, the equation for lattice parameter can be written as:

$$a = 0.9892 \times \frac{4}{\sqrt{3}}\left[xr_{La} + yr_{Sr} + (1-x-y)r_{Ce} + \left(\frac{2-\left\{\frac{x}{2}+y\right\}}{2}\right)r_o + \left(\frac{x}{4}r_{V_{\ddot{O}_t}} + 0.5yr_{V_{\ddot{O}_d}}\right)\right] \quad (7)$$

where $V_{\ddot{O}_t}$ and $V_{\ddot{O}_d}$ are oxygen vacancy produced from trivalent and divalent cations, respectively. Eq. (7) was used to determine theoretical value of lattice parameter for lanthanum and strontium co-doped ceria solid solutions. Lattice parameter for $Ce_{0.90}Sr_{0.10}O_{1.90}$ and $Ce_{0.85}La_{0.15}O_{1.925}$ can be calculated using Eqs. (8) and (9).

(a) $Ce_{0.90}Sr_{0.10}O_{1.90}$

$$a = 0.9892 \times \frac{4}{\sqrt{3}}\left[0.90r_{Ce} + 0.10r_{Sr} + \left(\frac{1.9}{2}\right)r_o + \left(\frac{0.10}{2}\right)r_{V_{\ddot{O}}}\right] \quad (8)$$

(b) $Ce_{0.85}La_{0.15}O_{1.925}$

$$a = 0.9892 \times \frac{4}{\sqrt{3}}\left[0.85r_{Ce} + 0.15r_{La} + \left(\frac{1.925}{2}\right)r_o + \left(\frac{0.075}{2}\right)r_{V_{\ddot{O}}}\right] \quad (9)$$

Substituting the lattice parameter of $Ce_{0.90}Sr_{0.10}O_{1.90}$ (5.429 Å) and $Ce_{0.85}La_{0.15}O_{1.925}$ (5.4582 Å) in Eqs. (8) and (9), calculated oxygen vacancy radii of $Ce_{0.90}Sr_{0.10}O_{1.90}$ and $Ce_{0.85}La_{0.15}O_{1.925}$ are 0.9498 and 1.154 Å, respectively.

The calculated results and experimental data of lattice parameters of lanthanum and strontium co-doped ceria systems are plotted as shown in Fig. 2(b).

Substituting the values of ionic radius of oxygen vacancy produced by trivalent and divalent dopant denoted by $r_{V_{\ddot{O}_t}}$ and $r_{V_{\ddot{O}_d}}$ as 1.154 and 0.9498 Å, respectively, in Eq. (7), the lattice parameters were calculated and are shown by line 1 in Fig. 2(b). These calculated values are different from the lattice parameter obtained from the experimental data as shown in Fig. 2(b). If the same value of $r_{V_{\ddot{O}_t}}$ and $r_{V_{\ddot{O}_d}}$ (average oxygen vacancy radius 1.16 Å) are substituted in Eq. (7), the calculated results of lattice parameter are shown by line 2. This result was found in good agreement with the experimental result. Therefore, it is found that the radii of oxygen vacancies formed by trivalent and divalent cations in lanthanum and strontium co-doped ceria systems are not different. These results are different from the results obtained by Yeh and Chou [22], where they found that radii of oxygen vacancies created by divalent and trivalent dopants are different.

Fig. 3(a)–(d) shows micrographs of thermally etched samples at 1250 °C. The surface micrograph of sintered pellets revealed a dense structure and well defined grains separated by grain boundaries. All the samples show grains having varying shape and size. The image of all the samples except CLO15 indicates the presence of faceted grains. It is interesting to notice that average grain size increases with increasing concentration of strontium up to 4 mol% and thereafter it decreases. The average grain size for the samples CLO15, CL11S2, CL7S4 and CL3S6 are found to be 1.0, 3.5, 4.0 and 2.9 μm, respectively.

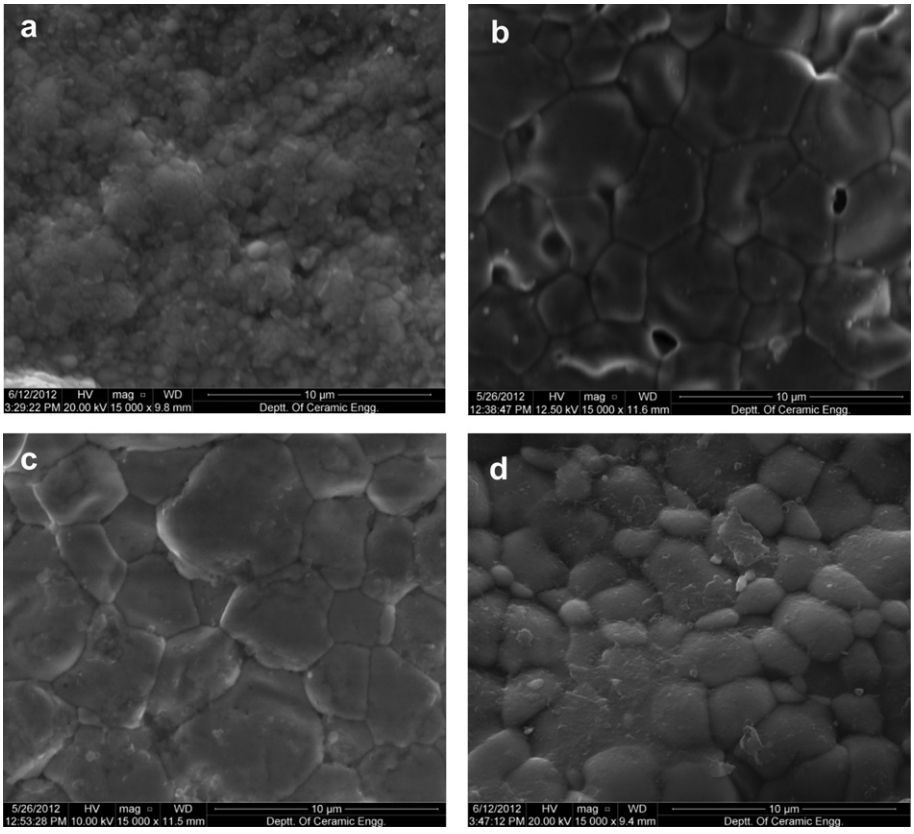

Fig. 3. Scanning electron micrographs of various compositions (a) CLO15, (b) CL11S2, (c) CL7S4, (d) CL3S6 etched at 1250 °C.

AC impedance analysis is well suited for the electrical conductivity measurements of ionic conductors. This method provides information on the contribution of grains and grain boundaries and electrode polarization to the total conductivity.

Complex plane impedance plots of all the samples in air at 200 °C as well as for CL7S4 sample at different temperatures are shown in Fig. 4a and b, respectively. At 200 °C, three contributions can be distinguished: an incomplete depressed semicircle at high frequency and two depressed arcs at lower frequencies. These arcs can be ascribed to contribution of grain polarization, grainboundary polarization, and electrodes polarization, respectively in order of decreasing frequency. In order to see clearly, the contribution of grains, the data is plotted on an expanded scale in the insets. Intercepts of the arcs due to grains and grain boundaries decrease with increase in Sr^{2+} concentration for $y \leq 0.04$. Thereafter these values decrease for $y > 0.04$. The time constant τ, for a dielectric relaxation decreases as temperature increases. This leads to shifting of arcs towards higher frequencies. Therefore, all the arcs are not observed at all temperatures in the limited range of frequency of the equipment. The arc corresponding to contribution of grains disappears at 325 °C. It is noted from Fig. 4(a) that total resistance given by $R_g + R_{gb}$ is minimum for CL7S4 among all the compositions. Arcs due to grains and grain boundaries are associated with the capacitances in the pF and nF ranges, respectively, determined from $2\pi f_{max} RC = 1$, where f_{max} is the applied frequency at the arc maximum and R is the resistance obtained from the intercept of the arcs on Z' axis. Total resistance of the electrolyte is given by:

$$R_t = R_g + R_{gb} \tag{10}$$

Conductivity σ at different temperatures can be obtained using the formula:

$$\sigma = \frac{L}{S \times R} \tag{11}$$

where L and S represent the thickness and electrode area of the sample surface, respectively.

Addition of trivalent or divalent cations to ceria produces oxygen vacancies responsible for ionic conduction in these oxides [27–29] as given below in the Eqs. (12) and (13).

$$La_2O_3 \xrightarrow{2CeO_2} 2La'_{Ce} + 3O_O + V_O^{\bullet\bullet} \tag{12}$$

$$SrO \xrightarrow{CeO_2} Sr''_{Ce} + O_O + V_O^{\bullet\bullet} \tag{13}$$

where all the species are written in accordance with Kroger Vink notation.

Arrhenius plots of bulk conductivity for all the samples are shown in Fig. 5. Ionic conductivity of grains increases with increasing strontium content up to 4 mol%. For higher concentration of Sr^{2+} ($y > 0.04$) it decreases. This is probably due to the dissolution of SrO in the ceria. Dissolution of Sr^{2+} ions in lanthanum-doped ceria sample will produce a higher association enthalpy for oxygen vacancies and hence lower conductivity [29]

Arrhenius plots of grain boundary conductance of the samples are shown in Fig. 6. It can be seen from Fig. 6 that the grain boundaries conductance of the samples depends strongly on the Sr content. It may be due to scavenging effect of Sr^{2+} ions to remove siliceous impurities. It has been reported by Gerhardt et al. [30], on the basis of scanning transmission electron microscopy (STEM) combined with energy dispersive X-ray microanalysis (EDXM) and electron energy loss spectroscopy (EELS) that in yttrium doped ceria there exists an amorphous silica thick layer surrounding the grains. This layer blocks the charge carriers leading to increase in

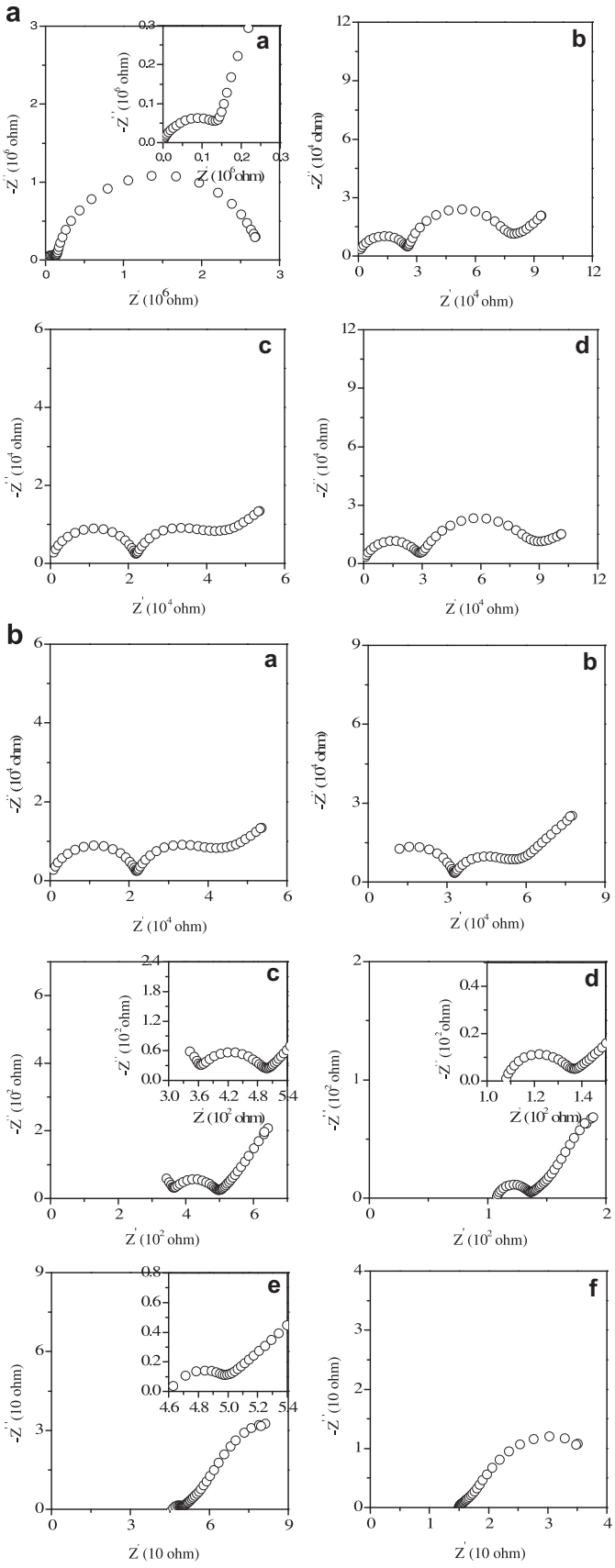

Fig. 4. (a) Impedance plots for various compositions (a) CLO15, (b) CL11S2, (c) CL7S4, (d) CL3S6 at 200 °C. (b) Impedance plots for the composition CL7S4 at (a) 200 °C, (b) 250 °C, (c) 325 °C, (d) 375 °C, (e) 425 °C and (f) 500 °C.

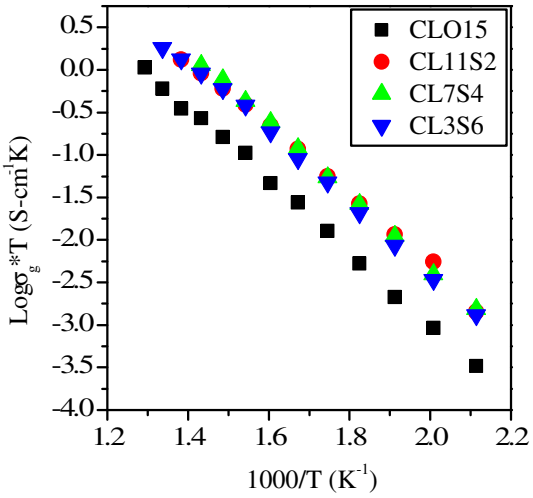

Fig. 5. log $\sigma_g \cdot T$ vs 1000/T plots of all the compositions of the system $Ce_{1-x-y}La_xSr_yO_{2-\{x/2+y\}}$.

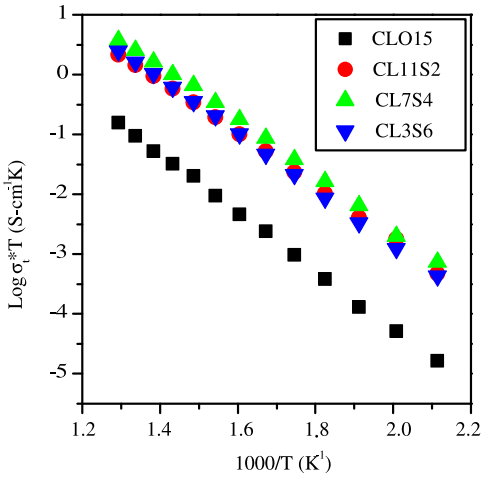

Fig. 7. log $\sigma_t \cdot T$ vs 1000/T plots of all the compositions of the system $Ce_{1-x-y}La_xSr_yO_{2-\{x/2+y\}}$.

the resistivity of the grain boundaries and hence the total resistivity. They also observed the formation of some silicate phases of yttrium. Similar silicate phases may form in the materials under present investigation. The exact compositions, morphology and distribution of these phases require analytical studies as mentioned above. Removal of silica decreases the resistivity of the grain boundaries leading to decrease in the total resistivity. They further observed that increase in ionic radius of the dopant increases its effectiveness in removing silica [31]. To confirm the scavenging effect of strontium for grain boundaries, the influence of the grain boundaries conductivity on the total conductivity is evaluated through the blocking factor (α_R) [31,32] given by

$$\alpha_R = \frac{R_{gb}}{R_g + R_{gb}} \tag{14}$$

where R_g and R_{gb} are resistance of grains and grain boundaries. α_R gives the fraction of charge carriers being blocked at the impermeable internal surface, under the measuring conditions, with respect to the total number of charge carriers in the samples. The blocking factor is minimum for the sample CL7S4 (0.21) at 375 °C.

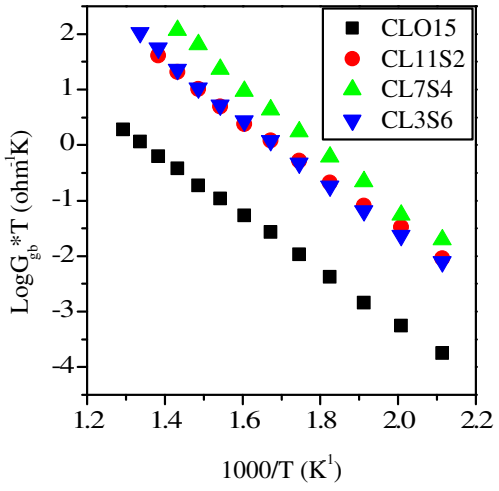

Fig. 6. log $G_{gb} \cdot T$ vs 1000/T plots of all the compositions of the system $Ce_{1-x-y}La_xSr_yO_{2-\{x/2+y\}}$.

For CLO15 its value at 375 °C is 0.90. This establishes that strontium is an effective grain boundaries scavenger.

Fig. 7 shows Arrhenius plots of the total ionic conductivity for the samples. Activation energy of conduction for the total conductivity was determined by fitting the conductivity data to the Arrhenius relation:

$$\sigma = \frac{A}{T} \exp - \frac{E}{kT} \tag{15}$$

where E is the activation energy for migration of O^{2-} ions, k is the Boltzman's constant, T is temperature in Kelvin, and A is the pre-exponential factor. Activation energies for conduction, calculated from the slopes of Arrhenius plots in the temperature range 200–500 °C are given in Table 2. It can be seen that the activation energies for conduction in co-doped ceria are less than those of ceria doped with La only.

It is found that addition of strontium improves the ionic conductivity. The composition $Ce_{0.89}La_{0.07}Sr_{0.04}O_{1.925}$ (CL7S4) shows the highest total conductivity among all the samples. Surprisingly, the ionic conductivity of $Ce_{0.89}La_{0.07}Sr_{0.04}O_{1.925}$ (CL7S4), (4.76×10^{-3} S-cm^{-1}) is about 20 times as high as that of $Ce_{0.85}La_{0.15}O_{1.925}$ (CLO15) (2.02×10^{-4} S-cm^{-1}) at 500 °C. It suggests that co-doping using an optimum ratio of La^{3+} and Sr^{2+} concentration enhances the ionic conductivity. Ionic conductivity of $Ce_{0.89}La_{0.07}Sr_{0.04}O_{1.925}$ at 600 °C (obtained by extrapolation) is more (Table 2) than the reported values of conductivity for compositions $Ce_{0.8}Sm_{0.2}O_{1.90}$ (1.20×10^{-2} S-cm^{-1}) [33] and $Ce_{0.8}Gd_{0.2}O_{1.90}$ (1.29×10^{-2} S-cm^{-1}) [34] at 600 °C.

In this study, the partial substitution of La with Sr causes four effects for the samples of $Ce_{1-x-y}La_xSr_yO_{2-\{x/2+y\}}$. Yamamura et al. [35] reported that the ordering of oxygen vacancies is suppressed

Table 2
Total conductivity (at 500 °C and 600 °C), activation energy of grains (E_g), grain-boundaries (E_{gb}) and total (E_t) conductivity of various compositions of the system $Ce_{1-x-y}La_xSr_yO_{2-\{x/2+y\}}$.

S.No.	Compositions	σ_t at 500 °C (S cm^{-1})	σ_t at 600 °C (S cm^{-1})[a]	E_g (eV)	E_{gb} (eV)	E_t (eV)
1.	$Ce_{0.85}La_{0.15}O_{1.925}$	2.02×10^{-4}	9.400×10^{-4}	0.89	0.98	0.97
2.	$Ce_{0.87}La_{0.11}Sr_{0.02}O_{1.925}$	2.79×10^{-3}	1.230×10^{-2}	0.79	0.98	0.88
3.	$Ce_{0.89}La_{0.07}Sr_{0.04}O_{1.925}$	4.75×10^{-3}	2.370×10^{-2}	0.85	1.11	0.91
4.	$Ce_{0.91}La_{0.03}Sr_{0.06}O_{1.925}$	3.19×10^{-3}	1.497×10^{-2}	0.83	1.05	0.92

[a] Data obtained by extrapolation.

due to doping. This decreases activation energy which enhances the conductivity. The number of $[La'_{Ce} - V_O^{\cdot\cdot}]^{\cdot}$ pairs decreases as twice the number of Sr^{2+} ions added. This decreases total number of associated pairs leading to enhancement of the ionic conductivity. Replacement of La^{3+} by Sr^{2+} increases the lattice strain [36] due to larger size of Sr^{2+} ion (1.26 Å) as compared to La^{3+} ion (1.16 Å). This causes the increase in association enthalpy of dopant–vacancy pairs $[\{Sr''_{Ce} - V_O^{\cdot\cdot}\}^{x}]$ [37,38]. Consequently activation energy increases and hence ionic conductivity decreases.

For compositions with $y \leq 0.04$, first two factors seem to dominate leading to an increase in ionic conductivity. For $y > 0.04$, the later two factors may start dominating causing a decrease in the ionic conductivity. $Y = 0.04$ seems to be an optimum value for molar concentration of Sr^{2+} which gives the maximum conductivity. Ionic conductivity increases also due to scavenging effect of strontium. The observed trend in the conductivity values may also be partly due to the same trend found in the average grain size of these samples mentioned earlier. Since conductivity of $Ce_{0.89}La_{0.07}Sr_{0.04}O_{1.925}$ composition is comparable to the highest conductivity reported for SDC and GDC, use of this material as a solid electrolyte for intermediate temperature solid oxide fuel cells will reduce the cost drastically. Its compatibility with other cell components, however, is necessary for its application in IT-SOFC and this need to be checked.

4. Conclusions

Samples of ceria co-doped with La and Sr, $Ce_{1-x-y}La_xSr_yO_{2-\{x/2+y\}}$ $\{(x = 0.15, y = 0), (x = 0.11, y = 0.02), (x = 0.07, y = 0.04)$ and $(x = 0.03, y = 0.06)\}$ having same number of oxygen vacancies $(x/2 + y)$ have been prepared by citrate-nitrate auto-combustion method. Density obtained by sintering at 1350 °C is more than 95% of theoretical density. It has been found that the average radius of oxygen vacancy formed by divalent and trivalent dopant cations in co-doped lanthanum and strontium systems is an important parameter for estimation of lattice parameter in this system. $Ce_{0.89}La_{0.07}Sr_{0.04}O_{1.925}$ shows higher conductivity (20 times) and lower activation energy than that of ceria doped with lanthanum only having the same number of oxygen vacancies This is also higher than the maximum value reported in the system, SDC and GDC. This increase in ionic conductivity is mainly due to decrease in grain boundary resistance.

Acknowledgement

Thanks are due to Department of Science and Technology, New Delhi for financial support.

References

[1] O. Yamamoto, Electrochim. Acta 45 (2000) 2423–2435.
[2] T.P. Chen, J.D. Wright, K. Krist, in: U. Stimming, S.C. Singhal, H. Tagawa, W. Lehnert (Eds.), SOFC V, The Electrochemical Society, Pennington, NJ, 1997, p. 69. PV 97-40.
[3] B.C.H. Steele, J. Mater. Sci. 36 (2001) 1053–1068.
[4] P. Holtappels, F.W. Poulsen, M. Mogensen, Solid State Ionics 135 (2000) 675–679.
[5] H.L. Tuller, in: H. Tuller, J. Schoonman, I. Riess (Eds.), Oxygen Ion and Mixed Conductors and Their Technological Applications, Kluwer (NATO ASI Series), Dordrecht, 2000, pp. 245–270.
[6] L. Minervini, M.O. Zacate, R.W. Grimes, Solid State Ionics 116 (1999) 339–349.
[7] T.H. Etsell, S.N. Flengas, Chem. Rev. 70 (1970) 339–376.
[8] H. Rickert, Electrochemistry of Solids. An Introduction, Springer-Verlag, Berlin, 1982.
[9] V.N. Chebotin, M.V. Perfilyev, Electrochemistry of Solid Electrolytes, Khimiya, Moscow, 1978.
[10] M.V. Perfilyev, A.K. Demin, B.L. Kuzin, A.S. Lipilin, High-temperature Electrolysis of Gases, Nauka, Moscow, 1988.
[11] V.V. Kharton, E.N. Naumovich, A.A. Vecher, J. Solid State Electrochem 3 (1999) 61–81.
[12] H. Inaba, H. Tagawa, Solid State Ionics 83 (1996) 1–16.
[13] H.J.M. Bouwmeester, A.J. Burggraaf, in: A. Burggraaf, L. Cot (Eds.), Fundamentals of Inorganic Membrane Science and Technology, Elsevier, Amsterdam, 1996, pp. 435–528.
[14] N.M. Sammes, G.A. Tompsett, H. Nafe, F. Aldinger, J. Eur. Ceram. Soc. 19 (1999) 1801–1826.
[15] M. Mogensen, N.M. Sammes, G.A. Tompsett, Solid State Ionics 129 (2000) 63–94.
[16] J.V. Herle, D. Seneviratne, A.J. McEvoy, J. Eur. Ceram. Soc. 19 (1999) 837–841.
[17] H. Yoshida, H. Deguchi, K. Miura, M. Horiuchi, Solid State Ionics 140 (2001) 191–199.
[18] H. Yoshida, T. Inagaki, K. Miura, M. Inaba, Z. Ogumi, Solid State Ionics 160 (2003) 109–116.
[19] S. Lubke, H.D. Wiemhofer, Solid State Ionics 117 (1999) 229–243.
[20] N. Kim, B.H. Kim, D. Lee, J. Power Sources 90 (2000) 139–143.
[21] F.Y. Wang, S. Chen, Q. Wang, S. Yu, S. Cheng, Catal. Today 97 (2004) 189–194.
[22] Tsung-Her Yeh, Chen-Chia Chou, Phys. Scr. T129 (2007) 303–307.
[23] S. Basu, P. Sujata Devi, H.S. Maiti, J. Mater. Res. 19 (2004) 3162–3171.
[24] N.K. Singh, P. Singh, M.K. Singh, D. Kumar, O. Parkash, Solid State Ionics 192 (2011) 431–434.
[25] S.J. Hong, A.V. Virkar, J. Am. Ceram. Soc. 78 (1995) 433–439.
[26] T.H. Yeh, W.C. Hsu, C.C. Chou, J. Phys. IV 128 (2005) 213–219.
[27] B.C.H. Steele, Solid State Ionics 180 (2009) 681–687.
[28] E. Ruiz-Trejo, A. Benitez-Rico, S. Gomez-Reynoso, M. Angeles-Rosas, J. Electrochem. Soc. 154 (4) (2007) A258–A262.
[29] N. Cioatera, V. Parvulescu, A. Rolle, R.N. Vannier, Solid State Ionics 180 (2009) 681–687.
[30] R. Gerhardt, A.S. Nowick, M.E. Mochel, I. Dumler, J. Am. Ceram. Soc. 69 (1986) 647–651.
[31] R. Gerhardt, A.S. Nowick, J. Am. Ceram. Soc. 69 (1986) 641–646.
[32] M.J. Verkerk, B.J. Middlehuis, A.J. Burggraaf, Solid State Ionics 6 (2) (1982) 159–170.
[33] G. Bryan Balazas, S. Robert Glass, Solid State Ionics 76 (1995) 155–162.
[34] Y.-P. Fu, S.-H. Chen, J.-J. Huang, Int. J. Hydrogen Energy 35 (2010) 745–752.
[35] H. Yamamura, E. Katoh, M. Ichikawa, K. Kakinuma, T. Mori, H. Haneda, Electrochemistry 68 (2000) 455–459.
[36] D.J. Kim, J. Am. Ceram. Soc. 72 (1989) 1415–1421.
[37] V. Butler, C.R.A. Catlow, B.E.F. Fender, J.H. Harding, Solid State Ionics 8 (1983) 109–113.
[38] J.A. Kilner, Solid State Ionics 8 (1983) 201–207.

Journal of Alloys and Compounds 577 (2013) 456–462

Contents lists available at SciVerse ScienceDirect

Journal of Alloys and Compounds

journal homepage: www.elsevier.com/locate/jalcom

Effect of Mg and Sr co-doping on the electrical properties of ceria-based electrolyte materials for intermediate temperature solid oxide fuel cells

Nandini Jaiswal [a], Devendra Kumar [a], Shail Upadhyay [b], Om Parkash [a,*]

[a] Department of Ceramic Engineering, Indian Institute of Technology, Banaras Hindu University, Varanasi 221 005, India
[b] Department of Applied Physics, Indian Institute of Technology, Banaras Hindu University, Varanasi 221 005, India

ARTICLE INFO

Article history:
Received 23 March 2013
Received in revised form 11 June 2013
Accepted 15 June 2013
Available online 27 June 2013

Keywords:
Ceramics
Chemical synthesis
Ionic conduction
Impedance spectroscopy
Scanning electron microscope and X-ray diffraction

ABSTRACT

Attempts have been made to synthesize a few compositions in the system $Ce_{0.90}Mg_{0.10-x}Sr_xO_{1.90}$ (x = 0.00, 0.02, 0.04 and 0.06) by citrate–nitrate auto-combustion method. XRD patterns reveal that all the samples have fluorite crystal structure similar to ceria. Microstructures of samples have been studied by scanning electron microscope. Ionic conductivity of singly doped and co-doped ceria has been investigated as a function of temperature by AC impedance spectroscopy in the temperature range 200–700 °C. Impedance plots show a significant decrease in grain boundary resistance after partial substitution of Sr in Mg-doped ceria in the intermediate temperature range. Composition with x = 0.04 shows the highest ionic conductivity (2.0×10^{-2} S/cm at 700 °C) among all the samples studied.

1. Introduction

Solid oxide electrolytes have received an increasing interest in recent years due to their excellent suitability as ionic conducting materials in solid oxide fuel cells (SOFCs). Currently yttria stabilized zirconia (YSZ) is widely used as an electrolyte due to its excellent chemical and mechanical stability. But it requires high operating temperature (1000 °C). High operating temperature can lead to complex material problems such as interfacial diffusion between electrodes and electrolyte, mechanical stress due to different thermal expansion coefficients, long term stability and high cost of interconnects and other construction materials [1]. Therefore, development of new cost effective electrolytes of high ionic conductivity in the intermediate temperature range (600–800 °C) such as lanthanum gallate and doped ceria based electrolytes have been proposed [2,3]. Among these new materials, ceria doped with aliovalent cations such as rare earth and alkaline earth ions has been widely investigated as solid electrolytes for intermediate temperature solid oxide fuel cells (IT-SOFCs) [4–6]. Substitution of aliovalent cations in ceria leads to incorporation of oxygen vacancies for charge compensation.

$$2CeO_2 \xrightarrow{M_2O_3} 2M'_{Ce} + 3O_O^{\times} + V_{\ddot{O}} \quad (1)$$

$$CeO_2 \xrightarrow{MO} M''_{Ce} + 2O_O^{\times} + V_{\ddot{O}} \quad (2)$$

where the symbols are used in accordance with Kroger Vink notation of defects. M'_{Ce} stands for a trivalent ion on Ce^{4+} site, M''_{Ce} stands for a divalent ion on Ce^{4+} site $V_{\ddot{O}}$ is oxygen vacancy with doubly positive effective charge and $O_O^{\times}$ represents that oxygen ion on O^{2-} site being neutral. Rare earth oxides have high solubility in ceria [7]. However, at high temperatures and low oxygen partial pressures, the electronic conductivity of doped ceria is considerably high. This is a problem for use of these materials as solid electrolyte for SOFC. Co-doped ceria appears to be a potential solution for this problem [8]. Gadolinium (Gd) and samarium (Sm) doped ceria have been widely used [9,10] because these have lattice parameter almost equal to un-doped ceria. Their substitution produces very small strain in the lattice which reduces activation energy for diffusion of oxide ions [11]. This has also been confirmed by atomistic computer simulation studies based on the binding energy between trivalent cations and oxygen vacancies and the corresponding lattice relaxation energy [12]. Jadhav et al. [13] studied the $Ce_{1-x}Gd_xO_{2-x/2}$ (x = 0.30) system which was synthesized by glycine–nitrate process and they found single phase formation in this system and the grain growth of sintered samples was observed to hindered with an increase in Gd content. Composition $Ce_{0.90}Gd_{0.10}O_{1.95}$ was synthesized using combustion technique by Jadhav et al. [14] and they found that the relative density of the sample was more than 90% at 1200 °C which was also confirmed by SEM analysis. The grain and grain boundary conductivity of a GDC ($Ce_{0.90}Gd_{0.10}O_{1.95}$) thin film

* Corresponding author. Tel.: +91 542 6701791; fax: +91 542 2368428.
E-mail address: oprakash.cer@itbhu.ac.in (O. Parkash).

0925-8388/$ - see front matter © 2013 Elsevier B.V. All rights reserved.
http://dx.doi.org/10.1016/j.jallcom.2013.06.094

deposited on NiO-GDC substrate has been found to be 0.103 and 0.0005 S/cm at 500 °C [15]. But Gd and Sm are very costly.

Alkaline earth oxides, such as CaO [16,17], SrO [18,19] and MgO have been investigated as dopant in CeO_2 to reduce the cost. Kim et al. [20] studied the scavenging effect of SrO. It reacts with SiO_2 and the resultant material gathers at triple point junction of the grain boundaries. This reduces the grain boundaries resistance. However, only a few reports on MgO doped ceria exist in the literature. Limited solubility of MgO in ceria has been reported to be due to difference in ionic radius of Ce^{4+} (0.97 Å) and Mg^{2+} (0.89 Å) [21]. $Ce_{0.90}Mg_{0.10}O_{1.90}$ exhibits very less conductivity (2×10^{-3} S-cm^{-1}) at 700 °C [22]. Solubility of SrO in ceria is between 5 and 10 mol% for similar reason (ionic radius of Sr^{2+} is 1.26 Å) [21]. It was considered worthwhile to investigate conductivity of ceria co-doped with one smaller cation (Mg^{2+}) and one larger cation (Sr^{2+}) as compared to Ce^{4+}. This is expected to enhance ionic conductivity.

Hence, the primary objective of the present work is to create new cost effective ceria based solid electrolyte having high ionic conductivity in the IT-range. Therefore a few compositions in the system $Ce_{0.90}Mg_{0.10-x}Sr_xO_{1.90}$ (x = 0.00, 0.02, 0.04 and 0.06) keeping total number of oxygen vacancies same have been prepared via citrate–nitrate route. Scavenging effect of Sr in Mg-doped ceria may have an advantageous effect on the overall conductivity because it can hinder the formation of a continuous and uniform Si phase along the grain boundaries.

2. Experimental

2.1. Powder synthesis

A series of compositions with the general formula $Ce_{0.90}Mg_{0.10-x}Sr_xO_{1.90}$ (x = 0.00, 0.02, 0.04 and 0.06) have been synthesized by citrate–nitrate auto-ignition method using ammonium ceric nitrate (99% purity, Qualikems), magnesium nitrate (99.5% purity, Qualigens), strontium nitrate (99.5% purity, Reidel Chemicals) and citric acid (purity 99.5%, Loba Chemie) as the starting materials. Compositions with x = 0.0, 0.02, 0.04 and 0.06 are abbreviated as CMO10, CM8S2, CM6S4 and CM4S6 respectively. Raw materials were weighted according to stoichiometric ratio and dissolved in distilled water. An aqueous solution of citric acid was added to the mixed solution of metal nitrates to achieve citrate to nitrate ratio C/N ~ 0.30 for controlled combustion [23]. The mixed solution was evaporated on a hot plate using a magnetic stirrer at approximately 200 °C. This solution became viscous and turned into a gel during heating. The gel slowly foamed and finally burnt on its own to produce light yellow ash. This ash was calcined at 800 °C in air and the calcined powder was milled using an agate mortor in air. The calcined powder was pelletized under a load of 50 kN into cylindrical pellets (diameter ~15 mm, thickness ~2.5 mm). These pellets were sintered at 1350 °C for 4 h in air. Density of the sintered pellets was determined using Archimedes principle.

2.2. Characterization

Crystal structure has been determined at room temperature by powder X-ray diffraction (Rigaku X-ray diffractometer) using Cu Kα radiation employing Ni filter in the 2θ range from 20° to 80°. The lattice constant was determined using "Unit Cell" software [24]. The crystallite size, D was estimated using Scherrer's formula:

$$D = 0.9\lambda/\beta\cos\theta \quad (3)$$

where β [in degree] is the full width at half maxima (FWHM) excluding instrumental broadening, λ is the wave length of X-rays [in nm] and θ is the Bragg angle [in degree]. β is taken for the strongest Bragg's peak corresponding to (1 1 1) reflection for all the samples. Micrographs of the fractured samples were taken with the help of a scanning electron microscope (INSPECT 50 FEI').

2.3. Electrical conductivity

Sintered pellets were polished on both the sides. Silver paint in an epoxy was applied on both the surfaces of polished pellets and pellets were heated at 700 °C for 15 min to form a smooth conducting silver layer on both the surfaces. Two probe AC impedance measurements were done on electroded pellets using a Novocontrol Alpha-A high-performance frequency analyzer. The measurements were done in the frequency and temperature range 1 Hz–1 MHz and 200–700 °C respectively in air by applying 20 mV ac signal. Data were collected using 'Win data' program and fitted to the corresponding equivalent circuit using ZView software. Total conductivity of the samples is given by following relation:

$$\sigma_t = \frac{L}{S \times R_t} \quad (4)$$

where σ_t is the total conductivity (S/cm), R_t is the total resistance (ohm), L is the thickness (cm) and S is the area (cm^2) of the sample.

3. Results and discussion

3.1. Crystal structure

To confirm the complete dissolution of dopants in CeO_2, XRD patterns were recorded for all the sintered samples. These are shown in Fig. 1. These results indicate that all the samples are single phase having cubic fluorite structure similar to CeO_2. Fig. 1 shows that 2θ values of co-doped ceria shift slightly towards lower angles with increasing Sr content. The ionic radius increases in the order $Mg^{2+} < Ce^{4+} < Sr^{2+}$. Therefore substitution of Sr^{2+} in CeO_2 in place of Mg^{2+} increases the lattice parameter. Diffraction patterns

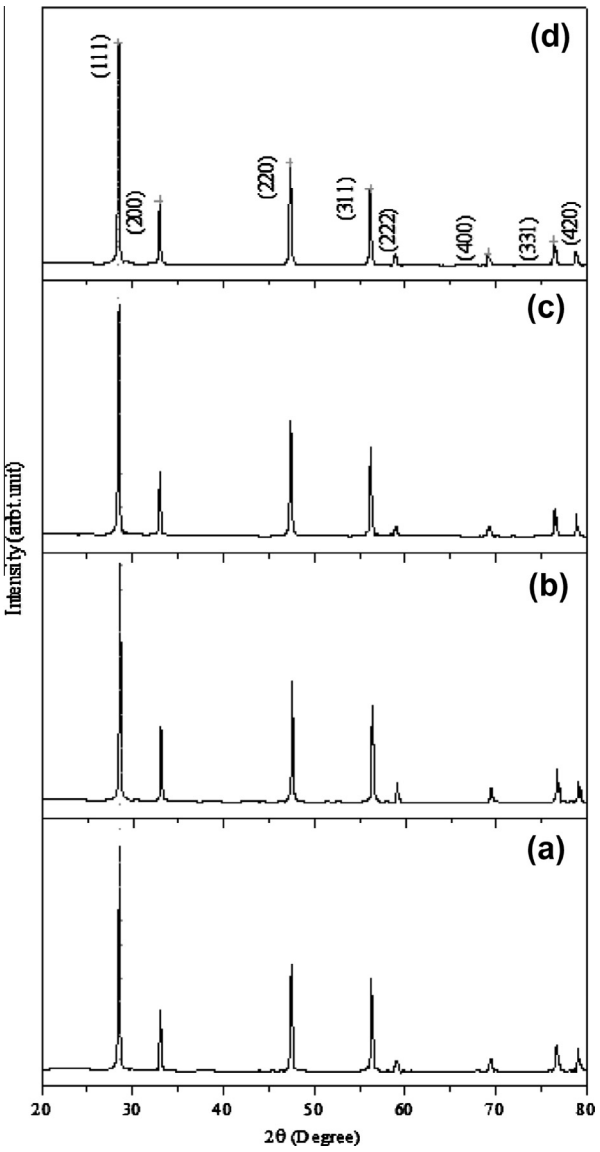

Fig. 1. Powder X-ray diffraction patterns of the system $Ce_{0.90}Mg_{0.10-x}Sr_xO_{1.90}$ for (a) x = 0.00 (b) x = 0.02 (c) x = 0.04 and (d) x = 0.06 sintered at 1350 °C.

were indexed on the basis of fluorite structure similar to CeO_2 using JCPDS file No. 43-1002.

Crystallite size of all the samples has been found to be in the range 46–60 nm. Pellets sintered at 1350 °C have densities more than 96% of the theoretical values (Table 1).

3.2. Microstructure

Fig. 2 shows micrographs of fractured surfaces of pellets sintered at 1350 °C. Micrographs show well-defined grains separated by grain boundaries. As strontium content increases, a narrowing of grain size distribution is observed. Average grain size of the compositions CMO10, CM8S2, CM6S4 and CM4S6 determined by linear intercept method is approx. 3.6, 2.1, 1.0 and 2.0 μm respectively. It is observed from Fig. 2 that average grain size decreases with increasing concentration of Sr up to $x = 0.04$ indicating that Sr acts as a grain growth inhibitor. This may be due to segregation of Sr^{2+} at grain boundaries due to elastic strain arising out of size mismatch of Sr^{2+} and Ce^{4+}. Grain boundaries are regions of high energy because of disordered present in them. Therefore, the dopant ions can be accommodated in the grain boundaries with minimum expenditure of extra energy i.e. dopants tends to segregate to the grain boundaries. This needs, however, to be confirmed using EDAX. The reason for increasing the grain size for the sample CM4S6 is not clear.

Table 1
Crystallite size, lattice parameter and % theoretical density of compositions of the system $Ce_{0.90}Mg_{0.10-x}Sr_xO_{1.90}$.

S. No.	Compositions	Crystallite size of sintered powder (nm)	Lattice parameter (Å)	% Theoretical density
1.	$Ce_{0.90}Mg_{0.10}O_{1.90}$	60	5.4099 ± 0.0002	97.5
2.	$Ce_{0.90}Mg_{0.08}Sr_{0.02}O_{1.90}$	46	5.4134 ± 0.0026	97.5
3.	$Ce_{0.90}Mg_{0.06}Sr_{0.04}O_{1.90}$	57	5.4260 ± 0.0006	96.0
4.	$Ce_{0.90}Mg_{0.04}Sr_{0.06}O_{1.90}$	57	5.4299 ± 0.0005	97.0

3.3. Electrical conductivity

Conductivity of doped-ceria has been reported to be ionic in air [25]. Therefore, the conductivity measured in air in these materials can be treated as oxide ion conductivity. Nyquist plots for all the compositions measured at 200 °C are shown in Fig. 3. Nyquist plot with an equivalent circuit for a typical composition with $x = 0.04$ at 225 °C is shown in Fig. 4. Impedance of the samples measured by two-probe method has the contributions from grains interior, grain boundaries, and electrode–electrolyte interface. These are reflected in a complex plane impedance plots by three successive circular arcs in the high frequency, intermediate frequency and low frequency range respectively. All of these arcs cannot be observed at a particular temperature due to limited frequency range available in the equipment. As temperature increases, relaxation frequency of all the polarization processes increases leading to shifting of the corresponding arcs to higher frequency. Impedance spectra were fitted to the equivalent circuits containing two parallel resistance-constant phase element subcircuits in series. The electrode/electrolyte contribution to the overall electrolyte resistance has not been considered in this work because total resistance of electrolyte is given by the sum of grains (R_g) and grain boundaries resistance (R_{gb}). Use of a simple capacitor is not sufficient to model the electrical response of the materials due to microstructural inhomogenieties of the sample. Due to this, a constant phase

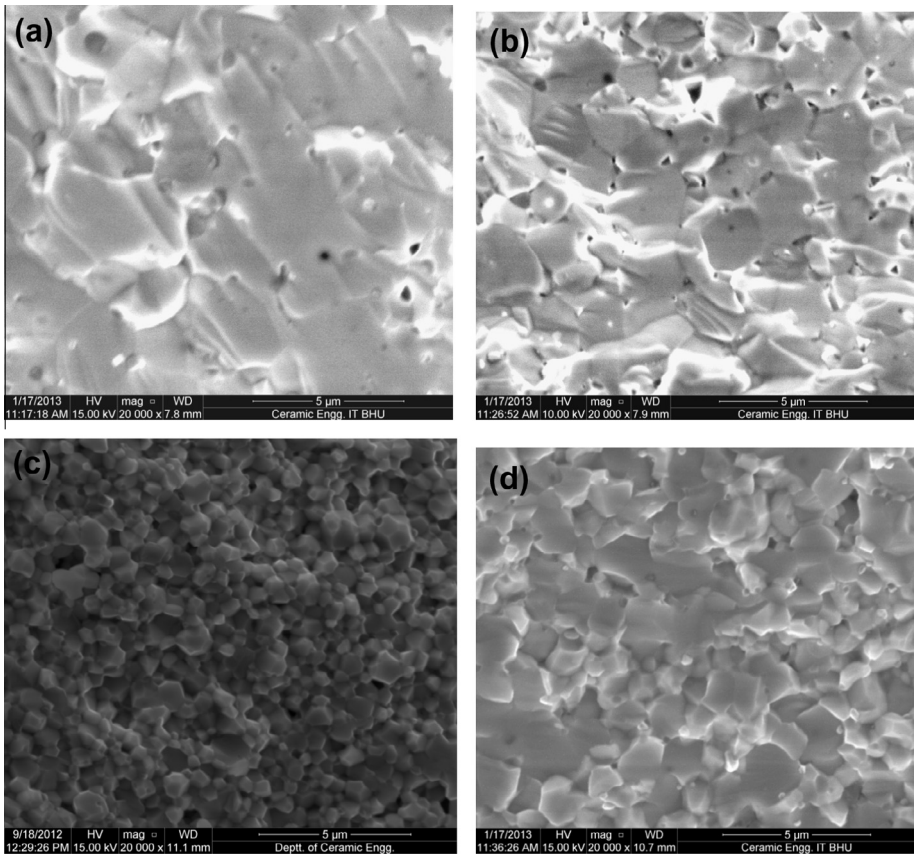

Fig. 2. Scanning electron micrograph of the fractured samples in the system $Ce_{0.90}Mg_{0.10-x}Sr_xO_{1.90}$ for (a) $x = 0.00$ (b) $x = 0.02$ (c) $x = 0.04$ and (d) $x = 0.06$.

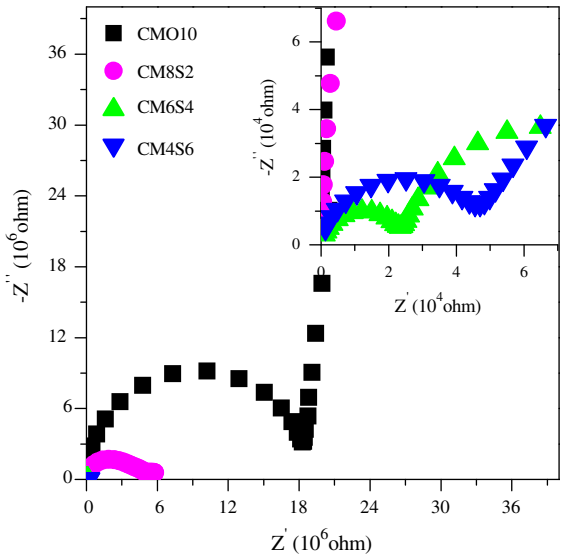

Fig. 3. Nyquist plots of the system $Ce_{0.90}Mg_{0.10-x}Sr_xO_{1.90}$ for (a) $x = 0.00$, (b) $x = 0.02$, (c) $x = 0.04$ and (d) $x = 0.06$ at 200 °C.

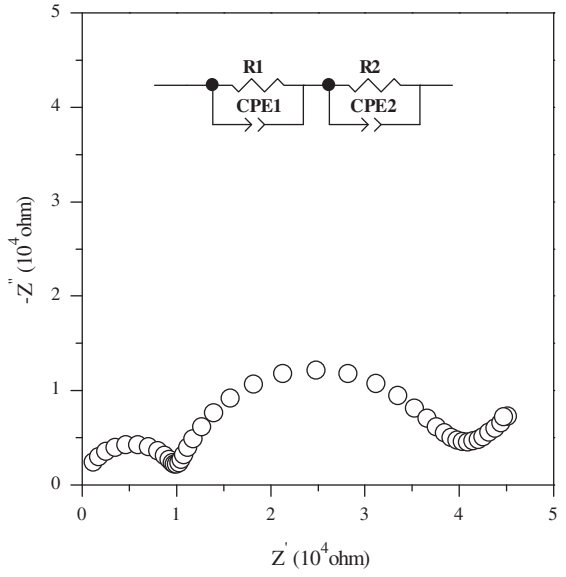

Fig. 4. Nyquist plot with an equivalent circuit for the composition $Ce_{0.90}Mg_{0.06}Sr_{0.04}O_{1.90}$ at 225 °C.

element (CPE) is used to fit the data [26]. CPE is equivalent to a distribution of capacitors in parallel. The capacitance associated with bulk and grain boundaries arcs are in the range pF and nF respectively determined from the relation $2\pi f_{max}RC = 1$, where f_{max} is the frequency at the arc maximum and R is the resistance determined from the intercept of the arc on Z' axis. From Fig. 3 it can be seen that co-doped samples have less values of grains and grain boundaries resistance than that of singly Mg-doped ceria. Further, total resistance given by $R_t = R_g + R_{gb}$ is minimum for the sample with $x = 0.04$ among all the compositions. Values of grains, R_g and grain boundaries, R_{gb} resistance can be determined by fitting the impedance plots as mentioned above.

Fig. 5 shows plots of Log $\sigma_g T$ vs. $1000/T$ for all the investigated samples. It can be seen from Fig. 5 that bulk conductivity first increases with increasing strontium content up to $x = 0.04$. The enhancement in bulk conductivity may be mainly ascribed to suppression of ordering of oxygen vacancies. This leads to an increase in the bulk conductivity due to decrease in activation energy for diffusion of O^{2-} ions [27]. At low temperatures, concentration of charge carriers is determined by the thermodynamic equilibrium between the free defects and defect associated defect pairs viz. $Mg''_{Ce} - V_{\ddot{O}}$ and $Sr''_{Ce} - V_{\ddot{O}}$ [28]. It is noted from Fig. 5 that Arrhenius plots show a change in the slope at 400 °C which is interpreted as a transition from associated defect pairs to dissociated defects. In the low temperature range, the activation energy is equal to sum of migration enthalpy and defect association enthalpy and in the high temperature region it contains only migration enthalpy. Activation energy of conduction for grains, E_g is determined by fitting the data in Fig. 5 to Arrhenius relationship:

$$\sigma_g = \frac{\sigma_{og}}{\tau} \exp\left(\frac{-E_g}{k\tau}\right) \quad (5)$$

where σ_{og} is the pre exponential factor, k is Boltzmann constant and T is absolute temperature. Values of E_g (in eV), measured at low and high temperatures are given in Table 2 for all the compositions and it is minimum for the composition CM6S4.

Specific grain boundary conductivity, σ^*_{gb} is calculated using the following equation:

$$\sigma^*_{gb} = \frac{C_g}{C_{gb}} \sigma_{gb} \quad (6)$$

where C_g and C_{gb} are measured grains and grain boundaries capacitance (in Farad) and its value can be calculated from equation:

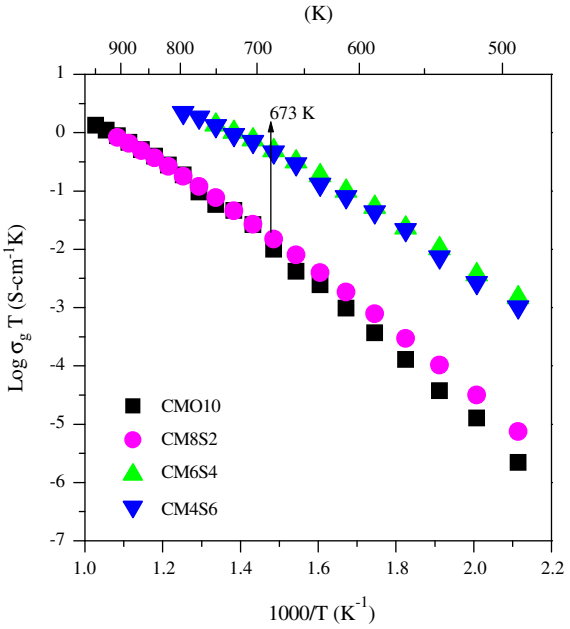

Fig. 5. Electrical conductivity of bulk vs. temperature plots for all the compositions in the system $Ce_{0.90}Mg_{0.10-x}Sr_xO_{1.90}$.

Table 2
Activation energy for conduction of grains, grain boundaries and total conductivity of various compositions in the system $Ce_{0.90}Mg_{0.10-x}Sr_xO_{1.90}$.

S. No.	Compositions	E_g (eV)		E_{gb} (eV)	E_t (eV)
		200–400 °C	400–700 °C		
1.	$Ce_{0.90}Mg_{0.10}O_{1.90}$	1.12	0.76	1.20	1.46
2.	$Ce_{0.90}Mg_{0.08}Sr_{0.02}O_{1.90}$	1.02	0.79	1.07	1.11
3.	$Ce_{0.90}Mg_{0.06}Sr_{0.04}O_{1.90}$	0.82	0.58	0.88	0.85
4.	$Ce_{0.90}Mg_{0.04}Sr_{0.06}O_{1.90}$	0.84	0.59	0.97	0.87

$$C = \frac{(RQ^{1/n})}{R} \quad (7)$$

σ_{gb} is the macroscopic grain boundaries conductivity (in S/cm) as it is calculated from R_{gb} and the macroscopic dimension of the sample (thickness/area) [29]. Specific grain boundaries conductivity exhibits a continuous increase with increasing strontium content up to $x = 0.04$ as shown in Fig. 6. This may be due to scavenging effect of strontium to remove siliceous impurities present at grain boundaries.

To confirm the scavenging effect of strontium for grain boundaries, the influence of the grain boundaries conductivity on the total conductivity is evaluated through the blocking factor [α_R] [30], defined by:

$$\alpha_R = R_{gb}/(R_g + R_{gb}) \quad (8)$$

where R_g and R_{gb} are resistance of grains and grain boundaries. α_R gives the fraction of charge carriers being blocked at the impermeable internal surface, under the measuring conditions, with respect to total number of charge carriers in the sample. The lowest blocking factor, 0.42 has been observed in the composition with $x = 0.04$ at 400 °C while it is 0.95 for the composition with $x = 0.00$. Therefore it is concluded that strontium is an effective grain boundary scavenger. It has been reported by Gerhardt et al. [31] in yttria doped ceria that there exists an amorphous silica thick layer surrounding the grains and it was confirmed on the basis of scanning transmission electron microscopy (STEM) combined with energy dispersive X-ray microanalysis (EDXM) and electron energy loss spectroscopy (EELS). The charge carriers are blocked by these layers leading to increase in the resistivity of the grain boundaries and hence the total resistivity. They observed the formation of some silicate phases of yttrium. Similar silicate phases may form in the materials under present investigation. The exact compositions, morphology and distribution of these phases require analytical studies as mentioned above. Removal of silica decreases the resistivity of the grain boundaries leading to decrease in the total resistivity. They also observed that increase in ionic radius of the dopant increases its effectiveness in removing silica [30].

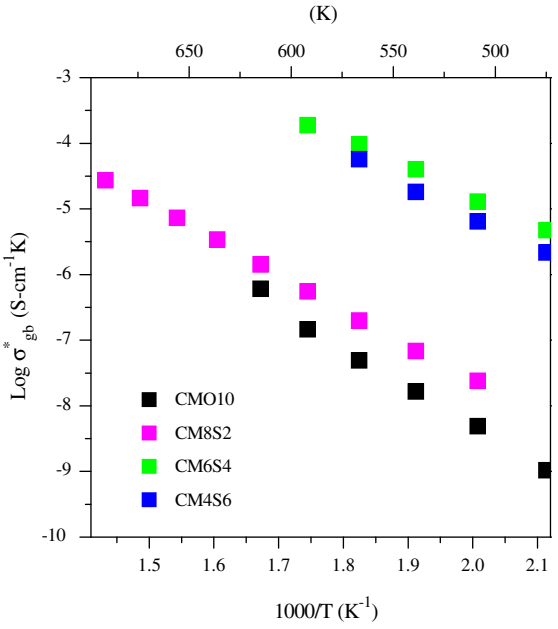

Fig. 6. Electrical conductivity of grain boundaries vs. temperature plots for all the compositions in the system $Ce_{0.90}Mg_{0.10-x}Sr_xO_{1.90}$.

It can be observed from Fig. 6 that specific grain boundaries conductivity increases with decreasing grain size. This also influences the total conductivity observed in these samples. Small grain size samples exhibits much higher grain boundary conductivity because grain boundaries area is so large that the finite amount of impurity contained in these samples is not sufficient to form a continuous and uniform glassy phase layer along grain boundaries and leaving the remaining grain boundary areas with clean grain to grain contact. Therefore, the transport of O^{2-} ions is through clean boundaries. This also accounts for the decrease in conductivity of the sample with $x = 0.06$.

Activation energy of conduction for grain boundaries, E_{gb} (in eV) for all the compositions is determined by fitting the data in Fig. 6 to Arrhenius equation and is given in Table 2. Value of E_{gb} is less for Sr co-doped samples and it is minimum for the sample, CM6S4.

Plots of Log $\sigma_t T$ vs. 1000/T for all the compositions are shown in Fig. 7. Fig. 7 shows that total conductivity increases with increase in Sr concentration up to $x = 0.04$ and decreases beyond this. Activation energy for total electrical conductivity, E_t (in eV) for all the compositions is determined by fitting the data in Fig. 7 to Arrhenius equation and is given in Table 2. Value of E_t is found to be minimum for composition CM6S4.

Values of total conductivity at 500 and 700 °C for all the compositions are given in Table 3. Composition CM6S4 has the highest ionic conductivity among all the samples. Its conductivity is about 94% higher than that of singly magnesium doped ceria. It is found that conductivity of composition CM6S4 (2.39×10^{-3} S/cm) is higher than the values reported for composition $Ce_{0.85}Ca_{0.09}Mg_{0.06-}$

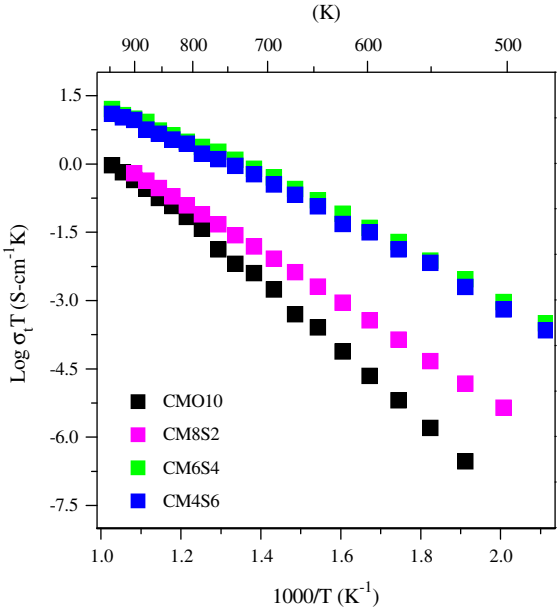

Fig. 7. Total electrical conductivity vs. temperature plots for all the compositions in the system $Ce_{0.90}Mg_{0.10-x}Sr_xO_{1.90}$.

Table 3
Total conductivity at 500 and 700 °C and configurational entropy of various compositions in the system $Ce_{0.90}Mg_{0.10-x}Sr_xO_{1.90}$.

S. No.	Compositions	σ_t at 500 °C (S cm^{-1})	σ_t at 700 °C (S cm^{-1})	Configurational entropy, S (J/K)
1.	$Ce_{0.90}Mg_{0.10}O_{1.90}$	1.71×10^{-5}	9.53×10^{-4}	2.70
2.	$Ce_{0.90}Mg_{0.08}Sr_{0.02}O_{1.90}$	6.05×10^{-5}	1.42×10^{-3}	3.12
3.	$Ce_{0.90}Mg_{0.06}Sr_{0.04}O_{1.90}$	2.40×10^{-3}	2.00×10^{-2}	3.26
4.	$Ce_{0.90}Mg_{0.04}Sr_{0.06}O_{1.90}$	1.64×10^{-3}	1.25×10^{-2}	3.26

$O_{1.85}$ under the same experimental conditions (2.09×10^{-3} S/cm [32] at 500 °C.

Fig. 8 illustrates activation energy of conduction for grains, grain boundaries and total conductivity for all the samples as a function of Sr content, x. It is seen that the activation energy of conduction for the samples change with Sr content exhibiting a minimum for CM6S4 (Table 2). The change in activation energy with composition appears to be correlated with variation in conductivity; the maximum value of total ionic conductivity corresponds to the minimum activation energy in agreement with the Meyer–Neldel compensation rule [33].

Effect of co-doping has been discussed in terms of configurational entropy [27]. It originates from random mixing of cations that suppresses the ordering of oxygen vacancies. This leads to an increase in ionic conductivity [27]. For example, assuming that the oxygen vacancy concentration is constant, the configurational entropy, S [in J/K] of $Ce_{0.90}Mg_{0.10-x}Sr_xO_{1.90}$ system is calculated using the following equation:

$$S = R\{0.9ln0.9 + (0.10 - x)\ln(0.10 - x) + xlnx \quad (9)$$

where R is the gas constant (in J/mol-K). The calculated values of configurational entropy of all the samples are given in Table 3. It is noted, from Table 3 that co-doped samples have larger values of S, and therefore have higher ionic conductivity.

Partial substitution of Mg with Sr in CeO_2 has some opposite competiting effects. Ordering of oxygen vacancies is suppressed as mentioned above. This leads to decrease in the activation energy for migration of O^{2-} ions leading to increase in the conductivity. Secondly, on substitution of Sr^{2+}, binding energy of oxygen decreases as compared to that in CeO_2. This decreases the activation energy for diffusion of oxygen ion leading to increase in conductivity. Number of associated defects pairs increases with increase in Sr^{2+} substitution. This leads to decrease in the ionic conductivity. Lattice parameter increases with increasing concentration of Sr^{2+}. This increases elastic strain in the lattice leading to an increase in the activation energy for diffusion of O^{2-} ions [11]. This causes a decrease in the conductivity. First two factors seems to dominate up to $x = 0.04$ while the later two factors starts dominating for $x > 0.04$ leading to decrease in the conductivity. Since $Ce_{0.90}Mg_{0.06}Sr_{0.04}O_{1.90}$ shows the highest conductivity among all the synthesized samples, use of this material as a solid electrolyte for intermediate temperature solid oxide fuel cells will reduce the cost drastically. Its compatibility with other cell components, however, is necessary for its application in IT-SOFC and this need to be checked.

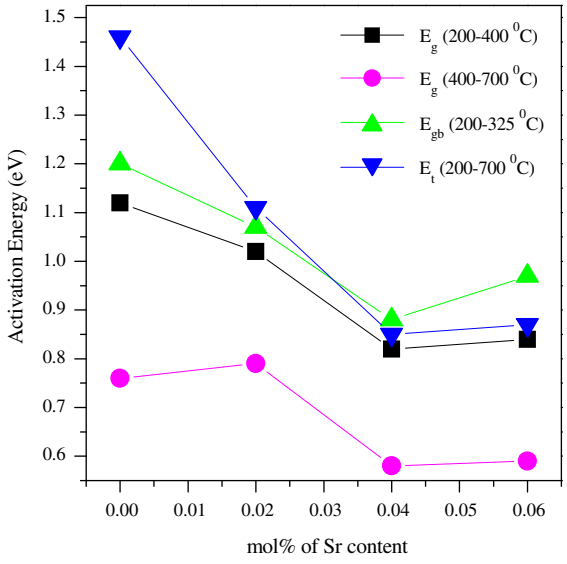

Fig. 8. Variation of activation energy for the conduction of grains, grain boundaries and total conductivity with Sr content in the system $Ce_{0.90}Mg_{0.10-x}Sr_xO_{1.90}$.

4. Conclusions

All the synthesized Mg and Sr co-doped samples have fluorite structure similar to ceria. The fine crystalline powders were sintered to >95% of theoretical density at 1350 °C. The results of ionic conductivity of magnesium and strontium co-doped ceria indicate that appropriate ratio of magnesium and strontium leads to an increase in the ionic conductivity as compared to that exhibited by ceria singly doped with Mg. Grain boundary as well as total conductivity increases due to scavenging effect of Sr and decrease in average grain size of the samples up to $x = 0.04$. Composition, CM6S4 shows higher ionic conductivity and lower activation energy than that of ceria doped with magnesium only.

Acknowledgement

Thanks are due to Department of Science and Technology, New Delhi for financial support.

References

[1] H. Tu, U. Stimming, Advances, aging mechanisms and life time in solid oxide fuel cells, J. Power Sources 127 (2004) 284–293.
[2] J.W. Fergus, Electrolytes for solid oxide fuel cells, J. Power Sources 162 (2006) 30–40.
[3] V.V. Kharton, F.M.B. Marques, A. Atkinson, Transport properties of solid oxide electrolyte ceramics, Solid State Ionics 174 (2004) 135–149.
[4] H. Inba, H. Tagawa, Ceria based solid electrolytes, Solid State Ionics 83 (1996) 1–16.
[5] B.C.H. Steele, Appraisal of $Ce_{1-y}Gd_yO_{2-y/2}$ electrolytes for IT-SOFC operation at 500 °C, Solid State Ionics 129 (2000) 95–110.
[6] S.W. Zha, C.R. Xia, G.Y. Meng, Effect of Gd (Sm) doping on properties of ceria electrolyte for solid oxide fuel cells, J. Power Sources 115 (2003) 44–48.
[7] V.V. Kharton, F.M. Figueirwdo, L. Navarro, E.N. Navarro, E.N. Naumovich, A.V. Kovalevsky, A.A. Yaremchenko, A.P. Viskup, A. Carneiro, F.M.B. Marques, J.R. Frade, Ceria based materials for solid oxide fuel cells, J. Mater. Sci. 36 (2001) 1105–1117.
[8] F.Y. Wang, B.Z. Wan, S. Cheng, Study on Gd^{3+} and Sm^{3+} co-doped ceria-based electrolytes, J. Solid State Electrochem. 9 (2005) 168–173.
[9] Z. Tianshu, P. Hing, H. Huang, J. Kilner, Ionic conductivity in the CeO_2–Gd_2O_3 system ($0.05 \leqslant Gd/Ce \leqslant 0.4$) prepared by oxalate co-precipitation, Solid State Ionics 148 (2002) 567–573.
[10] J.C.C. Abrantes, D. Perez-Coll, P. Nunez, J.R. Frdae, Electronic transport in $Ce_{0.8}Sm_{0.2}O_{1.9}$ ceramics under reducing conditions, Electrochem. Acta 48 (2003) 2761–2766.
[11] D.-J. Kim, Lattice parameters, ionic conductivities, and solubility limits in fluorite-structure MO_2 oxide [M = Hf^{4+}, Zr^{4+}, Ce^{4+}, Th^{4+}, U^{4+}] solid solutions, J. Am. Ceram. Soc. 72 (1989) 1415–1421.
[12] L. Minervini, M.O. Zacate, R.W. Grimes, Defect cluster formation in M_2O_3-doped CeO_2, Solid State Ionics 116 (1999) 339–349.
[13] L.D. Jadhav, M.G. Chourashiya, A.P. Jamale, A.U. Chavan, S.P. Patil, Synthesis and characterization of nanocrystalline $Ce_{1-x}Gd_xO_{2-x/2}$ ($x = 0.30$) solid solutions, J. Alloys Comp. 506 (2010) 739–744.
[14] L.D. Jadhav, M.G. Chourashiya, K.M. Subhedar, A.K. Tyagi, J.Y. Patil, Synthesis of Gd doped ceria by combustion technique, J. Alloys Comp. 470 (2009) 383–386.
[15] M.G. Chourashiya, L.D. Jadhav, Synthesis and characterization of 10%Gd doped ceria (GDC) deposited on NiO-GDC anode grade ceramic as half cell for IT-SOFCs, Int. J. Hydrogen Energy 36 (2011) 14984–14995.
[16] H. Arai, T. Kunisaki, Y. Shimizu, T. Seiyama, Electrical properties of calcia-doped ceria with oxygen ion conduction, Solid State Ionics 20 (1986) 241–248.
[17] J.E. Garnier, R.N. Blumenthal, R.J. Panlener, R.K. Sharma, A thermodynamic study on CaO-doped nonstoichiometric cerium dioxide, J. Phys. Chem. Solid 37 (1976) 368–378.
[18] H. Yahiro, K. Eguchi, H. Arai, Ionic conduction and microstructure of the ceria-strontia system, Solid State Ionics 21 (1986) 37–47.
[19] R.N. Blumenthal, J.E. Garnier, The electrical conductivity and thermodynamic behavior of SrO-doped nonstoichiometric cerium dioxide, Solid State Chem. 16 (1976) 21–34.
[20] Y.H. Cho, P.S. Cho, G. Auchterlonie, D.K. Kim, J.H. Lee, D.Y. Kim, et al., Enhancement of grain-boundary conduction in gadolinia-doped ceria by the scavenging of highly resistive siliceous phase, Acta Mater. 55 (2007) 4807.
[21] H. Yahiro et al., Electrical properties and microstructure in the system ceria–alkaline earth oxide, J. Mater. Sci. 23 (1988) 1036–1041.

[22] F.-Y. Wang et al., Study on Gd and Mg co-doped ceria electrolyte for intermediate temperature solid oxide fuel cells, Catal. Today 97 (2004). 189–194.S.
[23] S. Basu, P. Sujatha Devi, H.S. Maiti, Synthesis and properties of nanocrystalline ceria powders, J. Mater. Res. 19 (2004) 3162–3171.
[24] T.J.B. Holland, S.A.T. Redfern, Unit cell refinement from powder diffraction data: the use of regression diagnostics, Mineral. Maga. 61 (1997) 65–77.
[25] H. Inaba, H. Tagawa, Ceria based electrolytes, Solid State Ionics 83 (1996) 1–16.
[26] G.M. Christie, F.P.F. Berkel, Microstructure-ionic conductivity relationships in ceria-gadolinia electrolytes, Solid State Ionics 83 (1996) 17–27.
[27] H. Yamamura, E. Katoh, M. Ichikawa, K. Kakinuma, T. Mori, H. Haneda, Multiple Doping effect on the electrical conductivity in the $(Ce_{1-x-y}La_xM_y)O^{2-}$·DELTA. (M = Ca, Sr) system, Electrochemistry 68 (2000) 455–459.
[28] N. Cioatera, V. Parvulescu, A. Rolle, R.N. Vannier, Effect of strontium addition on europium-doped ceria properties, Solid State Ionics 180 (2009) 681–687.
[29] M. Buchi Suresh, Johnson Roy, The effect of strontium doping on densification and electrical properties of $Ce_{0.8}Gd_{0.20}O_{2-\delta}$ electrolyte for IT-SOFC application, Ionics 18 (2012) 291–297.
[30] R. Gerhardt, A.S. Nowick, Grain-boundary effect in ceria doped with trivalent cations: I, electrical measurements, J. Am. Ceram. Soc. 69 (1986) 641–646.
[31] R. Gerhardt, A.S. Nowick, M.E. Mochel, I. Dumler, Grain boundary effect in ceria doped with trivalent cations: II microstructure and microanalysis, J. Am. Ceram. Soc. 69 (1986) 647–651.
[32] Om Parkash, Namrata Singh, Nitish Kumar Singh, Devendra Kumar, Preparartion and characterization of ceria co-doped with Ca and Mg, Solid State Ionics 212 (2012) 100–105.
[33] W. Meyer, H. Neldel, A relation between the energy constant and the quantity constant in the conductivity temperature formula for oxide semiconductors, ZTechPhys 18 (1937) 588.

Available online at www.sciencedirect.com

ScienceDirect

journal homepage: www.elsevier.com/locate/he

Sm^{3+} and Sr^{2+} co-doped ceria prepared by citrate–nitrate auto-combustion method

Nandini Jaiswal [a], Shail Upadhyay [b], Devendra Kumar [a], Om Parkash [a,*]

[a] Department of Ceramic Engineering, Indian Institute of Technology, (Banaras Hindu University), Varanasi 221005, Uttar Pradesh, India

[b] Department of Applied Physics, Indian Institute of Technology, (Banaras Hindu University), Varanasi 221005, Uttar Pradesh, India

ARTICLE INFO

Article history:
Received 16 May 2013
Received in revised form
25 September 2013
Accepted 2 October 2013
Available online 12 November 2013

Keywords:
Citrate–nitrate process
Doped ceria
Co-doping effect
Ionic conductivity
IT-SOFC

ABSTRACT

A few compositions in the system, $Ce_{1-x-y}Sm_xSr_yO_{1.90}$ have been prepared by citrate–nitrate auto-combustion method. X-ray diffraction data show that all the compositions are solid solution having cubic fluorite structure. Density of the samples sintered at 1350 °C has been found to be more than 95% of the theoretical value. Surface morphology has been studied by scanning electron microscope. AC impedance spectroscopy measurements have been carried out to study the grains, grain boundaries and total ionic conductivity of the samples in the temperature range 200–600 °C. The composition, $Ce_{0.82}Sm_{0.16}Sr_{0.02}O_{1.90}$ shows the maximum conductivity i.e. 2.67×10^{-2} S-cm^{-1} at 600 °C among all the compositions investigated. This is about two times higher than that of $Ce_{0.80}Sm_{0.20}O_{1.90}$.

1. Introduction

Solid oxide fuel cells (SOFCs) are the energy converters. These convert chemical energy into electrical energy. Solid oxide electrolytes with high ionic conductivity at low temperatures are the key component for SOFCs. So far, yttria-stabilized zirconia (YSZ) has been used as a solid electrolyte due to its high ionic conductivity and stability at high temperature. Sealing of SOFC units using YSZ requires high temperature. This puts constraint of using expensive materials for various components of the cells. To be cost effective, it is necessary therefore, to develop solid electrolytes having high ionic conductivity at lower temperatures (500–700 °C).

Gd-doped ceria (GDC) and Sm-doped ceria (SDC) are considered to be the most promising low temperature solid electrolytes for such applications because of their high oxide ion conductivity in the temperature range 500–700 °C [1]. But both Gd and Sm are very costly. In order to reduce the cost and to identify new systems, a co-doping approach has been introduced [2–4]. Van Herle et al. [4] found that ceria doped with two or more cations showed significantly higher ionic conductivity than the best singly doped ceria. Co-doping suppresses the ordering of oxygen vacancies leading to increase in ionic conductivity [5]. $Ce_{1-x-y}Sm_xCa_yO_{2-\delta}$ [6] and $Ce_{0.85}Gd_{0.10}Mg_{0.05}O_{2-\delta}$ [7] are well known examples. Yifeng et al. [8] studied the electrical properties of $Ce_{0.80}Sm_{20-x}Mg_xO_{2-\delta}$ samples synthesized by solid state reaction at

* *Corresponding author*. Department of Ceramic Engineering, Indian Institute of Technology, (Banaras Hindu University), Varanasi 221005, Uttar Pradesh, India. Tel.: +91 542 6701791; fax: +91 542 2368428.
E-mail address: oprakash.cer@itbhu.ac.in (O. Parkash).
0360-3199/$ – see front matter Copyright © 2013, Hydrogen Energy Publications, LLC. Published by Elsevier Ltd. All rights reserved.
http://dx.doi.org/10.1016/j.ijhydene.2013.10.009

1550 °C. They found that co-doping with appropriate ratio of samarium and magnesium leads to an improvement in the ionic conductivity.

Readily available alkaline earth oxides are more cost effective than the rare earth oxides. The most distinguished feature of using alkaline earth ions as co-dopants is the scavenging of siliceous impurities present at grain boundaries thereby, increasing the grain boundaries conductivity. Previous results have shown that MgO, CaO, SrO and BaO are effective grain boundaries scavengers for Gd-doped ceria (GDC) [9–12]. Many attempts have been made to increase the grain boundary conductivity by adding various additives such as Al_2O_3, Fe_2O_3, and alkaline earth oxides [12–17]. Kim et al. [12] studied the scavenging effect of SrO. It reacts with SiO_2 and the resultant material gathers at triple point junction of the grain boundaries. This reduces the grain boundaries resistance.

Cioatera et al. [18] studied the effect of strontium addition on the properties of europium-doped ceria. They found a significant diminution of grain boundaries resistance after partial substitution of europium and strontium. Some other examples of strontium co-doped electrolytes are $Ce_{0.80-x}Sm_{0.20}Sr_xO_{2-\delta}$ [19], (1 − x)SDC − xSr [20] $Ce_{0.80-x}Gd_{0.20}Sr_xO_{2-\delta}$ [21], and $Ce_{0.80}Y_{0.20-x}Sr_xO_{2-\delta}$ [22]. In all these compositions studied the concentration of oxygen vacancies changes with concentration of Sr^{2+} (x).

$Ce_{1-x-y}Sm_xSr_yO_{1.90}$ compositions have been studied in the present work because Sm has been proved to be a very good dopant that produces the highest conductivity and also decreases the reducibility of ceria [23]. Nanocrystalline $Ce_{0.80}Sm_{0.20}O_{1.90}$, $Ce_{0.82}Sm_{0.16}Sr_{0.02}O_{1.90}$, $Ce_{0.84}Sm_{0.12}Sr_{0.04}O_{1.90}$ and $Ce_{0.91}Sm_{0.08}Sr_{0.06}O_{1.90}$ having same number of total oxygen vacancies have been prepared using citrate–nitrate auto-combustion method. The purpose of the study is to investigate the effect of co-doping of Sr^{2+} only on the ionic conductivity keeping total number of oxygen vacancies constant. A significant improvement of the electrical conductivity is observed by co-doping ceria with samarium and strontium.

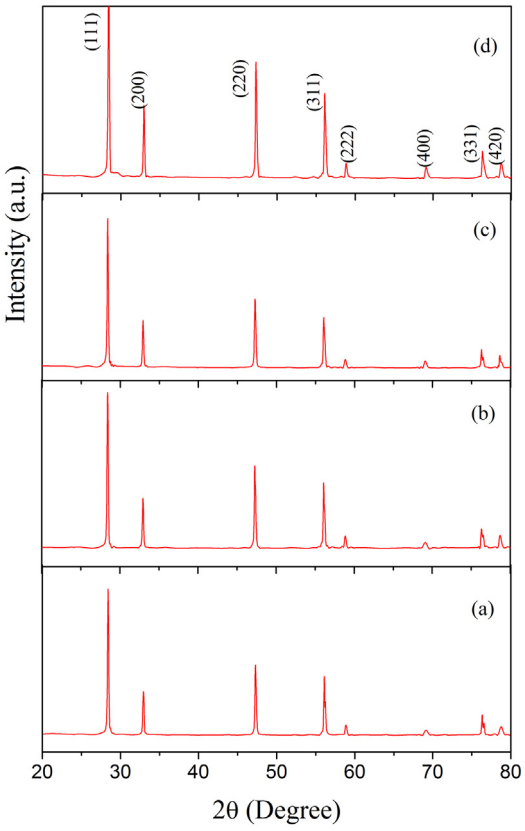

Fig. 1 – Powder X-ray diffraction patterns of $Ce_{1-x-y}Sm_xSr_yO_{1.90}$ system with (a) x = 0.20, y = 0.00 (b) x = 0.16, y = 0.02 (c) x = 0.12, y = 0.04 (d) x = 0.08, y = 0.06 sintered at 1350 °C.

2. Experimental

2.1. Powder synthesis

A series of solid solutions having the general formula, $Ce_{1-x-y}Sm_xSr_yO_{1.90}$ where (x = 0.20, y = 0), (x = 0.16, y = 0.02), (x = 0.12, y = 0.04) and (x = 0.08, y = 0.06) were synthesized by citrate–nitrate auto-combustion method using ammonium ceric nitrate (purity 99.00%), samarium nitrate (99.90%), strontium nitrate (99.50%), and citric acid (99.90%). The raw materials were weighted according to stoichiometric ratio and thoroughly mixed in distilled water. An aqueous solution of citric acid was added to this mixed solution of nitrates to achieve citrate–nitrate molar ratio ~0.3 [24]. This ratio is used to ensure smooth combustion. The solution was heated on a hot plate at 200 °C until excess free water evaporated. This was followed by ignition. Within a few seconds, the combustion reaction completed giving a yellow porous ash. The ash was calcined at 800 °C in air for 4 h. The calcined powders were dry-pressed uniaxially into pellets (about 15 mm in diameter and 1.5 mm thickness) by applying 50 kN load. The pellets were sintered at 1350 °C for 4 h and furnace cooled.

2.2. Structural and morphology characterization

Powder X-ray diffraction patterns were recorded using a Rigaku high resolution powder X-ray diffractometer employing Cu $K_{\alpha 1}$ radiation using Ni-filter at room temperature. Data were collected in the 2θ range from 20 to 80°. Lattice parameter was determined using nonlinear least square fitting program 'Unit Cell' [25]. The crystallite size, D was estimated using Scherrer's formula

$$D = 0.9\lambda/\beta\cos\theta \quad (1)$$

where β is the full width at half maxima (FWHM) excluding instrumental broadening, λ is the wavelength of X-rays and θ is the Bragg angle. β is taken for the strongest Bragg's peak corresponding to (111) reflection for all the samples. Density of the sintered pellets was determined using Archimedes method. Theoretical density can be calculated using following formula:

$$\text{Theoretical Density} = \frac{n \times \text{moleculer wt. of sample}}{N \times a^3} \quad (2)$$

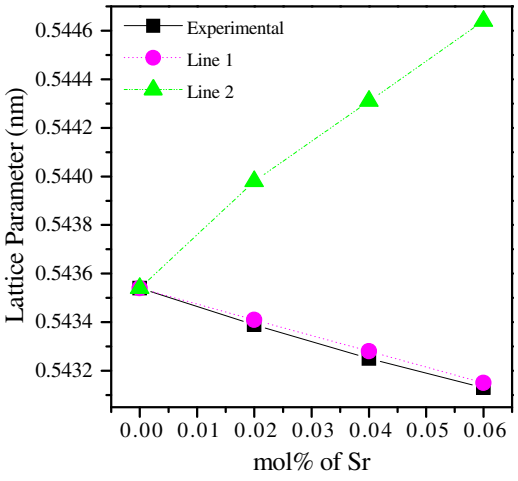

Fig. 2 – Variation of lattice parameter of the system $Ce_{1-x-y}Sm_xSr_yO_{1.90}$ with Sr content.

where n is the number of atoms per unit cell, N is the Avogadro's number and a is the lattice parameter.

Microstructure and chemical compositions were studied using a FEI QUANTA Scanning Electron Microscope. The sintered pellet was polished using emery papers of grade 1/0, 2/0, 3/0, and 4/0 (Sia, Switzerland) followed by polishing on a velvet cloth using diamond paste of grade1/4-OS-475 (HIFIN). Then these were etched thermally at 1250 °C and coated with gold for microstructural analysis.

2.3. *Electrical characterization*

Impedance measurements were made using Novocontrol Alpha-A High Performance Frequency Analyzer in air in the temperature range 200–600 °C and frequency range 1 Hz–1 MHz with an ac signal of 20 mV. Data were collected using 'Win data' program and fitted to the corresponding equivalent circuits using 'ZView' software. Ag-paste was brushed on both the surfaces of the pellet, followed by annealing at 700 °C (for 15 min) producing conducting layers on both the sides of the pellets.

3. Results and discussion

3.1. *Phase analysis*

Powder X-ray diffraction patterns of all the samples sintered at 1350 °C are shown in Fig. 1. These show the formation of a single phase solid solution having cubic fluorite structure similar to that of CeO_2. XRD patterns for the calcined powders are similar to those obtained after sintering except that the diffraction lines become sharper as shown in Fig. 1. This is due to grain growth occurring during sintering. Fig. 1 also shows that the 2θ values of co-doped ceria shift slightly toward lower angles with increasing Sr content. Diffraction patterns were indexed on the basis of structure of CeO_2 using JCPDS file no. 43-1002. Lattice parameter was determined using "Unit Cell" software. Lattice parameter increases from 5.4019 ± 0.0016 Å [26] to 5.4354 ± 0.0009 Å on addition of 20 mol% Sm to CeO_2 because ionic radius of Sm^{3+} (1.079 Å) is larger than that of Ce^{4+} (0.97 Å) [27]. Lattice parameter decreases with increasing Sr content as shown in Fig. 2 because total dopant content decreases to maintain the molar concentration of oxygen vacancies same in all the samples. Average crystallite size, D, of powders, calculated by Scherrer's formula from X-ray line broadening is in the range 55–67 nm (Table 1). Pellets sintered at 1350 °C have density more than 95% of the theoretical values (Table 1).

Lattice parameter of co-doped ceria was calculated using following equation given by hard sphere model [28]:

$$a = \frac{4}{\sqrt{3}}(r_{anion} + r_{cation}) \tag{3}$$

where r_{anion} and r_{cation} are radii of the dopant cations and anions, respectively. The equation of the system $Ce_{1-x-y}Sm_xSr_yO_{1.90}$ can be written as

$$xSmO_{1.5} + ySrO + (1-x-y)CeO_2 = xSm'_{Ce} + ySr''_{Ce} + \left(\frac{x}{2}+y\right)V_{\ddot{O}} + (1-x-y)Ce_{Ce} + [2-(x/2+y)]O_O \tag{4}$$

where all the species are written in accordance with Kroger Vink notation of defects. Radii of cations and anions can be calculated using the following Eqns. (5) and (6):

$$r_{cation} = xr_{Sm} + yr_{Sr} + (1-x-y)r_{Ce} \tag{5}$$

$$r_{anion} = \left(\frac{2-\left(\frac{x}{2}+y\right)}{2}\right)r_o + \left(\frac{\frac{x}{2}+y}{2}\right)r_{\bar{V}_O} \tag{6}$$

where r_{Ce}, r_{Sr}, r_{Sm}, $r_{V_{\ddot{O}}}$ and r_o are radii of Ce^{4+}, Sr^{2+}, Sm^{3+}, oxygen vacancy and oxygen ion respectively. From Eqs. (5) and (6), lattice parameter of the system, $Ce_{1-x-y}Sm_xSr_yO_{1.90}$ can be written as

$$a = \frac{4}{\sqrt{3}}\left[xr_{Sm} + yr_{Sr} + (1-x-y)r_{Ce} + \left(\frac{1.9}{2}\right)r_o + \left(\frac{x}{4}r_{V_{\ddot{O}_t}} + 0.5yr_{V_{\ddot{O}_d}}\right)\right] \tag{7}$$

where $V_{\ddot{O}_d}$ and $V_{\ddot{O}_t}$ are radii of oxygen vacancy produced by

Table 1 – Crystallite size, lattice parameter and % theoretical density of all the compositions in the system $Ce_{1-x-y}Sm_xSr_yO_{1.90}$.

S. No.	Compositions	Crystallite size of sintered powder (nm)	Lattice parameter (Å)	% of theoretical density
1.	$Ce_{0.80}Sm_{0.20}O_{1.90}$	66	5.4354 ± 0.0009	97.0
2.	$Ce_{0.82}Sm_{0.16}Sr_{0.02}O_{1.90}$	58	5.4339 ± 0.0006	98.0
3.	$Ce_{0.84}Sm_{0.12}Sr_{0.04}O_{1.90}$	67	5.4325 ± 0.0007	95.0
4.	$Ce_{0.91}Sm_{0.08}Sr_{0.06}O_{1.90}$	55	5.4313 ± 0.0005	95.0

divalent and trivalent cations respectively in the system $Ce_{1-x-y}Sm_xSr_yO_{1.90}$. Lattice parameter of pure ceria calculated by using this model is 5.473 Å while the actual value is 5.414 Å from JCPDS file. Therefore, a multiplication factor of 0.9892 was taken in above equation. Now Eq. (7) can be written as

$$a = 0.9892 \times \frac{4}{\sqrt{3}}\left[xr_{Sm} + yr_{Sr} + (1-x-y)r_{Ce} + \left(\frac{1.9}{2}\right)r_o + \left(\frac{x}{4}r_{V_{\dot{O}_t}} + 0.5yr_{V_{\dot{O}_d}}\right)\right] \quad (8)$$

Equations for lattice parameter of $Ce_{0.90}Sr_{0.10}O_{1.90}$ and $Ce_{0.80}Sm_{0.20}O_{1.90}$ can be written as

(a) $Ce_{0.90}Sr_{0.10}O_{1.90}$

$$a = 0.9892 \times \frac{4}{\sqrt{3}}\left[0.90r_{Ce} + 0.10r_{Sr} + \left(\frac{1.9}{2}\right)r_o + \left(\frac{0.10}{2}\right)r_{V_{\dot{O}}}\right] \quad (9)$$

(b) $Ce_{0.80}Sm_{0.20}O_{1.90}$

$$a = 0.9892 \times \frac{4}{\sqrt{3}}\left[0.80r_{Ce} + 0.20r_{Sm} + \left(\frac{1.9}{2}\right)r_o + \left(\frac{0.1}{2}\right)r_{V_{\dot{O}}}\right] \quad (10)$$

By using lattice parameter of $Ce_{0.80}Sm_{0.20}O_{1.90}$ (5.4354 Å from Table 1) and $Ce_{0.90}Sr_{0.10}O_{1.90}$ (5.429 Å) from Ref. [29], radius of oxygen vacancy for trivalent, $r_{V_{\dot{O}_t}}$ and divalent dopant cation, $r_{V_{\dot{O}_d}}$ can be calculated using Eqs. (9) and (10). Values of $r_{V_{\dot{O}_t}}$ and $r_{V_{\dot{O}_d}}$ are found to be 1.149 Å and 0.9498 Å respectively. Theoretical value of lattice parameter has been obtained by substituting the values of $r_{V_{\dot{O}_t}}$ and $r_{V_{\dot{O}_d}}$ in Eq. (8). For comparing the results, the theoretical and experimental data of lattice parameter is plotted in Fig. 2 (Line-1). It can be seen from Fig. 2 that the theoretical values are in good agreement with the experimental values.

In the second case when the same values of $r_{V_{\dot{O}_t}}$ and $r_{V_{\dot{O}_d}}$ are substituted in Eq. (8) i.e. average oxygen vacancy radius 1.16 [19] then the results are different from the experimental values (as shown in Fig. 2 by Line-2).

From this investigation it is clear that the radius of oxygen vacancy formed by trivalent and divalent dopants are different and it is larger for trivalent dopant. Larger radius of oxygen vacancy produces wider conducting channel for easy migration of oxygen ions leading to increase in the conductivity.

3.2. *Microstructure analysis*

Fig. 3(a)–(d) shows micrographs of thermally etched samples at 1250 °C. Surface scanning electron micrographs of sintered

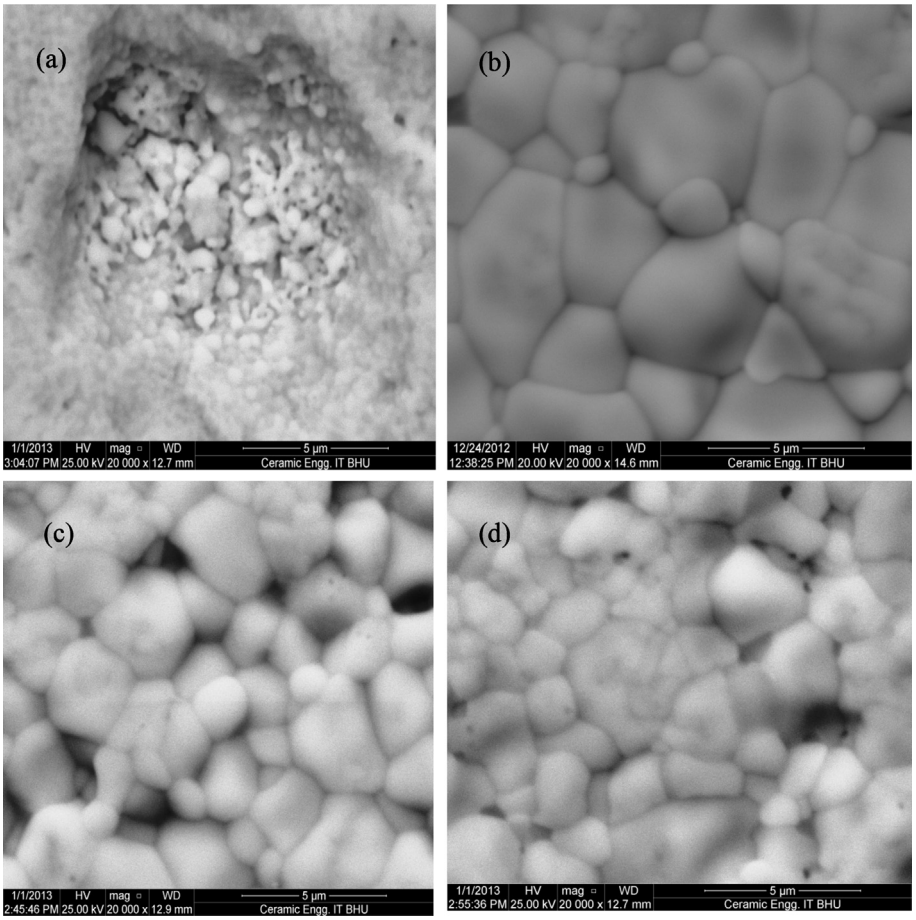

Fig. 3 – Scanning electron micrographs of the system $Ce_{1-x-y}Sm_xSr_yO_{1.90}$ (a) $x = 0.20$, $y = 0.00$ (b) $x = 0.16$, $y = 0.02$ (c) $x = 0.12$, $y = 0.04$ (d) $x = 0.08$, $y = 0.06$ sintered at 1350 °C.

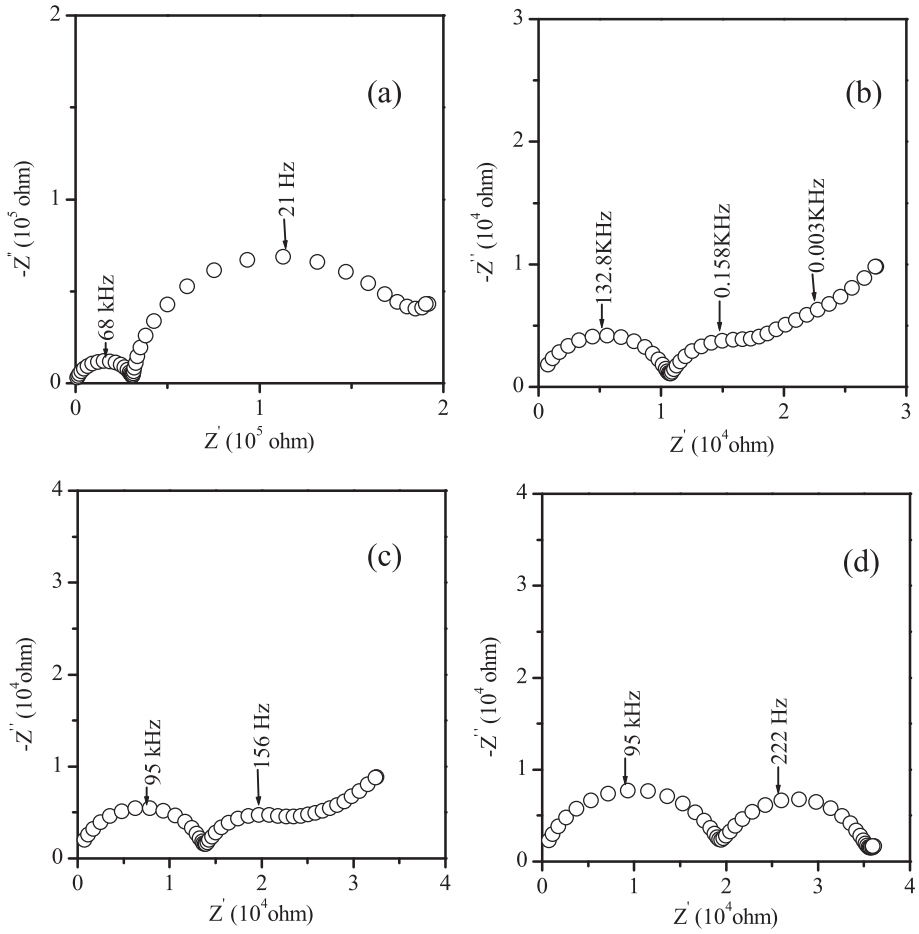

Fig. 4 – Nyquist plots for $Ce_{1-x-y}Sm_xSr_yO_{1.90}$ system with (a) $x = 0.20$, $y = 0.00$ (b) $x = 0.18$, $y = 0.02$ (c) $x = 0.12$, $y = 0.04$ (d) $x = 0.08$, $y = 0.06$ at 200 °C.

pellets show a dense structure and well defined grains separated by grain boundaries. All the samples show grains of varying size. Image of all the samples except for the sample with $x = 0.20$, $y = 0.00$ indicates presence of faceted grains. It is interesting to notice that average grain size increases on substitution of strontium. The average grain size for the samples with ($x = 0.20$, $y = 0.00$), ($x = 0.16$, $y = 0.02$), ($x = 0.12$, $y = 0.04$) and ($x = 0.08$, $y = 0.06$) is found to be 1.0, 3.0, 2.4 and 2.3 μm respectively. Substitution of Sr influences the grain size of the samples. Composition with $y = 0.02$ exhibits large grain size.

3.3. *Impedance analysis*

Impedance analysis is a powerful tool to study the electrical properties of solid electrolytes. AC impedance spectroscopy employs the frequency domain to separate the contributions of the bulk, grain boundaries and electrode resistance to the total observed resistance in polycrystalline ceramics. Experimentally one can determine the real part (Z') and the imaginary part (Z'') of impedance, Z by applying a small sinusoidal voltage across the sample and measuring the amplitude and phase angle, θ, of the current. Z'' vs. Z' plots known as Nyquist plot are drawn. Conductivity of doped-ceria has been reported to be ionic in air [30]. In the present study all the measurements have been made below 800 °C in air.

Nyquist plots of all the samples in air at 200 °C are shown in Fig. 4. Fig. 5 shows Nyquist plot with an equivalent circuit for the sample $Ce_{0.82}Sm_{0.16}Sr_{0.02}O_{1.90}$ at 250 °C. It is noted that two complete depressed circular arcs and a part of the third arc are clearly seen in Fig. 4. The arc in the highest frequency range corresponds to contribution of grains, arc in intermediate frequency corresponds to contribution of grain boundaries and the arc in lowest frequencies gives contribution of electrode/specimen interface polarization to the total polarization. At intermediate temperatures, only arcs due to contribution of the grain boundaries and electrodes are observed. The time constant τ, for a dielectric relaxation process decreases as the temperature increases. This leads to shifting of arcs toward higher frequencies. Therefore, all the arcs are not observed at all temperatures in the limited range of frequency of the equipment. Impedance spectra were fitted to the equivalent circuits containing two parallel resistance-constant phase element subcircuits in series. The electrode/electrolyte contribution to the overall electrolyte resistance has not been considered in this work because total resistance of electrolyte is given by the sum of grains (R_g) and grain boundaries resistance (R_{gb}). Use of a simple capacitor is not

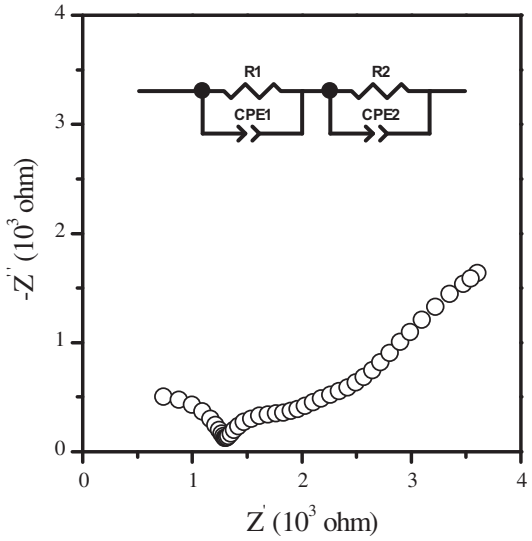

Fig. 5 – Nyquist plot with an equivalent circuit for the composition $Ce_{0.82}Sm_{0.16}Sr_{0.02}O_{1.90}$ at 250 °C.

sufficient to model the electrical response of the materials due to microstructural inhomogenieties of the sample. Therefore, a constant phase element (CPE) is used to fit the data [31]. CPE is equivalent to a distribution of capacitors in parallel. The capacitance of CPE can be given as

$$C = \frac{(RQ^{1/n})}{R} \tag{11}$$

Here R is resistance, and Q is pseudocapacitance. Here the exponent $n = 1$ for pure capacitor.

It is clear from the Fig. 4 that arcs corresponding to grain boundaries of co-doped samples are much smaller than those of the samples singly doped with Sm. This clearly shows that doping with Sr has significant influence on the grain boundaries contribution. It is observed from Fig. 4 that total resistance is minimum for the composition with $x = 0.16$ and $y = 0.02$.

Arcs due to grains and grain boundaries are associated with capacitances in the pF and nF range respectively, determined from the relation $2\pi f_{max}RC = 1$, where f_{max} is the applied frequency at the arc maximum, R is the resistance and C is the capacitance of a particular contribution.

3.4. *Electrical conductivity*

Total ionic conductivity σ is calculated from the resistance of grains (R_g) and grain boundaries (R_{gb}), using following Eqns. (12) and (13):

$$R_t = R_g + R_{gb} \tag{12}$$

$$\sigma = \frac{L}{A \times R_t} \tag{13}$$

where, L and A represent the thickness and area of the sample respectively. R_t is the total resistance.

Specific grain boundary conductivity, σ^*_{gb} is calculated using following equation:

$$\sigma^*_{gb} = \frac{C_g}{C_{gb}}\,\sigma_{gb} \tag{14}$$

where C_g and C_{gb} are measured grain and grain boundary capacitance. σ_{gb} is the macroscopic grain boundaries conductivity as it is calculated from R_{gb} and the macroscopic dimension of the sample (thickness/area) [32].

Figs. 6–8 show Arrhenius plots for the bulk conductivity, σ_g, specific grain boundaries conductivity, σ^*_{gb}, and total conductivity, σ_t, of the system $Ce_{1-x-y}Sm_xSr_yO_{1.90}$. It can be seen from Fig. 6 that bulk conductivity is nearly same for all the compositions. On the contrary, σ^*_{gb} and σ_t are higher for Sr co-doped samples (Figs. 7 and 8).

It can be seen from Fig. 7 that grain boundaries conductivity is higher for Sr co-doped samples and it is maximum for composition $Ce_{0.82}Sm_{0.16}Sr_{0.02}O_{1.90}$. This may be due to scavenging effect of Sr. To confirm this point, the grain boundary blocking factor, α_R, has been calculated [33,34]. It is defined as

$$\alpha_R = \frac{R_{gb}}{R_g + R_{gb}} \tag{15}$$

where R_g and R_{gb} are the resistance of grains and grain boundaries.

Values of α_R for all the samples are given in Table 3. The blocking factor at 400 °C for the sample, $Ce_{0.82}Sm_{0.16}Sr_{0.02}O_{1.90}$ is 0.19 while composition $Ce_{0.80}Sm_{0.20}O_{1.90}$ has value 0.66. By analogy with previously reported results in zirconia and ceria ceramics [35] it can be deduced that Sr has also reacted with Si present at the grain boundaries to produce a different silicate phase that segregates at the triple points. At these positions the presence of these secondary phases has less effect on the conductivity than a Si phase at the grain boundaries.

It has been reported by Gerhardt et al. [36], on the basis of scanning transmission electron microscopy (STEM) combined with energy dispersive X-ray microanalysis (EDXM) and electron energy loss spectroscopy (EELS) that in yttrium doped ceria there exists an amorphous silica thick layer surrounding the grains. This layer blocks the charge carriers leading to increase in the resistivity of the grain boundaries and hence the total resistivity. They also observed the formation of some

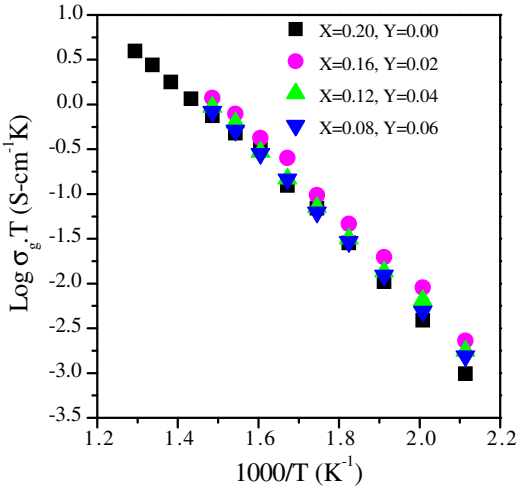

Fig. 6 – Arrhenius plots for bulk conductivity of all the compositions in the system $Ce_{1-x-y}Sm_xSr_yO_{1.90}$.

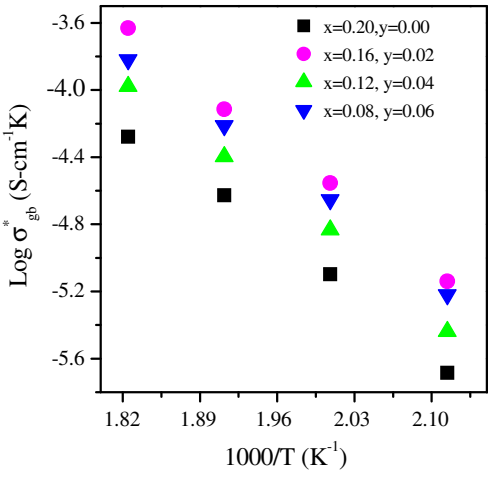

Fig. 7 – Arrhenius plots for specific grain boundary of all the compositions in the system $Ce_{1-x-y}Sm_xSr_yO_{1.90}$.

silicate phases of yttrium. Similar silicate phases may form in the materials under present investigation. The exact compositions, morphology and distribution of these phases require analytical studies as mentioned above. Removal of silica decreases the resistivity of the grain boundaries leading to decrease in the total resistivity. They further observed that increase in ionic radius of the dopant increases its effectiveness in removing silica [33].

Activation energy of conduction for the total conductivity was determined by using Arrhenius relationship for thermally activated conduction

$$\sigma_t = \frac{\sigma_0}{T}\exp -\frac{E_a}{kT} \quad (16)$$

where E_a is the activation energy for migration of O^{2-} ions, k is the Boltzmann's constant, T is temperature in K, and σ_0 is the pre-exponential factor.

From Fig. 8, it is clear that there is a change in slope at 500 °C, which indicates that mechanism of conduction at low (200–500 °C) temperature and high (500–600 °C) temperature is different. Activation energy at low temperature is the sum of association enthalpy (ΔH_a) of the defects pairs such as $Sm'_{Ce} - V_{\ddot{O}}$ /$Sr''_{Ce} - V_{\ddot{O}}$ and migration enthalpy (ΔH_m) of oxygen ions [37]. In the low temperature regime oxygen vacancies form associated defect pairs with dopant ions. As the temperature increases the dissociation of these defect pairs takes place and oxygen vacancies are free to take part in conduction. Arrhenius plots for total ionic conductivity have been fitted by two straight lines. Association enthalpy ΔH_a, is determined from the difference between activation energy at low and high temperature. The association enthalpy obtained is less being in the range 0.17–0.33 eV. These values are similar from the value ($\Delta H_a = 0.28$ eV) obtained by Arachi et al. [38] in 8 mol% YSZ. Fig. 9 illustrates the activation energy of conduction for grains, grain boundaries and for total conductivity measured above and below 500 °C as a function of Sr content, y. It is seen that the activation energy for the samples change with Sr content exhibiting a minimum for $x + y = 0.18$ (Table 2). The change in activation energy with composition appears to be correlated with variation in conductivity the maximum value of total ionic conductivity corresponds to the minimum activation energy in agreement with the Meyer–Neldel compensation rule [39].

Value of total conductivity at 300 °C for composition with $x = 0.16$, $y = 0.02$ is 1.024×10^{-4} S-cm^{-1}. This is much higher than the value 5.68×10^{-5} S-cm^{-1} reported for $Ce_{0.8}Sm_{0.18}Ca_{0.02}O_{1.90}$ sintered at 1300 °C by Maure et al. [40]. Composition, $Ce_{0.82}Sm_{0.16}Sr_{0.02}O_{1.90}$ shows the highest conductivity 2.67×10^{-2} S-cm^{-1} at 600 °C, (Table 3) which is about 50% more than the compared to Sm singly doped sample $Ce_{0.80}Sm_{0.20}O_{1.90}$. Its conductivity is higher than the highest value reported for 0.94SDC–0.06Sr [20] (~1.13×10^{-2} S-cm^{-1}), $Ce_{0.70}Sm_{0.2}Ca_{0.10}O_{2-\delta}$ (2.58×10^{-2} S-cm^{-1}) [41], $Ce_{0.8-x}Sm_{0.10}Mg_{0.10}O_{2-\delta}$ (1.491×10^{-2} S-cm^{-1}) [8] and $Ce_{0.8}Sm_{0.10}Y_{0.10}O_{1.9}$ (1.44×10^{-2} S-cm^{-1}) [42] at 600 °C.

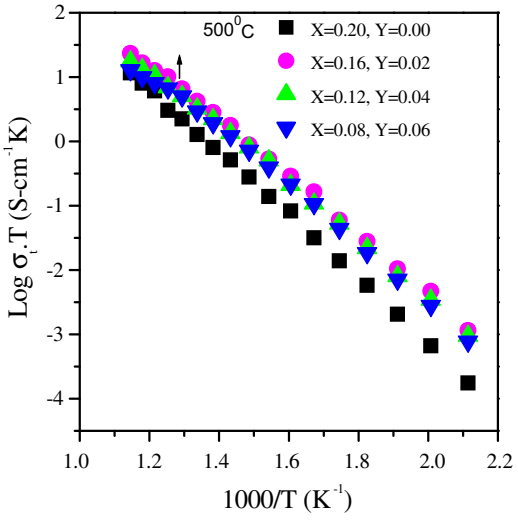

Fig. 8 – Arrhenius plots for total conductivity of all the compositions in the system $Ce_{1-x-y}Sm_xSr_yO_{1.90}$.

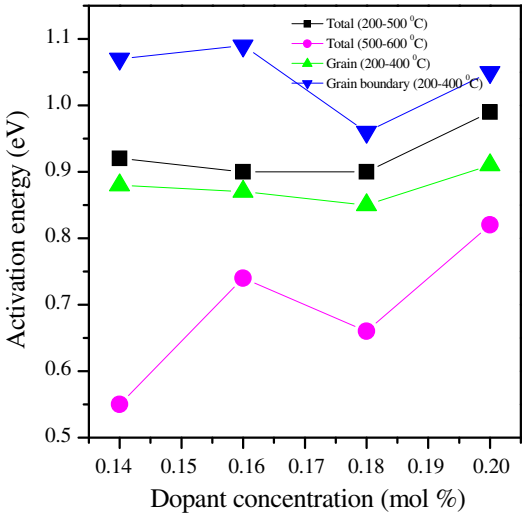

Fig. 9 – Plots of variation of activation energy with dopant concentration for $Ce_{1-x-y}Sm_xSr_yO_{1.90}$ system.

Table 2 – Activation energy of grains (E_g), grain boundaries (E_{gb}) and total (E_t) conductivity of all the compositions in the system $Ce_{1-x-y}Sm_xSr_yO_{1.90}$.

S.No.	Compositions	E_g (eV) (200–400 °C)	E_{gb} (eV) (200–400 °C)	E_t (eV)	
				(200–500 °C)	(500–600 °C)
1.	$Ce_{0.80}Sm_{0.20}O_{1.90}$	0.91	1.04	0.99	0.82
2.	$Ce_{0.82}Sm_{0.16}Sr_{0.02}O_{1.90}$	0.85	0.99	0.90	0.66
3.	$Ce_{0.84}Sm_{0.12}Sr_{0.04}O_{1.90}$	0.87	1.08	0.91	0.74
4.	$Ce_{0.91}Sm_{0.08}Sr_{0.06}O_{1.90}$	0.88	1.08	0.92	0.59

In the present study, for the $Ce_{1-x-y}Sm_xSr_yO_{1.90}$ system, partial substitution of Sr causes four effects. According to Yamamura et al. [5] co-doping suppresses the ordering of oxygen vacancies. Suppressing ordering of oxygen vacancies decreases the activation energy. This leads to increase in the ionic conductivity. The number of $[Sm'_{Ce} - V_{\ddot{O}}]^{\cdot}$ pairs decreases as twice the number of Sr^{2+} ions added. This decreases total number of associated pairs leading to enhancement of the ionic conductivity. According to Kim [43], a large lattice mismatch between the host and dopant cations produces strain in the lattice. It decreases the conductivity leading to increase in activation energy. The lattice mismatch between Sr^{2+}(1.26 Å) and Ce^{4+} (0.97 Å) is more than that between Sm^{3+} (1.079 Å) and Ce^{4+} (0.97 Å). This causes an increase in association enthalpy of dopant–vacancy pairs $[\{Sr''_{Ce} - V_{\ddot{O}}\}^{x}]$ [44,45]. Consequently activation energy increases and hence ionic conductivity decreases. The first two factors dominate upto $y \leq 0.02$ and the last two factors starts dominating for $y > 0.02$. Sr^{2+} content upto 2 mol% seems to be an optimum value for molar concentration of Sr^{2+} which gives the maximum conductivity. Ionic conductivity increases also due to scavenging effect of strontium. The observed trend in the conductivity values may also be partly due to the same trend found in the average grain size of these samples mentioned earlier. Since conductivity of $Ce_{0.82}Sm_{0.16}Sr_{0.02}O_{1.90}$ sample is comparable to the highest conductivity reported for some electrolytes as mentioned above, use of this material as a solid electrolyte for intermediate temperature solid oxide fuel cells will reduce the cost drastically. Its compatibility with other cell components and thermodynamic stability, however, is necessary for its application in IT-SOFC and this needs to be studied.

4. Conclusions

Co-doped ceria samples with nominal compositions $Ce_{1-x-y}Sm_xSr_yO_{1.90}$ where ($x = 0.20$, $y = 0$), ($x = 0.16$, $y = 0.02$), ($x = 0.12$, $y = 0.04$) and ($x = 0.08$, $y = 0.06$) have been synthesized and studied to compare the conductivity ceria doped singly with Sm. Single phase solid solution has formed in all the samples. More than 95% of theoretical density has been achieved by sintering at 1350 °C. Grain boundaries as well as total conductivity increases due to scavenging effect of strontium. Composition $Ce_{0.82}Sm_{0.16}Sr_{0.02}O_{1.90}$ shows the highest ionic conductivity among all the samples studied. This makes it a potential candidate as a solid electrolyte for IT-SOFCs being much cheaper than ceria doped singly with Sm.

Table 3 – Grain boundary blocking factor at 400 °C and total ionic conductivity of all the compositions in the system $Ce_{1-x-y}Sm_xSr_yO_{1.90}$ at temperatures 600 °C.

S. No.	Compositions	α_{gb} at 400 °C	σ_t at 600 °C (S cm^{-1})
1.	$Ce_{0.80}Sm_{0.20}O_{1.90}$	0.66	1.33×10^{-2}
2.	$Ce_{0.82}Sm_{0.16}Sr_{0.02}O_{1.90}$	0.19	2.67×10^{-2}
3.	$Ce_{0.84}Sm_{0.12}Sr_{0.04}O_{1.90}$	0.21	2.00×10^{-2}
4.	$Ce_{0.91}Sm_{0.08}Sr_{0.06}O_{1.90}$	0.15	1.47×10^{-2}

Acknowledgment

Thanks are due to Department of Science and Technology, New Delhi for financial support.

REFERENCES

[1] Minh NQ, Takahashi T. Science and technology of ceramic fuel cells. New York: Elsevier Science BV; 1995.
[2] Omar S, Wachsman ED, Nino JC. A co-doping approach towards enhanced ionic conductivity in fluorite based electrolytes. Solid State Ionics 2006;177:3199–203.
[3] Sha X, Lü Z, Huang X, Miao J, Ding Z, Xin X, et al. Study on La and Y co-doped ceria-based electrolyte materials. J Alloys Compd 2007;428:59–64.
[4] Van Herle J, Senevirante D, McEvoy AJ. Lanthanide co-doping of solid electrolytes: AC conductivity behavior. J Eur Ceramic Soc 1999;19:837–41.
[5] Yamamura H, Katoh E, Ichikawa M, Kakinuma K, Mori T, Haneda H. Multiple doping effect on the electrical conductivity in the $(Ce_{1-x-y}La_xM_y)O_\delta$ (M = Ca, Sr) system. Electrochemistry 2000;68:455–9.
[6] Mori T, Drennan J, Lee JH, Li JG, Ikegami T. Oxide ionic conductivity and microstructures of Sm- or La-doped CeO_2-based systems. Solid State Ionics 2002;154–155:461–6.
[7] Wang FY, Chen SY, Wang Q, Yu SX, Cheng SF. Study on Gd and Mg co-doped ceria electrolyte for intermediate temperature solid oxide fuel cells. Catal Today 2004;97:189–94.
[8] Yifeng Zheng, Haitao Gu, Han Chen, Ling Gao, Xiaofang Zhu, Lucun Guo. Effect of Sm and Mg co-doping on the properties of ceria based electrolyte materials for IT-SOFCs. Mater Res Bull 2009;44:775–9.
[9] Cho PS, Cho YH, Park SY, Lee SB, Kim DY, Park HM, et al. Grain-boundary conduction in gadolinia-doped ceria: the effect of SrO addition. J Electrochem Soc 2009;156:B339–44.
[10] Cho PS, Lee SB, Cho YH, Kim DY, Park HM, Lee JH. Effect of CaO concentration on enhancement of grain-boundary

conduction in gadolinia-doped ceria. J Power Sources 2008;183:518–23.
[11] Park SY, Cho PS, Lee SB, Park HM, Lee JH. Improved of grain boundary conduction in SiO_2-doped GDC by BaO addition. J Electrochem Soc 2009;156:B891–6.
[12] Cho YH, Cho PS, Auchterlonie G, Kim DK, Lee JH, Kim DY, et al. Enhancement of grain-boundary conduction in gadolinia-doped ceria by the scavenging of highly resistive siliceous phase. Acta Mater 2007;55:4807–15.
[13] Jasinski Piotr, Petrovsky Vladimir, Suzuki Toshio, Anderson Harlan U. Impedance studies of diffusion phenomena and ionic and electronic conductivity of cerium oxide. J Electrochem Soc 2005;152:J27–32.
[14] Verkerk MJ, Winnubst AJA, Burggraaf AJ. Effect of impurities on sintering and conductivity of yttria-stabilized zirconia. J Mater Sci 1992;17:3113–22.
[15] Zhang TS, Ma J, Kong LB, Chan SH, Hing P, Kilner JA. Iron oxide as an effective sintering aid and a grain boundary scavenger for ceria-based electrolytes. Solid State Ionics 2004;167:203–7.
[16] Kim DK, Cho PS, Lee JH, Kim DY, Park HM, Auchterlonie G, et al. Mitigation of highly resistive grain-boundary phase in gadolinia-doped ceria by the addition of SrO. Electrochem Solid State Lett 2007;10:B91–5.
[17] Cho PS, Lee SB, Kim DS, Lee JH, Kim DY, Park HM. Improvement of grain-boundary conduction in gadolinia doped ceria by the addition of CaO. Electrochem Solid State Lett 2006;9:A399–402.
[18] Cioatera N, Parvulescu V, Rolle A, Vannier RN. Effect of strontium addition on europium-doped ceria properties. Solid State Ionics 2009;180:681–7.
[19] Yeh Tsung-Her, Chou Chen-Chia. Ionic conductivity investigation in samarium and strontium co-doped ceria system. Phys Scr 2007;T129:303–7.
[20] Zheng Yifeng, He Shoucheng, Ge Lin, Zhou Ming, Chen Han, Guo Lucan. Effect of Sr on Sm-doped ceria electrolyte. Int J Hydrogen Energy 2011;36:5128–35.
[21] Ramesh S, Vishnuvardhan Reddy C. Electrical properties of co-doped ceria electrolyte $Ce_{0.80-x}Gd_{0.20}Sr_xO_{2-\delta}$ ($0 \le x \le 0.10$). Acta Phys Pol 2009;A115:909–13.
[22] Zheng Yifeng, Wu Liqiang, Gu Haitao, Gao Ling, Chen Han, Guo Lucun. The effect of Sr on the properties of Y-doped ceria electrolyte for IT-SOFCs. J Alloys Compd 2009;486:586–9.
[23] Mogensen M, Sammes NM, Tompsett GA. Physical, chemical and electrochemical properties of pure and doped ceria. Solid State Ionics 2000;129:63–94.
[24] Basu S, Sujata Devi P, Maiti HS. Synthesis and properties of nanocrystalline ceria powders. J Mater Res 2004;19:3162–71.
[25] Holland TJB, Redfern SAT. Unit cell refinement from powder diffraction data: the use of regression diagnostics. Mineral Mag 1997;61:65–77.
[26] Singh NK, Singh P, Singh MK, Kumar D, Parkash O. Auto-combustion synthesis and properties of $Ce_{0.85}Gd_{0.15}O_{1.925}$ for intermediate temperature solid oxide fuel cells electrolyte. Solid State Ionics 2011;192:431–4.
[27] Shannon RD. Revised effective ionic radii in halides and chalcogenides. Acta Crystallogr 1976;A32:751–67.
[28] Hong SJ, Virkar AV. Lattice parameters and densities of rare-earth oxide doped ceria electrolytes. J Am Ceram Soc 1995;78:433–9.
[29] Jaiswal Nandini, Kumar Singh Nitish, Kumar Devendra, Parkash Om. Effect of strontium (Sr) doping on the conductivity of ceria. J Power Sources 2012;202:78–84.
[30] Inaba H, Tagawa H. Ceria based electrolytes. Solid State Ionics 1996;83:1–16.
[31] Christie GM, Berkel FPF. Microstructure-ionic conductivity relationships in ceria-gadolinia electrolytes. Solid State Ionics 1996;83:17–27.
[32] Macdonald JR. Impedance spectroscopy. NewYork: Wiley; 1987.
[33] Gerhardt R, Nowick AS. Grain-boundary effect in ceria doped with trivalent cations: I. Electrical measurements. J Am Ceram Soc 1986;69:641–6.
[34] Verkerk MJ, Middlehuis BJ, Burggraaf AJ. Effect of grain boundaries on the conductivity of high purity ZrO_2-Y_2O_3 ceramics. Solid State Ionics 1982;6:159–70.
[35] Guo Xin, Waser Rainer. Electrical properties of the grain boundaries of oxygen ion conductors: acceptor-doped zirconia and ceria. Prog Mater Sci 2006;51:151–210.
[36] Gerhardt R, Nowick AS, Mochel ME, Dumler I. J Am Ceram Soc 1986;69:647–51.
[37] Zhang TS, Ma J, Kong LB, Chan SH, Kilner JA. Aging behavior and ionic conductivity of ceria-based ceramics: a comparative study. Solid State Ionics 2004;170:209–17.
[38] Arachi Y, Sakai H, Yamamoto O, Takeda Y, Imanishai N. Electrical conductivity of the ZrO_2-Ln_2O_3 systems. Solid State Ionics 1999;121:133–9.
[39] Meyer W, Neldel H. A relation between the energy constant and the quantity constant in the conductivity temperature formula for oxide semiconductors. ZTechPhys 1937;18:588.
[40] Moure A, et al. A significant improving of the processing and electric properties of CeO_2 co-doped with Ca and Sm by mechanosynthesis. J Power Sources 2011;196:10543–9.
[41] Ramesh S, Prashanth Kumar V, Kistaiah P, Vishnuvardhan Reddy C. Preparation, characterization and thermo electrical properties of co-doped $Ce_{0.8-x}Sm_{0.2}Ca_xO_{2-\delta}$ materials. Solid State Ionics 2010;181:86–91.
[42] Sha Xueqing, Lu Zhe, Huanga Xiqiang, Miaoa Jipeng, Jia Li, Xin Xianshuang, et al. Preparation and properties of rare earth co-doped $Ce_{0.8}Sm_{0.20-x}Y_xO_{2-\delta}$ electrolyte materials for SOFC. J Alloys Compd 2006;424:315–21.
[43] Kim DJ. Lattice parameters, ionic conductivities, and solubility limits in fluorite structure MO_2 oxide ($M = Hf^{4+}$, Zr^{4+}, Ce^{4+}, Th^{4+}, U^{4+}) solid solutions. J Am Ceram Soc 1989;72:1415–21.
[44] Butler V, Catlow CRA, Fender BEF, Harding JH. Dopant ion radius and ionic conductivity in cerium oxide. Solid State Ionics 1983;8:109–13.
[45] Kilner JA. Fast ion transport in solids. Solid State Ionics 1983;8:201–7.

Ionics
DOI 10.1007/s11581-013-0936-8

ORIGINAL PAPER

Ceria co-doped with calcium (Ca) and strontium (Sr): a potential candidate as a solid electrolyte for intermediate temperature solid oxide fuel cells

Nandini Jaiswal · Devendra Kumar · Shail Upadhyay · Om Parkash

Received: 22 March 2013 / Revised: 5 June 2013 / Accepted: 6 June 2013

Abstract Co-doped samples of $Ce_{0.95-x}Ca_{0.05}Sr_xO_{1.95-x}$, where ($x$=0.00, 0.01, 0.02, and 0.03), have been prepared by auto-combustion method and characterized to explore their use as a solid electrolyte for intermediate temperature solid oxide fuel cells (IT-SOFCs). Crystal structure, microstructure, and ionic conductivity have been characterized by X-ray diffraction, scanning electron microscopy, and impedance spectroscopy, respectively. All the compositions have been found to be single phase. Results show that the samples co-doped with Ca and Sr exhibit higher ionic conductivity than the samples singly doped with Ca in the intermediate temperature range. $Ce_{0.93}Ca_{0.05}Sr_{0.02}O_{2-\delta}$ exhibits maximum conductivity among all the compositions. This may be a potential candidate as a solid electrolyte for IT-SOFCs.

Keywords Doped ceria electrolyte · Co-doping effect · Ionic conductivity · Solid oxide fuel cells

Introduction

Oxide ion conductors are used in oxygen sensors [1–3] and solid oxide fuel cells (SOFCs) [4–6]. Among these applications, SOFCs are especially developed as a clean and efficient power source for generating electricity from a variety of fuels. For the commercial application of the SOFCs for the distributed heat-power co-generation, an operation temperature in the range 500–700 °C is highly desirable. This is in view of the cost effectiveness because inexpensive stainless steel may be used for this purpose.

Doped ceria electrolytes have attracted great interest in recent years because of their potential as a solid electrolyte for intermediate temperature solid oxide fuel cells (IT-SOFCs) application [7]. In CeO_2, temperature facilitates movement of oxygen ions through oxygen vacancies which are produced in the oxygen sublattice to neutralize the deficiency of charge created by lower valent dopant cations. Doped ceria oxides show much higher ionic conductivity at relatively low temperatures (500–700 °C) as compared with yttria-stabilized zirconia. These have been extensively studied as the most promising electrolyte materials for IT-SOFCs. Among the various ceria compositions investigated so far [8–19], Gd- and Sm-doped ceria (GDC and SDC) are considered as the most suitable low-temperature solid electrolytes for IT-SOFCs application. Both Gd_2O_3 and Sm_2O_3, however, are very costly. Therefore, there is an increasing interest to develop new cost-effective ceria-based electrolytes.

Ceria doped with alkaline earth oxides such as CaO [20, 21] and SrO [22, 23] has been studied extensively. Electrical conductivity of CaO- and SrO-doped ceria is much higher than that of undoped ceria. The highest conductivity was found in the composition $Ce_{0.90}Ca_{0.10}O_{1.90}$ by Shing et al. [24] which is ~10^{-3} S cm^{-1} at 600 °C. Yamashita et al. [25] found that the composition $Ce_{0.90}Ca_{0.10}O_{1.90}$ has the highest conductivity which is ~10^{-2} S cm^{-1} at 600 °C. Banerjee et al. [26] studied the electrical properties of $Ce_{1-x}Ca_xO_{2-\delta}$ ($0.05 \le x \le 0.20$) samples prepared by a mixed fuel process followed by sintering at 1,250 °C. They found that the composition $Ce_{0.80}Ca_{0.20}O_{1.80}$ exhibits the highest conductivity (1.29×10^{-2} S cm^{-1}) at 600 °C. Compositions $Ce_{1-x}Ca_xO_{2-\delta}$ with $0.05 \le x \le 0.20$ have been prepared by auto-combustion method and characterized.

N. Jaiswal · D. Kumar · O. Parkash (✉)
Department of Ceramic Engineering, Indian Institute of Technology, Banaras Hindu University, Varanasi 221005, India
e-mail: oprakash.cer@itbhu.ac.in

S. Upadhyay · O. Parkash
Department of Applied Physics, Indian Institute of Technology, Banaras Hindu University, Varanasi 221005, India

Published online: 11 July 2013

$Ce_{0.95}Ca_{0.05}O_{1.95}$ exhibits the maximum conductivity in this system. Composition exhibiting maximum conductivity in this system has been reported to be different by different authors. This may be due to minor changes in the purity of raw materials and mainly changes in the processing conditions.

Co-doping of ceria has been found to be very effective for enhancement of conductivity in recent years [27–37]. Most of these compounds contain rare earth elements as a constituent. In the present investigations, effect of co-doping has been studied using Sr as a co-dopant in the composition $Ce_{0.95}Ca_{0.05}O_{1.95}$, which exhibits the maximum conductivity in our investigation as mentioned above.

Co-doping with Sr in some rare earth singly doped ceria has been reported to enhance their conductivity [38–41]. In order to explore cheaper solid electrolyte for IT-SOFCs, a few samples of ceria co-doped with Ca and Sr, viz.

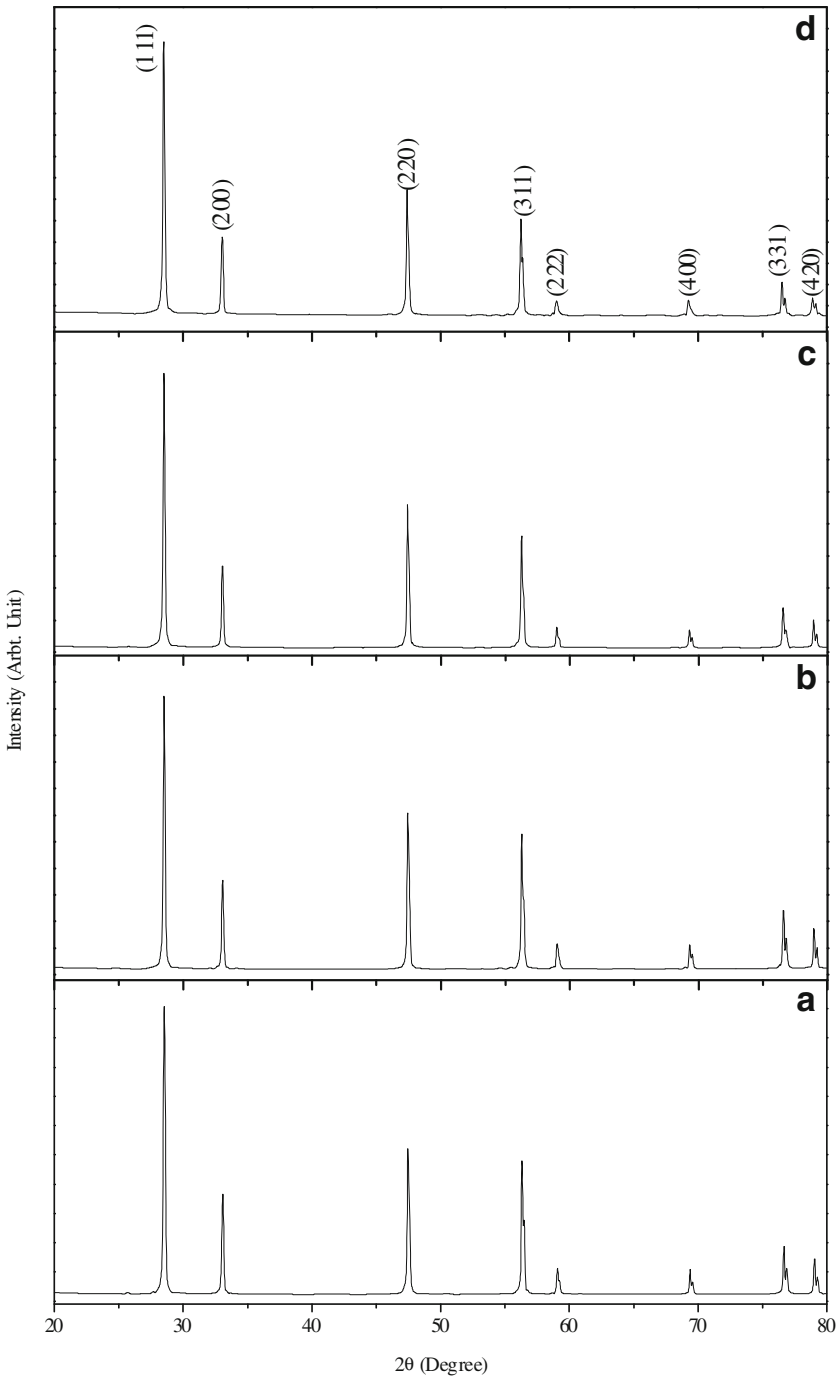

Fig. 1 Powder X-ray diffraction patterns of various compositions. **a** CCO5. **b** CC5S1. **c** CC5S2. **d** CC5S3 sintered at 1,350 °C

Table 1 Crystallite size, lattice parameter, and percent theoretical density of compositions in the system $Ce_{0.95-x}Ca_{0.05}Sr_xO_{1.95-x}$

S. no.	Compositions	Crystallite size of sintered powder (nm)	Lattice parameter (Å)	Experimental density (g/cc)	Percent of theoretical density
1.	$Ce_{0.95}Ca_{0.05}O_{1.95}$	56	5.4120±0.0003	6.60±0.02	97.0
2.	$Ce_{0.94}Ca_{0.05}Sr_{0.01}O_{1.94}$	47	5.4174±0.0002	6.69±0.02	98.3
3.	$Ce_{0.93}Ca_{0.05}Sr_{0.02}O_{1.93}$	57	5.4192±0.0002	6.70±0.03	98.5
4.	$Ce_{0.92}Ca_{0.05}Sr_{0.03}O_{1.92}$	55	5.4201±0.0006	6.62±0.03	97.5

$Ce_{0.95}Ca_{0.05}O_{1.95}$ (CCO5), $Ce_{0.94}Ca_{0.05}Sr_{0.01}O_{1.94}$ (CC5S1), $Ce_{0.93}Ca_{0.05}Sr_{0.02}O_{1.93}$ (CC5S2), and $Ce_{0.92}Ca_{0.05}Sr_{0.03}O_{1.92}$ (CC5S3), have been synthesized by citrate–nitrate route and characterized. Our results show that there is an enhancement in ionic conductivity by co-doping.

Experimental

Sample preparation

Starting chemicals used for the synthesis were ceric ammonium nitrate $(NH_4)_2[Ce(NO_3)_6]$, (Qualikems, India; 99.00 %), calcium carbonate (Reidel, India; >99.5 % purity), strontium nitrate (Reidel, India; >99.5 % purity), and citric acid (Loba Chemie, India; 99.5 %) for the synthesis of powders. Aqueous solutions of metal nitrates were mixed with an aqueous solution of citric acid maintaining a constant citrate to nitrate ratio of 0.3 [42]. The mixed solution was evaporated with continuous stirring at 200±5 °C until it gelled and finally burnt. Within a few seconds, the combustion reaction completed giving yellow porous ash filling the container. The ash was calcined at 600 °C in air for 4 h. Calcined powder was uniaxially pressed under a load of 70 kN into green pellets having 15 mm diameter. The green pellets were sintered at 1,350 °C for 4 h in air.

Sample characterization

Crystal structure of sintered powder was determined using a Rigaku high-resolution powder X-ray diffractometer employing

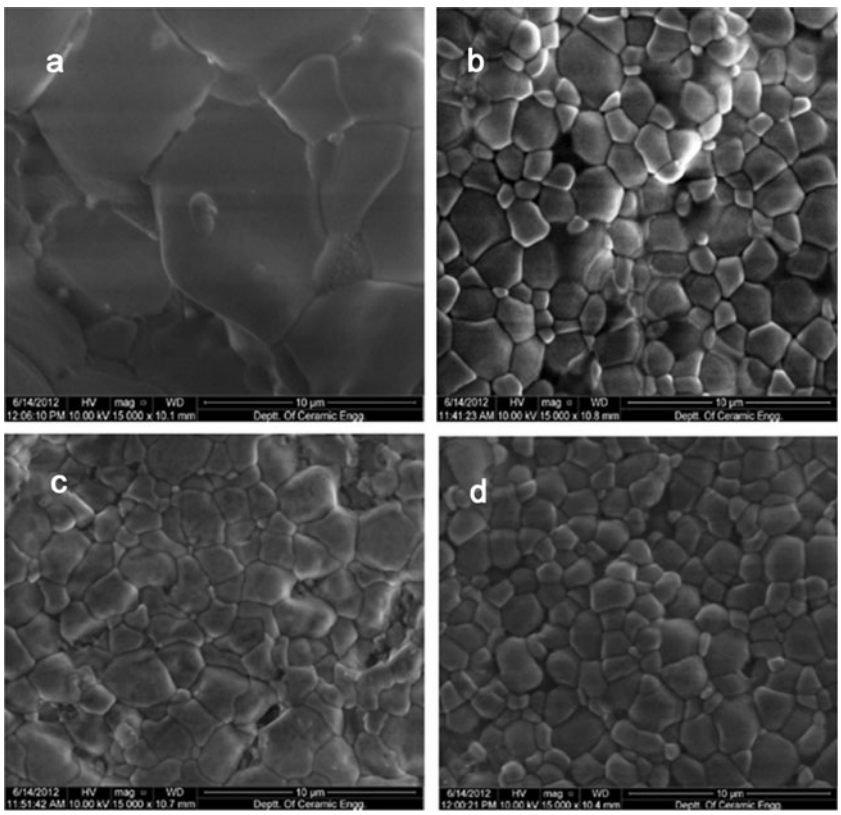

Fig. 2 Scanning electron micrographs of various compositions. **a** CCO5. **b** CC5S1. **c** CC5S2. **d** CC5S3 thermally etched at 1,250 °C

Cu $K_{\alpha 1}$ radiation and Ni filter. Data were collected in the Bragg angle range of $20° \leq 2\theta \leq 80°$. The crystallite size, D of the sintered powder, was determined using Scherrer's formula:

$$D = \frac{0.9\lambda}{\beta \cos\theta} \quad (1)$$

where β is the full width at half maxima excluding instrumental broadening, λ is the wave length of X-ray radiation, and θ is the Bragg angle. β is taken for the strongest Bragg's peak corresponding to (111) reflection for all the samples. Lattice parameters were calculated using "Unit Cell" software [43]. Density of sintered pellets was determined by Archimedes method and expressed as percentage of theoretical density determined from the lattice parameter and molecular weight of the compound. Sintered pellets were polished using emery papers of grade 1/0, 2/0, 3/0, and 4/0 (Sia, Switzerland) followed by polishing on a velvet cloth using diamond paste of grade1/4-OS-475 (HIFIN). Then, these were etched thermally at 1,250 °C. Micrographs were taken with the help of a scanning electron microscope (INSPECT 50 FEI').

Conductivity measurement

For conductivity measurements, Ag paste was applied on both surfaces of the pellet. The paint was cured at 700 °C for 15 min to form silver electrodes. Conductivity was determined by impedance spectroscopy. Impedance measurements were made using a Novocontrol Alpha-A High-Performance Frequency Analyzer with an applied voltage of 20 mV in air in the temperature and frequency range 200–600 °C and 1 Hz to 1 MHz, respectively. Data were collected using "Win data" program and fitted to the corresponding equivalent circuit using ZView software.

Results and discussion

Crystal structure

Figure 1 shows X-ray diffraction patterns of the powders of sintered pellets for the system $Ce_{0.95-x}Ca_{0.05}Sr_xO_{1.95-x}$ (x=0.00, 0.01, 0.02, and 0.03). Characteristic lines of constituent oxides are not observed in the diffraction patterns. All the samples are single phase having cubic fluorite structure. X-ray diffraction (XRD) patterns of the calcined powders are similar to those obtained after sintering except that the diffraction lines become sharper as shown in Fig. 1. This is due to grain growth occurring during sintering. There is a slight shift in 2θ values from the corresponding 2θ values of undoped ceria. Diffraction patterns were indexed on the basis of fluorite structure similar to CeO_2 using JCPDS file no. 43–1002. Lattice parameter of all the samples is given in Table 1. Lattice parameter is found to increase with strontium content because ionic radius of Sr^{2+} (1.26 Å) is larger than that of Ce^{4+} (0.97 Å) and Ca^{2+} (1.12 Å) [44]. Crystallite size, D of the calcined powder calculated from X-ray line broadening using Scherrer's formula, is in the range 47–57 nm. Density of the sintered pellets of all the samples, determined by Archimedes principle, is more than 97 % of the theoretical density (Table 1).

Figure 2 shows micrographs of thermally etched samples at 1,250 °C. Micrographs of the surface of the sintered samples show well-defined grains separated by grain boundaries. All sintered samples have grains with varying sizes. As strontium content increases, a narrowing of grain size distribution is observed. Average grain size of the compositions with x=0.00, 0.01, 0.02, and 0.03 determined by linear intercept method is approx. 6.0, 2.5, 2.0, and 1.5 μm, respectively. It is observed from Fig. 2 that average grain size decreases with increasing concentration of Sr, indicating that Sr acts as a grain growth inhibitor. This may be due to segregation of Sr^{2+} at grain boundaries due to elastic strain arising out of size mismatch of Sr^{2+} and Ce^{4+}. Whenever we dope a material with another ion, two types of strains are developed. Elastic strain arises due to difference between the ionic radii of the host ion and dopant ion. Electrostatic strain arises due to difference in their valency. Both these strains lead to increase in the energy of the materials. Grain boundaries are regions of high energy because of disorder present in them. Therefore, the dopant ions can be accommodated in the grain boundaries with minimum expenditure of extra energy, i.e., dopants tend to segregate to the grain boundaries. In the present materials, the excess concentration of dopants (Sr^{2+} in this case) may not be enough at grain boundaries so that it appears as a different phase in XRD. This can however be studied by using EDX and electron microprobe analysis.

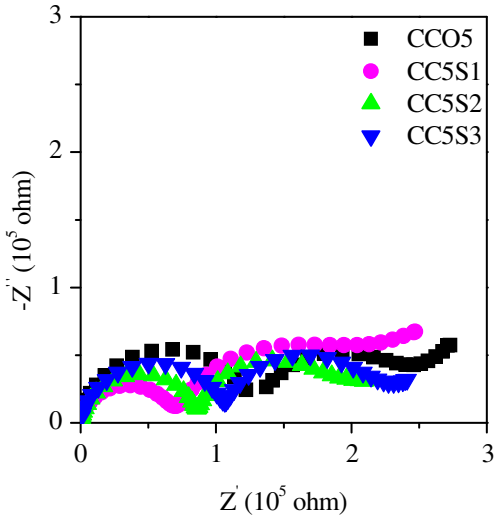

Fig. 3 Impedance plots of all the compositions in the system $Ce_{0.95-x}Ca_{0.05}Sr_xO_{1.95-x}$ at 200 °C

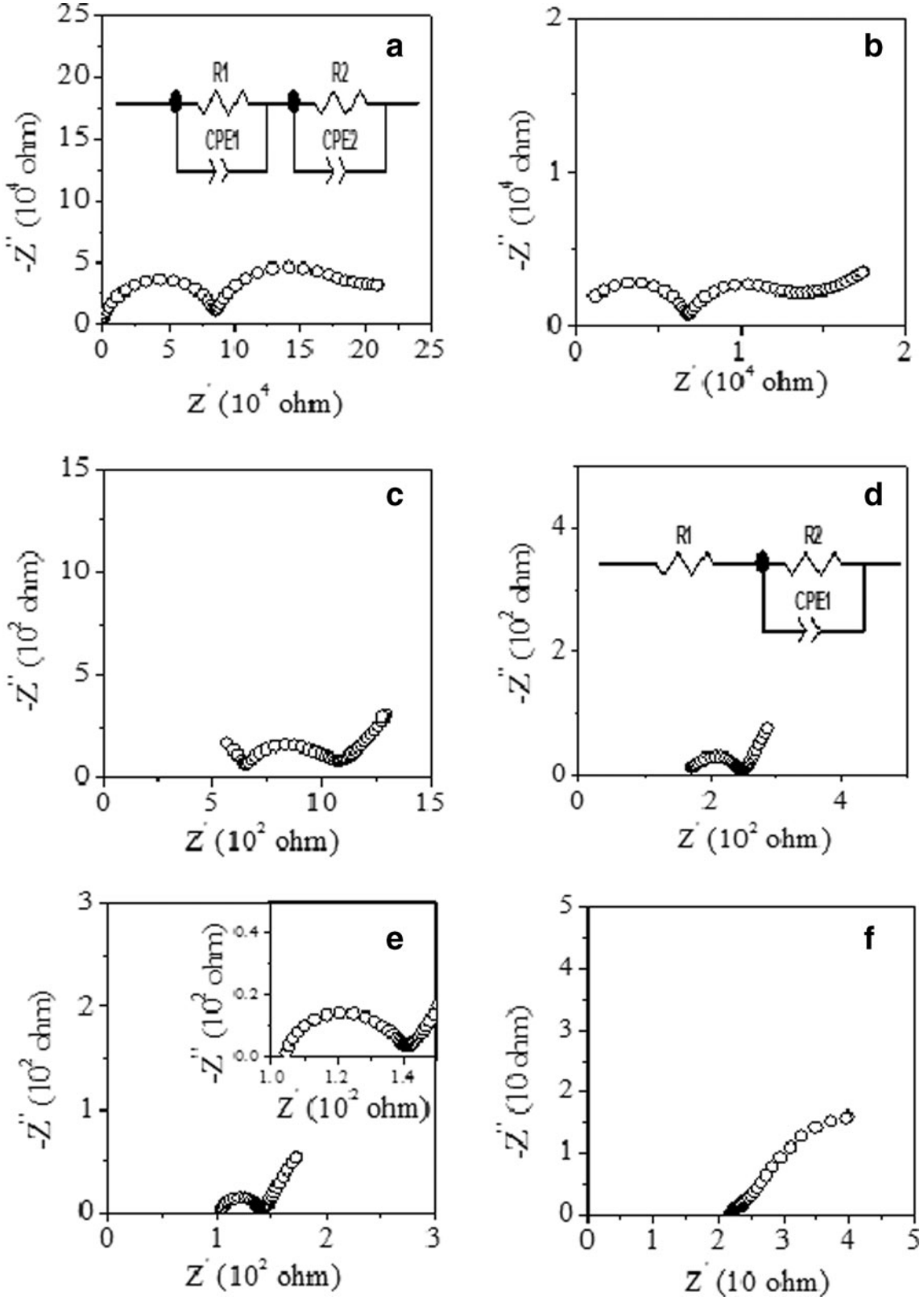

Fig. 4 Impedance plots of the composition CC5S2 at **a** 200 °C, **b** 250 °C, **c** 325 °C, **d** 375 °C, **e** 425 °C, and **f** 500 °C

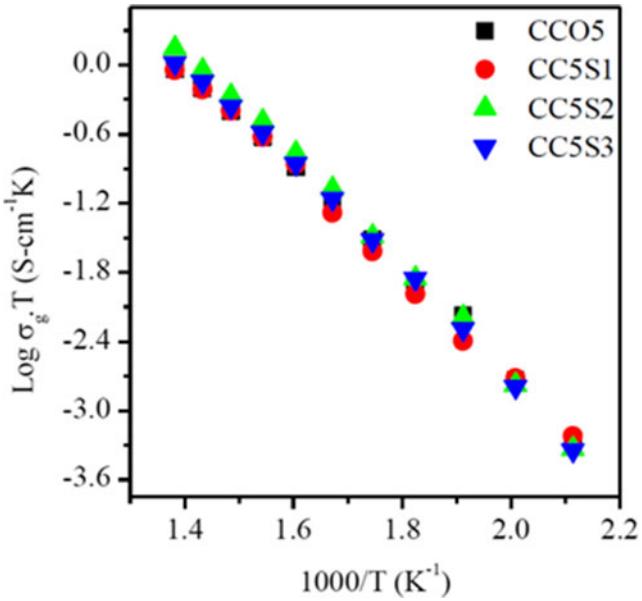

Fig. 5 Arrhenius plots for grain ionic conductivity of all the compositions in the system $Ce_{0.95-x}Ca_{0.05}Sr_xO_{1.95-x}$

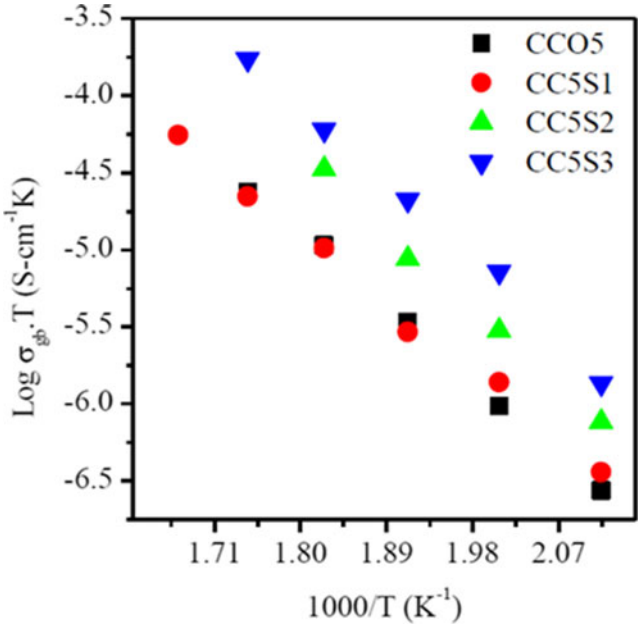

Fig. 6 Arrhenius plots for specific grain boundary conductivity of all the compositions in the system $Ce_{0.95-x}Ca_{0.05}Sr_xO_{1.95-x}$

Electrical conductivity

Conductivity of doped ceria in air has been reported to be completely ionic in nature [34]. In this paper, the conductivity measured in air can be treated as oxide ion conductivity. Electrical conductivity of the samples was studied using complex plane impedance analysis. Complex plane impedance plots at 200 °C of all the compositions studied are shown in Fig. 3. Impedance plots of CC5S2 composition at different temperatures are plotted in Fig. 4. Typically, three arcs are observed in the complex plane impedance plots of polycrystalline materials. The arc present in the highest frequency range is attributed to intragrain behavior, one in the intermediate frequencies is attributed to grain boundaries, and the third arc in the lowest frequency range is assigned to electrode–electrolyte interface polarization. Impedance plots at 200 °C (Fig. 3) exhibit two distinct arcs corresponding to grains and grain boundaries, and a third arc corresponding to electrode–electrolyte interface starts appearing. As the temperature increases, the arcs shift to higher frequency leading to disappearance of the arcs due to contributions of grains and grain boundaries. The grain arc disappeared at temperature above 325 °C, and beyond 450 °C, grain boundary arc also disappeared. At higher temperatures, only electrode arc appears. All the three arcs are not clearly seen in the impedance plots at all temperatures because of limited frequency range available in the equipment. The grains and grain boundaries arcs are associated with the capacitances in the pF (10^{-10}–10^{-12}) and nF (10^{-7}–10^{-9}) ranges [45]. These are determined from the relation $2\pi f_{max}RC=1$, where f_{max} is the applied frequency at the arc maximum, R is the resistance, and C is the capacitance of a particular contribution. In order to see clearly the contribution of the grain boundaries, the data is plotted on an expanded scale in the insets. Impedance spectra were fitted using the equivalent circuit containing two parallel resistance (R)—constant phase element (CPE) circuits connected in series one for the bulk and other for the grain boundaries. In the present analysis, a CPE [46] is used for fitting the data instead of a capacitor (Fig. 4). The CPE accounts for the microstructure inhomogeneity within the sample, and it is equivalent to a

Table 2 Total conductivity at 600 °C (σ_t), activation energy of grains (E_g), grain boundaries (E_{gb}), total (E_t) conductivity, and thickness of the grain boundary (δ_{gb}) of various compositions in the system $Ce_{0.95-x}Ca_{0.05}Sr_xO_{1.95-x}$

S. no.	Compositions	δ_{gb} (nm)	σ_t at 600 °C (S cm^{-1})	E_g (eV) (200–450 °C)	E_{gb} (eV) (200–450 °C)	E_t (eV) (200–600 °C)
1.	$Ce_{0.95}Ca_{0.05}O_{1.95}$	5.42	7.98×10^{-3}	0.88±0.08	1.06±0.12	0.93±0.06
2.	$Ce_{0.94}Ca_{0.05}Sr_{0.01}O_{1.94}$	3.78	1.04×10^{-2}	0.89±0.07	0.97±0.15	0.99±0.05
3.	$Ce_{0.93}Ca_{0.05}Sr_{0.02}O_{1.93}$	4.66	1.66×10^{-2}	0.94±0.08	1.10±0.23	0.97±0.05
4.	$Ce_{0.92}Ca_{0.05}Sr_{0.03}O_{1.92}$	4.56	1.22×10^{-2}	0.92±0.07	1.11±0.19	0.95±0.04

distribution of capacitors in parallel. In Fig. 4, R_1, R_2, CPE1, and CPE2 stand for grain resistance, grain boundary resistance, CPE of grains, and CPE of grain boundaries, respectively. The contribution of the electrode–specimen interface (which is given by the third arc) is not considered here because total resistance of electrolyte is given by the sum of grain (R_g) and grain boundary resistance (R_{gb}). These circuits are used to obtain the best fit and adequately determine the electrolyte resistance.

Total resistance of the sample is given by $R_t=R_g+R_{gb}$. Resistance of grains (R_g) and grain boundaries (R_{gb}) can be determined by fitting the impedance data. Total conductivity (σ_t) has been determined using the formula:

$$\sigma_t = \frac{1}{R} \times \frac{L}{S} \tag{2}$$

where L is the thickness and S is the area of the sample.

An important feature of ceria is its tolerance to doping due to its relatively open structure. Addition of divalent cations in ceria produces oxygen vacancies responsible for ionic conduction [47, 48] as given below in the Eqs. 3 and 4:

$$\mathrm{SrO} \overset{\mathrm{CeO_2}}{\rightarrow} \mathrm{Sr''_{Ce}} + O_o + V_o^{\bullet\bullet} \tag{3}$$

$$\mathrm{CaO} \overset{\mathrm{CeO_2}}{\rightarrow} \mathrm{Ca''_{Ce}} + O_o + V_o^{\bullet\bullet}. \tag{4}$$

Arrhenius plots of bulk conductivities for all the samples in the temperature range 200–450 °C are shown in Fig. 5. It can be seen from Fig. 5 that the value of bulk conductivity is highest for the sample $Ce_{0.93}Ca_{0.05}Sr_{0.02}O_{1.93}$ and starts decreasing beyond x (Sr)=0.02. Value of grain ionic conductivity for the sample $Ce_{0.93}Ca_{0.05}Sr_{0.02}O_{1.93}$ is 1.39×10^{-4} S cm^{-1} at 325 °C, which is much higher than the value 6.0×10^{-6} S cm^{-1} reported by Junior et al. [49] for the sample $Ce_{0.90}Ca_{0.05}Sr_{0.05}O_{1.90}$ at 320 °C. These plots are linear having a single slope. Activation energy of conduction (E_g) has been determined using Arrhenius relationship:

$$\sigma_g = \frac{\sigma_{0g}}{T} \cdot \exp\left(\frac{-E_g}{kT}\right), \tag{5}$$

where σ_{0g} is the pre-exponential factor, k is the Boltzmann constant, and T is the absolute temperature. Values of activation energy of bulk ionic conductivity (E_g) for all the samples determined from the plots by least square fitting of the data points in Fig. 5 are given in Table 2.

According to Verkerk [50] and Christie et al. [46], there exists a relation between apparent grain boundaries conductivity (σ_{gb}) determined from the grain boundary arc of impedance plot and specific grain boundaries conductivity σ_{gb}^* as given by Eq. 6:

$$\sigma_{gb}^* = \left(\frac{\delta_{gb}}{d_g}\right)\sigma_{gb} \tag{6}$$

where δ_{gb} is the thickness of the grain boundary and d_g is the average grain size. If bulk and grain boundary permittivities are similar, then Eq. 6 can be written as:

$$\sigma_{gb}^* = \frac{C_g}{C_{gb}}\sigma_{gb} \tag{7}$$

where C_g and C_{gb} are bulk and grain boundary capacitance determined from the impedance plots.

Arrhenius plots for specific grain boundary conductivity are shown in Fig. 6. Thickness of grain boundary can be calculated from Eqs. 6 and 7, and it is in the range of 2–5 nm (given in Table 2) in agreement with the values reported by Guo et al. [51].

It is seen from Fig. 6 that the grain boundary conductivity depends on Sr content, and it is higher for co-doped samples. This may be due to two factors. One is due to scavenging effect of Sr. Grain boundary blocking factor ($\propto_{gb}$) has been used to confirm the scavenging effect of Sr [50, 52]. It is defined as:

$$\propto_{gb} = \frac{R_{gb}}{R_g + R_{gb}}. \tag{8}$$

Blocking factor $\propto_{gb}$ gives the fraction of charge carriers being blocked at the impermeable internal surface, under the

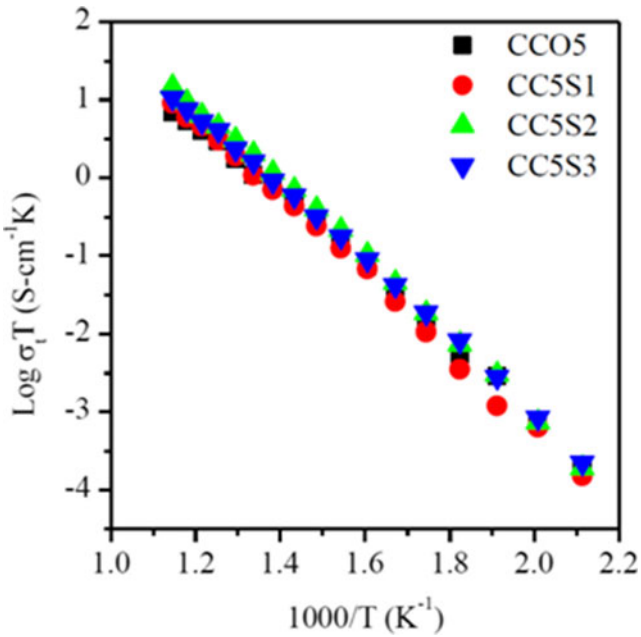

Fig. 7 Arrhenius plots for total ionic conductivity of all the compositions in the system $Ce_{0.95-x}Ca_{0.05}Sr_xO_{1.95-x}$

measuring conditions, with respect to the total number of charge carriers in the samples. Value of $\propto_{gb}$ is 0.37 for the sample $Ce_{0.95}Ca_{0.05}O_{1.95}$ which is maximum and 0.11 for $Ce_{0.93}Ca_{0.05}Sr_{0.02}O_{1.93}$ at 400 °C being minimum of all the samples. This may be due to scavenging effect of Sr^{2+} ions to remove siliceous impurities. It has been reported by Gerhardt et al. [52] that grain boundary effect depends on dopant concentration and dopant size. The grain boundary resistivity decreases sharply with increasing concentration and size of the dopants. Concentration and nature of the dopants control how much Si goes into solid solution and how much is segregated. On the basis of scanning transmission electron microscopy combined with energy dispersive X-ray microanalysis and electron energy loss spectroscopy, Gerhardt et al. [53] reported that in yttrium-doped ceria, there exists an amorphous silica thick layer surrounding the grains. This layer blocks the charge carriers leading to increase in the resistivity of the grain boundaries. They also observed the formation of some silicate phases of yttrium. The amount of these phases increases as the yttrium concentration increases. These phases pocket at the triple point junction, leaving clean grain to grain contacts area. Therefore, the amount of Si decreases as the concentration of dopants increases, i.e., less amount of Si is available for the formation of thick boundary layer. Similar silicate phases may form in the materials under present investigation. The exact compositions, morphology, and distribution of these phases require analytical studies as mentioned above. Removal of silica decreases the resistivity of the grain boundaries leading to decrease in the total resistivity. In the present investigation, an optimum value of Sr for scavenging effect is 2 mol %. Beyond this concentration, elastic strain seems to dominate leading to decrease in the conductivity.

Second is the decrease in the average grain size. It can be observed from Fig. 6 that specific grain boundary conductivity increases with decreasing grain size. Small grain size samples exhibit much higher grain boundary conductivity. This is because of the large grain boundary area for which the finite amount of impurity contained in these samples is not sufficient to form a continuous and uniform glassy phase layer along grain boundaries. This leaves the remaining grain boundary area for clean grain to grain contact [54]. Therefore, the transport of O^{2-} ions becomes faster across the grains through clean grain boundaries.

Values of activation energy of grain boundary conduction (E_{gb}) are given in Table 2. These values of E_{gb} are consistently higher than the corresponding E_g values.

Plots of Log $\sigma_t T$ vs. 1,000/T for all the compositions are shown in Fig. 7. These plots are linear with a single slope. Values of activation energy of total conductivity determined from the slope of these plots are given in Table 2.

Values of σ_t at 600 °C for different compositions are given in Table 2. Values of σ_t increase with increasing Sr content up to 2 mol%. In the present study, an addition of Ca and Sr to ceria leads to some opposite competing effects. First is the ordering of oxygen vacancies is suppressed due to co-doping reported by Yamamura et al. [55]. This decreases the activation energy for migration of O^{2-} ion, consequently increasing the conductivity. Second is due to scavenging effect of grain boundaries by Sr^{2+} leading to increase in the grain boundaries as well as total conductivity. Third is that the ionic size mismatch between Sr^{2+} (1.26 Å) and Ce^{4+} (0.97 Å) is larger than that between Ca^{2+} (1.12 Å) and Ce^{4+} (0.97 Å) [56]. The elastic strain therefore increases with increasing x (Sr). This decreases the conductivity because of an increase in activation energy for diffusion of O^{2-} ion. Concentration of oxygen vacancies also increases with increasing x. At the same time, the probability of the formation of associated defect pairs ($Ca_{Ce}''-V_O^{\bullet\bullet}$ or $Sr_{Ce}''-V_O^{\bullet\bullet}$) also increases with increasing x. Because of the complex interplay of these opposite competing effects, conductivity increases up to x=0.02 and decreases thereafter.

Composition, $Ce_{0.93}Ca_{0.05}Sr_{0.02}O_{1.93}$ shows the highest conductivity among all the compositions studied. Its conductivity at 600 °C (1.66×10^{-2} S cm^{-1}) is higher than the reported values of conductivity for the compositions $Ce_{0.80}Sm_{0.20}O_{1.90}$ (1.20×10^{-2} S cm^{-1}) [57] and $Ce_{0.80}Gd_{0.20}O_{1.90}$ (1.29×10^{-2} S cm^{-1}) [58] at 600 °C. Conductivity of composition for $Ce_{0.93}Ca_{0.05}Sr_{0.02}O_{1.93}$ is also higher than the maximum value reported for singly Sr-doped ceria $Ce_{0.95}Sr_{0.05}O_{1.95}$ (1.53×10^{-2} S cm^{-1}) at 600 °C [59]. It is concluded that the composition $Ce_{0.93}Ca_{0.05}Sr_{0.02}O_{1.93}$ has more conductivity than that of ceria singly or co-doped with rare earth ions such as Sm^{3+} and Gd^{3+}. Use of this material as a solid electrolyte for IT-SOFC is expected to reduce the cost drastically. Measurement of thermal expansion coefficient as a function of temperature and long-term stability needs to be studied for its application in IT-SOFCs.

Conclusions

Samples in the system, $Ce_{0.95-x}Ca_{0.05}Sr_xO_{1.95-x}$ (x=0.00, 0.01, 0.02, and 0.03), have been prepared by citrate–nitrate route. Single-phase solid solution forms in all the compositions at low temperature as 600 °C. Density of all the compositions is more than 97 % of the theoretical value. Conductivity of compositions increases with an increase in Sr concentration up to 2 mol % and then it decreases. Composition with x=0.02 exhibits the maximum ionic conductivity. This is higher than the maximum values reported in SDC and GDC. This may make this material suitable as a solid electrolyte for IT-SOFCs application.

Acknowledgment Thanks are due to the Department of Science and Technology, New Delhi for financial support.

References

1. Arai H (1992) Oxygen ion conductor and its application. J Bull Ceram Soc Jpn 27:100–104
2. Miura N, Kurosawa H, Hasei M, Lu G, Yamazoe N (1996) Stabilized zirconia-based sensor using oxide electrode for detection of NOx in high-temperature combustion-exhausts. Solid State Ionics 86–88:1069–1073
3. Yamazoeand N, Miura N (1996) Prospect and problems of solid electrolyte-based oxygenic gas sensors. Solid State Ionics 86–88:987–993
4. Minh NQ (1993) Ceramic fuel cells. J Am Ceram Soc 76:563–588
5. Hibino T, Iwahara H (1994) Improvement of CAPCIUS cell using $SrCe_{0.95}Yb_{0.05}O_{3-\alpha}$ as a solid electrolyte. Chem Lett 35:485–488
6. Sasaki H, Otoshi S, Suzuki M, Sogi T, Kajimura A, Sagiura N, Ippommatsu M (1994) Fabrication of high power density tabular type solid oxide fuel cells. Solid State Ionics 72:253–256
7. Inaba H, Tagawa H (1996) Ceria based solid electrolytes. Solid State Ionics 83:1–16
8. Stefanik ST, Tuller LH (2001) Ceria-based gas sensors. J Eur Ceram Soc 21:1967–1970
9. Jurado JR (2001) Present several items on ceria-based ceramic electrolytes: synthesis, additive effects, reactivity and electrochemical behavior. J Mater Sci 36:1133–1139
10. Kharton VV, Figueiredo FM, Navarro L, Naumovich EN, Kovalevsky AV, Yaremchenko AA, Viskup AP, Carneiro A, Marques FMB, Frade JR (2001) Ceria based materials for solid oxide fuel cells. J Mater Sci 36:1105–1117
11. Doshi R, Richards VL, Carter JD, Wang X, Krumpelt M (1999) Development of solid oxide fuel cells that operate at 500°C. J Electrochem Soc 146:1273–1278
12. Godickemeier M, Gauckler LJ (1998) Engineering of solid oxide fuel cells with ceria-based electrolytes. J Electrochem Soc 145:414–421
13. Zhu B, Liu X, Sun M, Ji Sun S (2003) Calcium doped ceria-based materials for cost-effective intermediate temperature solid oxide fuel cells. J Solid State Sci 5:1127–1134
14. Bellon O, Sammes NM, Staniforth J (1998) Mechanical properties and electrochemical characterisation of extruded doped cerium oxide for use as an electrolyte for solid oxide fuel cells. J Power Sources 75:116–121
15. Wang S, Kobayashi T, Dokiya M, Hashimoto T (2000) Electrical and ionic conductivity of Gd-doped ceria. J Electrochem Soc 147:3606–3609
16. Wang Y, Mori T, Li JG, Yajima Y (2003) Low-temperature fabrication and electrical property of 10 mol% Sm_2O_3-doped CeO_2 ceramics. Sci Technol Adv Mater 4:229–238
17. Kim DJ (1989) Ionic conductivities, and solubility limits in fluorite-structure MO_2 oxide [M=Hf^{4+}, Zr^{4+}, Ce^{4+}, Th^{4+}, U^{4+}] solid solutions. J Am Ceram Soc 72:1415–1421
18. Yahiro H, Ohuchi T, Eguchi K, Arai H (1988) Electrical properties and microstructure in the system ceria-alkaline earth oxide. J Mater Sci 23:1036–1041
19. Sameshima S, Ichikawa T, Kawaminami M, Hirata Y (1999) Thermal and mechanical properties of rare earth-doped ceria ceramics. Mater Chem Phys 61:31–35
20. Blumenthal RN, Pinz BA (1967) Nature of the electrical conduction transients observed in CeO_2 and Ca–doped CeO_2. J Appl Phys 38:2376–2378
21. Arai H, Kunisaki T, Shimizu Y, Seiyama T (1986) Electrical properties of calcia-doped ceria with oxygen ion conduction. Solid State Ionics 20:241–248
22. Blumenthal RN, Garnier JE (1976) The electrical conductivity and thermodynamic behavior of SrO-doped nonstoichiometric cerium dioxide. J Solid State Chem 16:21–34
23. Yahiro H, Eguchi K, Arai H (1986) AC conductivity and conductivity relaxation studies in the CeO_2–Y_2O_3 system. Solid State Ionics 21:49–53
24. Ong Poh Shing, Tan Yen Ping, and Taufiq Yap Yun Hin (2011) Mechanochemical synthesis and characterization of calcium doped ceria oxide ion conductor Material Science and Engineering 17: doi:10.1088/1757-899X/17/1/012017
25. Yamashita K, Ramanujachary KV, Greenblatt M (1995) Hydrothermal synthesis and low temperature conduction properties of substituted ceria ceramics. Solid State Ionics 81:53–60
26. Banerjee S, Devi PS (2008) Understanding the effect of calcium on the properties of ceria prepared by a mixed fuel process. Solid State Ionics 179:661–669
27. Holtappels P, Poulsen FW, Mogensen M (2000) Electrical conductivities and chemical stabilities of mixed conducting pyrochlores for SOFC applications. Solid State Ionics 135:675–679
28. Tuller HL, Tuller H, Schoonman J, Riess I (2000) Oxygen ion and mixed conductors and their technological applications. In: Riess I (ed) Defects and transport. Kluwer (NATO ASI series), Dordrecht, pp 245–270
29. Etsell H, Flengas SN (1970) The electrical properties of solid oxide electrolytes. Chem Rev 70:339–376
30. Rickert H (1982) Electrochemistry of solids—an introduction. Springer-Verlag, Berlin
31. Chebotin VN, Perfilyev MV (1978) Electrochemistry of solid electrolytes. Khimiya, Moscow
32. Perfilyev MV, Demin AK, Kuzin BL, Lipilin AS (1988) High temperature electrolysis of gases. Nauka, Moscow
33. Kharton VV, Naumovich EN, Vecher AA (1999) Research on the electrochemistry of oxygen ion conductors in the former Soviet Union I ZrO_2-based ceramic materials. J Solid State Electrochem 3:61–81
34. Inaba H, Tagawa H (1996) Ceria based electrolytes. Solid State Ionics 83:1–16
35. Bouwmeester HJM, Burggraaf AJ (1996) In: Burggraaf A, Cot L (eds) Fundamentals of inorganic membrane science and technology. Elsevier, Amsterdam, pp 435–528
36. Sammes NM, Tompsett GA, Nafe H, Aldinger F (1999) Bismuth based oxide electrolytes—structure and ionic conductivity. J Eur Ceram Soc 19:1801–1826
37. Mogensen M, Sammes NM, Tompsett GA (2000) Physical chemical and electrochemical properties of pure and doped ceria. Solid State Ionics 129:63–94
38. Yeh T-H, Chou C-C (2007) Ionic conductivity investigation in samarium and strontium co-doped ceria system. Phys Scr 129:303–307
39. Cioatera N, Parvulescu V, Rolle A, Vannier RN (2009) Effect of strontium addition on europium-doped ceria properties. Solid State Ionics 180:681–687
40. Zheng Y, Liqiang W et al (2009) The effect of Sr on the properties of Y-doped ceria electrolyte for IT-SOFCs. J Alloys Compd 486:586–589
41. Ramesh S, Vishnuvardhan Reddy C (2009) Electrical properties of co-doped ceria electrolyte $Ce_{0.8-x}Gd_{0.20}Sr_xO_{2-\delta}$ ($0.0<x<0.1$). Acta Phys Polon A 115:909–912
42. Basu S, Sujata Devi P, Maiti HS (2004) Synthesis and properties of nanocrystalline ceria powders. J Mater Res 19:3162–3171
43. Holland TJB, Redfern SAT (1997) Unit cell refinement from powder diffraction data: the use of regression diagnostics. Mineral Mag 61:65–77
44. Shannon RD (1976) Revised effective ionic radii and systematic studies of interatomic distances in halides and chalcogenides. Acta Crystallogr A 32:751–761
45. Hodge IM, Ingram MD, West AR (1976) Impedance and modulus spectroscopy of polycrystalline solid electrolytes. J Electro Anal Chem 74:125–143

46. Christie GM, Berkel FPF (1996) Microstructure-ionic conductivity relationships in ceria-gadolinia electrolytes. Solid State Ionics 83:17–27
47. Ruiz-Trejo E, Benitez-Rico A, Gomez-Reynoso S, Angeles-Rosas M (2007) Nanoparticles and nano-grain sized Y-doped CeO_2 ceramics. J Electrochem Soc 154:A258–A262
48. Wang DY, Norwick AS (1981) Dielectric relaxation from a network of charged defects in dilute CeO_2:Y_2O_3solid solutions. Solid State Ionics 5:551–555
49. Junior JMS et al (2012) Raman and Rietveld structure characterization of sintered alkaline earth doped ceria. Mater Chem Phys 135:957–964
50. Verkerk MJ, Middelhuis BJ, Burggraaf AJ (1982) Effect of grain boundaries on the conductivity of high-purity ZrO_2-Y_2O_3 ceramics. Solid State Ionics 6:159–170
51. Guo X, Waser R (2006) Electrical properties of the grain boundaries of oxygen ion conductors: acceptor doped zirconia and ceria. Prog Mater Sci 51:151–210
52. Gerhardt R, Nowick AS (1986) The grain boundary conductivity effect in ceria doped with trivalent cations. Part-I electrical behavior. J Am Ceram Soc 69:641–646
53. Gerhardt R, Nowick AS, Mochel ME, Dumler I (1986) Grain boundary effect in ceria doped with trivalent cations: II microstructure and microanalysis. J Am Ceram Soc 69:647–651
54. Tian C, Chan SW (2000) Ionic conductivities, sintering temperatures and microstructures of bulk ceramics CeO_2 doped with Y_2O_3. Solid State Ionics 134:89–102
55. Yamamura H, Katoh E, Ichikawa M, Kakinuma K, Mori T, Haneda H (2000) Multiple doping effect on the electrical conductivity in the ($Ce_{1-x-y}La_xM_y$) $O_{2-\delta}$ (M=Ca, Sr) system. Electrochemistry 68:455–459
56. Kim DK, Cho PS, Lee JH, Kim DY, Park HM, Auchterlonie G et al (2007) Mitigation of highly resistive grain-boundary phase in gadolinia-doped ceria by the addition of SrO. Electrochem Solid State Lett 10:B91–B95
57. Bryan Balazas G, Robert Glass S (1995) AC impedance studies of rare earth oxide doped ceria. Solid State Ionics 76:155–162
58. Fu Y-P, Chen S-H, Huang J-J (2010) Preparation and characterization of $Ce_{0.8}M_{0.2}O_{2-\delta}$ (M=Y, Gd, Sm, Nd, La) solid electrolyte materials for solid oxide fuel cells. Int J Hydrogen Energy 35:745–752
59. Jaiswal N, Singh NK, Kumar D, Parkash O (2012) Effect of strontium (Sr) doping on the conductivity of ceria. J Power Sources 202:78–84

Ionics
DOI 10.1007/s11581-014-1190-4

ORIGINAL PAPER

Preparation and characterization of $Ce_{0.85}La_{0.15-x}Sr_xO_{\{2-(0.075+x/2)\}}$ solid electrolytes for intermediate temperature solid oxide fuel cells

Nandini Jaiswal · Devendra Kumar · Shail Upadhyay · Om Parkash

Received: 28 October 2013 / Revised: 19 May 2014 / Accepted: 16 June 2014

Abstract A few compositions in the system $Ce_{0.85}La_{0.15-x}Sr_xO_{\{2-(0.075+x/2)\}}$ have been prepared using citrate-nitrate method. More than 95 % of theoretical density has been obtained by sintering at 1,350 °C for 4 h in air. Solid solution forms in all the compositions. Surface morphology has been studied by scanning electron microscope (SEM). Morphology of powder has been studied by bright field transmission electron microscopy (BFTEM). Complex plane impedance measurements have been made in the frequency range 1 Hz–1 MHz between 200 and 600 °C to separate the contributions of grains, grain boundaries, and electrode-specimen interface polarizations. Composition, $Ce_{0.85}La_{0.125}Sr_{0.025}O_{1.9125}$, exhibits the maximum conductivity 1.50×10^{-2} S/cm at 600 °C which is much higher than that of ceria doped with La only in the intermediate temperature range. Co-doping with Sr increases the bulk as well as grain boundary conductivity.

Keywords Doped ceria electrolyte · Co-doping effect · Ionic conductivity · Solid oxide fuel cells

Introduction

Increase in the energy demand has focused on the alternate energy conversion technologies. Solid oxide fuel cells (SOFCs) offer far more efficiency in conversion of chemical energy in fuels into electricity (65 % for electric power and 85 % efficient for cogeneration). There is worldwide interest in reducing the operating temperature of SOFCs to 500–700 °C for long-term stability and lower cost [1]. This, however, requires increased ionic conductivity of the electrolyte in this temperature range. SOFCs using such electrolytes are called intermediate temperature solid oxide fuel cells (IT-SOFCs).

There is a lot of literature on the improvement of ionic conductivity of solid electrolyte materials, e.g., zirconia, ceria, lanthanum gallate, and bismuth-based oxides [2–6]. Among these materials, ceria doped with aliovalent cations of rare earth and alkaline earth elements has been found to be a promising electrolyte for IT-SOFCs [7–9]. Ionic conductivity of doped ceria resulting from oxygen vacancies depends on the nature and concentration of the dopant [7, 10]. Doped ceria electrolytes such as $Ce_{1-x}Gd_xO_{2-\delta}$ (GDC), $Ce_{1-x}Sm_xO_{2-\delta}$ (SDC), and $Ce_{1-x}Y_xO_{2-\delta}$ (YDC) show high ionic conductivity. Ceria-doped singly with Sm has been reported to exhibit the highest conductivity among the singly doped ceria materials [11, 12]. But, Sm_2O_3 is very costly. It is important to develop new cost-effective ceria-based electrolyte materials having higher ionic conductivity for IT-SOFCs.

In order to reduce the cost and increase ionic conductivity, co-doping approach has been used and found to be effective. Herle et al. [13] found that co-doping of ceria with rare earth and alkaline earth ions showed significantly higher ionic conductivity than the singly doped materials. Some co-doped ceria electrolytes which have been investigated are $Ce_{1-x-y}Sm_xCa_yO_{2-\delta}$ [14], $Ce_{0.80}Sm_{0.20-x}Y_xO_{2-\delta}$ [15], $Ce_{1-x}Sm_{0.15-x}Gd_xO_{1.925}$ [16], $Ce_{0.85}Gd_{0.10}Mg_{0.05}O_{2-\delta}$ [17], and $Ce_{1-x-y}Gd_xPr_yO_{2-\delta}$ [18]. Yifeng et al. [19] studied electrical properties of $Ce_{0.80}Sm_{0.20-x}Mg_xO_{2-\delta}$ samples synthesized by solid state reaction by sintering at 1,550 °C. They found that substitution of Mg for Sm up to 50 mol% increases slightly the conductivity than that of ceria doped with Sm only. Yifeng [19] and Yueming Shi et al. [20] studied the electrical properties of $Ce_{1-x}La_{x-y}Ca_yO_{2-\delta}$

N. Jaiswal · D. Kumar · O. Parkash (✉)
Department of Ceramic Engineering, Indian Institute of Technology (Banaras Hindu University), Varanasi 221005, India
e-mail: oprakash.cer@itbhu.ac.in

S. Upadhyay
Department of Physics, Indian Institute of Technology (Banaras Hindu University), Varanasi 221005, India

Published online: 27 June 2014

electrolyte materials and observed that the composition $Ce_{0.85}La_{0.10}Ca_{0.05}O_{2-\delta}$ has the maximum conductivity (3.56×10^{-2} at 700 °C) of all the compositions studied. Cioatera et al. [21] studied the effect of addition of Sr on properties of europium-doped ceria. It was found that an optimum ratio of europium/strontium increased the conductivity, and this increase was mainly due to decrease in the grain boundary resistance. Some other co-doped ceria electrolytes studied are $Ce_{0.80-x}Sm_{0.20}Sr_xO_{2-\delta}$ [22], $Ce_{0.80-x}Gd_{0.20}Sr_xO_{2-\delta}$ [23], and $Ce_{0.80}Y_{0.20-x}Sr_xO_{2-\delta}$ [24]. An improvement in the conductivity has been found in these systems due to decrease in the grain boundary resistance.

In our previous reports, effect of strontium addition on conductivity of singly La-doped ceria, $Ce_{0.85}La_{0.15}O_{1.925}$ samples having the same number of oxygen vacancies was studied [25]. In the present work, La and Sr co-doped ceria viz $Ce_{0.85}La_{0.15-x}Sr_xO_{\{2-(0.075+x/2)\}}$ have been prepared to study the effect of increasing oxygen vacancies on the ionic conductivity by changing the concentration of Sr. It was considered worthwhile to study ionic conductivity of these materials because if these have more or comparable conductivity with Sm- or Gd-doped ceria as mentioned above, their use will reduce the cost drastically. A significant improvement in the electrical conductivity has been observed by co-doping ceria with lanthanum and strontium.

Experimental

Sample preparation

A series of samples in the system $Ce_{0.85}La_{0.15-x}Sr_xO_{\{2-(0.075+x/2)\}}$ (x=0.0, 0.025, 0.050, and 0.075) have been prepared by citrate-nitrate route using ammonium ceric nitrate (99 % purity, Qualikems, India), lanthanum oxide (99.9 %, Sigma-Aldrich), strontium nitrate (99.5 % purity, Reidel Chemicals, India), and citric acid (99.5 % purity, Loba Chemie, India) as starting materials. $La(NO_3)_3$ has been prepared by dissolving required amount of La_2O_3 in dilute nitric acid followed by heating at 100 °C to dryness water. This gives $La(NO_3)_3$ which is then dissolved in distilled water to get an aqueous solution. Solutions of other metal nitrates in distilled water were prepared separately. An aqueous solution of citric acid was added to the mixed solution of nitrates to give a citrate to nitrate ratio, C/N ~0.3 for controlled combustion [26]. The mixed solution was evaporated on a hot plate with constant stirring at approx 200 °C. The solution became viscous and turned into a gel during heating. The gel slowly foamed and finally burnt on its own giving light yellow color ash. Ash was calcined at 800 °C for 4 h. The calcined powder was pressed under a load of 50 kN into cylindrical pellets having ~15 mm diameter and ~2 mm thickness. These pellets were sintered at 1,350 °C for 4 h in air.

Characterization

Powder X-ray diffraction (XRD) patterns were recorded with the help of a Rigaku high resolution powder X-ray diffractometer employing $CuK_{\alpha1}$ radiation using Ni filter at room temperature. Data were collected in the 2θ range from 20° to 80°. Lattice parameter was determined using nonlinear least square fitting "UnitCell" software [27]. Average crystallite size, D, was determined using Scherrer's formula:

$$D = 0.9\lambda \Big/ \beta cos\theta \tag{1}$$

where β is the full width at half maxima (FWHM) excluding instrumental broadening, λ is the wavelength of X-rays, and θ is Bragg angle. β is taken for the strongest Bragg's peak corresponding to (111) reflection for all the samples. For determining instrumental broadening, XRD of a single crystal of Si is done by scanning at a very slow speed around strongest peak of Si which occurs at 2θ=28.424° corresponding to (111) reflection. The broadening of the peak, β_s, corresponding to (111) plane is 0.132° which is taken as instrumental broadening. β is calculated by using the formula:

$$\beta = \sqrt{\beta_m^2 - \beta_s^2}$$

where β_m is the FWHM of $Ce_{0.85}La_{0.15-x}Sr_xO_{\{2-(0.075+x/2)\}}$ calcined powders determined by XRD. Density of sintered pellets was determined using Archimedes principle. Sintered samples were weighed in air. Samples were then immersed in kerosene in a beaker and kept in a vacuum desiccator for 2 h to ensure that kerosene filled the open pores completely. Then, weights were taken in suspended state in kerosene and after removing from kerosene, wiping out the pellet with a tissue paper (soaked weight). Bulk density was calculated as follows:

$$Bulk\,Density = \frac{W_d}{W_s - W_a} \times Density\,of\,Kerosene \tag{2}$$

where W_d, W_s, and W_a are the dry weight, soaked weight, and suspended weight of the sample, respectively. Density of kerosene is 0.81 gm/cm^3.

Bright field transmission electron micrographs of the calcined powders were taken using Technai-G^2 (FEI, Eindhoven, Netherlands) electron microscope equipped with SIS Mega View III CCD camera (FEI, Eindhoven, Netherlands) at 120 KV employing Analysis software (SIS, Muenster, Germany). Samples were dispersed in

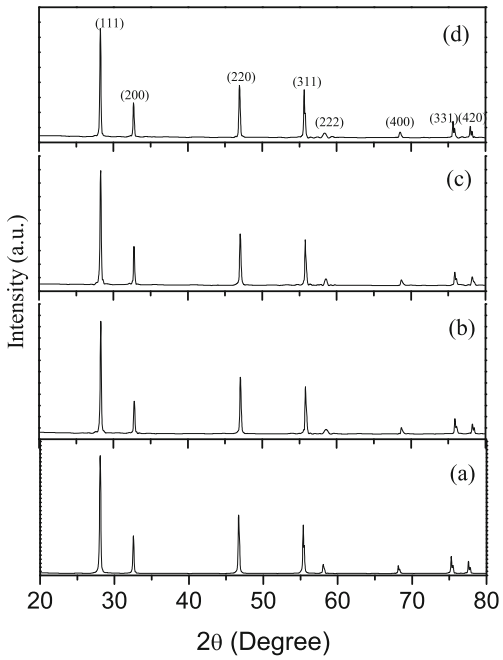

Fig. 1 Powder X-ray diffraction patterns of the system $Ce_{0.85}La_{0.15-x}Sr_xO_{\{2-(0.075+x/2)\}}$ for **a** x=0.0, **b** x=0.025, **c** x=0.050, and **d** x=0.075

double distilled water by sonication and dropped on a conventional carbon-coated copper grid. Sintered pellets were polished using emery papers of grade 1/0, 2/0, 3/0, and 4/0 (Sia, Switzerland) followed by polishing on a velvet cloth using diamond paste of grade 1/4-OS-475 (HIFIN). Then, these were etched thermally at 1,250 °C. Micrographs of thermally etched samples were taken using a scanning electron microscope (INSPECT 50 FEI').

Impedance analysis

Both the surfaces of sintered pellets were polished. Silver paint was applied on both the surfaces. The paint was matured by heating at 700 °C for 15 min. Impedance measurements were made in the temperature range 200–600 °C using a Novocontrol Alpha-A High Performance Frequency Analyzer in the frequency range 1 Hz to 1 MHz by applying 20-mV external ac signal. Data were collected using "Win data" program and fitted to equivalent circuit using ZView software.

Results and discussion

Crystal structure

Powder XRD patterns were recorded to check the phase purity of powder and to determine the crystal structure. Figure 1a–d shows powder XRD patterns of all the samples. Diffraction patterns were indexed on the basis of fluorite structure similar to CeO_2 using JCPDS file no. 43-1002. It has been observed that (111) and (200) peaks shift toward lower 2θ angle with increasing Sr content (x). This indicates that unit cell of co-doped ceria expands with increasing concentration of dopants. Lattice parameters determined by nonlinear least square fitting of the X-ray data using UnitCell program are given in Table 1. Increase in lattice parameter on substitution of La^{3+} and Sr^{2+} is attributed to larger ionic radius of La^{3+} (1.16 Å) and Sr^{2+} (1.26 Å) as compared to Ce^{4+} (0.97 Å) [28]. Variation of lattice parameter with strontium concentration is shown in Fig. 2. It can be seen that lattice parameter increases linearly with increase in Sr content following Vegard's law [29]. This variation can be represented as

$$a(x) = 0.54557 + 0.04228x \quad (3)$$

Average crystallite size calculated using Eq. (1) is given in Table 1. Sintered pellets have density more than 95 % of the theoretical values (Table 1).

Microstructure

Typical bright field transmission electron micrographs of the calcined powder of $Ce_{0.85}La_{0.15-x}Sr_xO_{\{2-(0.075+x/2)\}}$ are shown in Fig. 3a, b. These images clearly indicate that some particles are spherical and some are faceting in nature. Some agglomerated particles are also observed. TEM images show that average crystallite size lies in the range 18–30±4 nm. This is in good agreement with the results obtained from XRD data of calcined powders (given in Table 1). Figure 4a–d show scanning electron micrographs of samples thermally etched at 1,250 °C. Micrographs reveal a dense structure and well-defined grains separated by grain

Table 1 Crystallite size (determined from the X-ray line broadening), lattice parameter, and % theoretical density of compositions of the system $Ce_{0.85}La_{0.15-x}Sr_xO_{\{2-(0.075+x/2)\}}$

S. No.	Compositions	Crystallite size of calcined powder (nm)	Lattice parameter (Å)	% Theoretical density
1.	$Ce_{0.85}La_{0.15}O_{1.925}$	21	5.4582±0.0005	98.3 %
2.	$Ce_{0.85}La_{0.125}Sr_{0.025}O_{1.9125}$	24	5.4650±0.0004	98.2 %
3.	$Ce_{0.85}La_{0.10}Sr_{0.05}O_{1.9000}$	26	5.4760±0.0007	97.0 %
4.	$Ce_{0.85}La_{0.075}Sr_{0.075}O_{1.8875}$	25	5.4891±0.0009	95.0 %

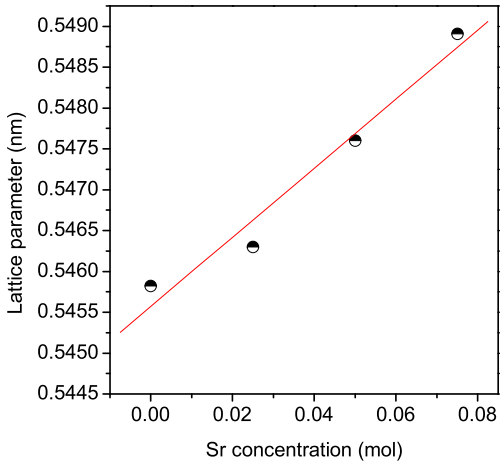

Fig. 2 Variation of lattice parameter as a function of Sr concentration for the system $Ce_{0.85}La_{0.15-x}Sr_xO_{\{2-(0.075+x/2)\}}$

boundaries. All the samples have grains of varying size. It is observed that average grain size increases with increasing concentration of Sr. Average grain size determined using linear intercept method is approx 1.0, 2.0, 4.5, and 5 μm for samples with x=0.0, 0.025, 0.05, and 0.075, respectively.

Electrical conductivity

Electrical conductivity of the samples has been determined using complex plane impedance analysis. Impedance plots for all the compositions at 200 °C are shown in Fig. 5. Typical impedance plots of the composition with x=0.025 at different temperatures are shown in Fig. 6. At 200 °C, arcs corresponding to grains and grain boundaries are clearly seen. As temperature increases, relaxation frequency of various polarization processes increases leading to shifting of arcs toward higher frequency. Therefore, all the three arcs are not observed at all the temperatures in the limited range of frequency of measurements. Arcs due to grains and grain boundaries are associated with capacitance in the pF and nF range, respectively, determined from the relation $2\pi f_{max} RC=1$, where f_{max} is the applied frequency at the arc maximum and R is the resistance obtained from the intercept of the arcs on Z′ axis. Impedance spectra were fitted to the equivalent circuits shown in Fig. 6. In equivalent circuits, the terms R_1-CPE1 and R_2-CPE2 refer to the resistance and constant phase element of the grains and grain boundaries, respectively. Use of a simple capacitor is not sufficient to model the electrical response of these materials due to microstructural inhomogenieties in the sample. A constant phase element (CPE) is, therefore, used to

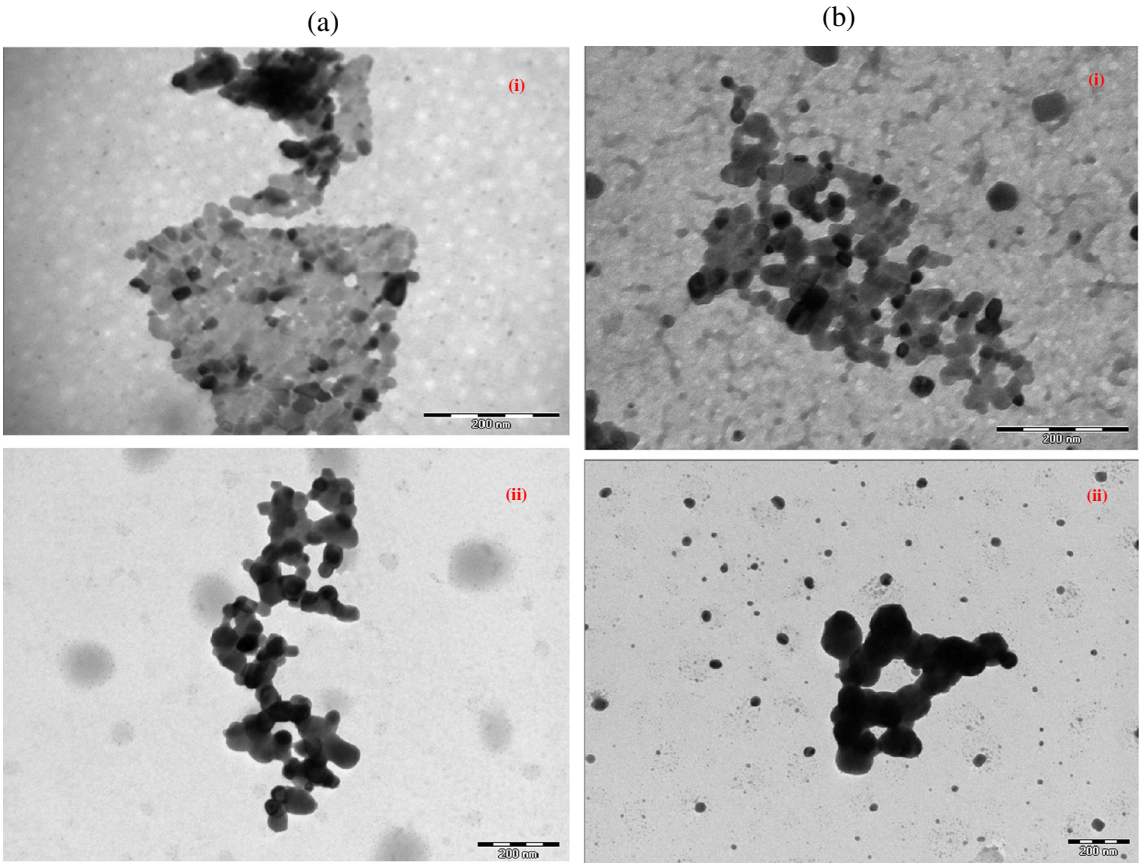

Fig. 3 **a** BFTEM images of the compositions in the system $Ce_{0.85}La_{0.15-x}Sr_xO_{\{2-(0.075+x/2)\}}$ with x=0.0 and 0.025. **b** BFTEM images of the compositions in the system $Ce_{0.85}La_{0.15-x}Sr_xO_{\{2-(0.075+x/2)\}}$ with x=0.05 and 0.075

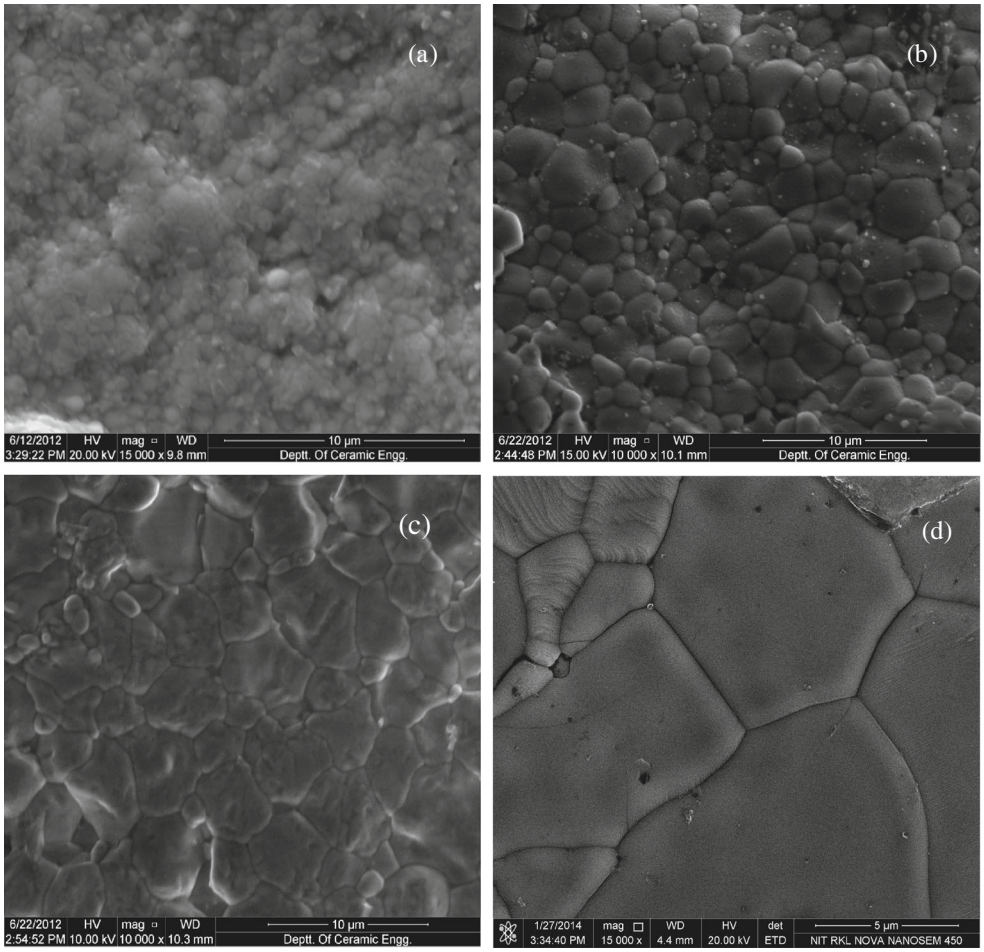

Fig. 4 Scanning electron micrographs of the system $Ce_{0.85}La_{0.15-x}Sr_xO_{\{2-(0.075+x/2)\}}$ for **a** x=0.0, **b** x=0.025, **c** x=0.050, and **d** x=0.075 thermally etched at 1,250 °C

fit the data [30]. CPE is equivalent to a distribution of capacitors in parallel. Total resistance (R_t) of the electrolyte is given by the sum of resistance of grains (R_g) and grain boundaries (R_{gb}). Conductivity, σ, at different temperatures can be obtained using the formula:

$$\sigma = \frac{L}{S \times R_t} \tag{4}$$

where L and S represent the thickness and area of the sample, respectively.

Arrhenius plots for ionic conductivity of grains for all the compositions are shown in Fig. 7. It is clear that conductivity of grains increases for the composition with x=0.025 followed by a decrease at higher concentration of Sr^{2+}. The enhancement in bulk conductivity is ascribed to an increase in the number of oxygen vacancies and suppression of ordering of oxygen vacancies which leads to a decrease in the activation energy for diffusion of O^{2-} ions [31]. Bulk conductivity decreases at higher concentration of Sr^{2+}. It may be due to increase in the number of neutral associated defect pairs $[Sr''_{Ce} - V_O^{\cdot}]^x$ which reduces free oxygen vacancies leading to a decrease in the conductivity [21].

It is noted from Fig. 7 that Arrhenius plots of co-doped samples show a change in the slope at 350 °C. It is interpreted as a transition from associated defect pairs (regions where oxygen vacancies are bound to cation defects) to dissociated defects (regions where oxygen

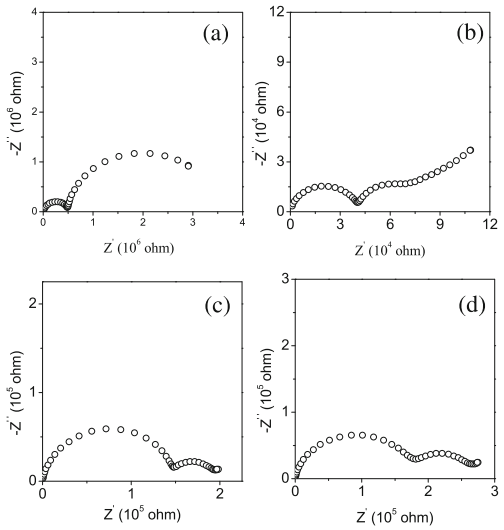

Fig. 5 Impedance plots of system $Ce_{0.85}La_{0.15-x}Sr_xO_{\{2-(0.075+x/2)\}}$ for **a** x=0.0, **b** x=0.025, **c** x=0.050, and **d** x=0.075 at 200 °C

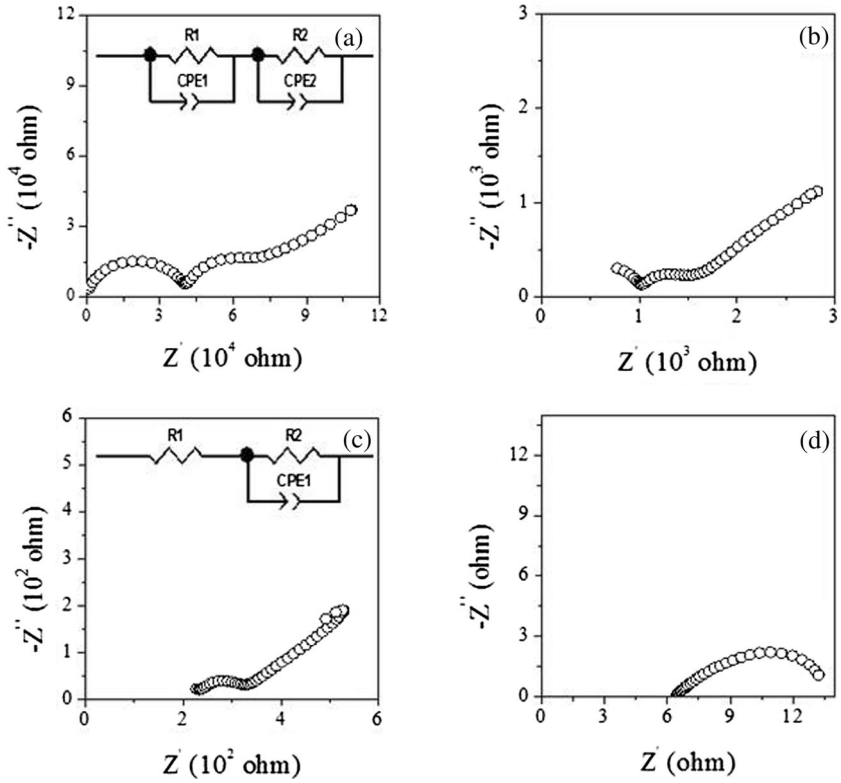

Fig. 6 Impedance plots for the composition with y=0.025 at temperature **a** 200 °C, **b** 300 °C, **c** 350 °C, and **d** 600 °C

vacancies are free). In the low temperature range, activation energy (E_a) is equal to sum of migration enthalpy (E_M) and association enthalpy (E_A), and in the high temperature region, it is equal to migration enthalpy only. At low temperatures, concentration of charge carriers is determined by the thermodynamic equilibrium between the free defects and associated defect pairs viz $[La'_{Ce}-V_O^{\cdot}]^{\cdot}$ and $[Sr''_{Ce}-V_O^{\cdot}]^{x}$ [21]. Activation energy of conduction, E_g, has been determined using Arrhenius relationship:

$$\sigma_g = \frac{\sigma_{0g}}{T}\cdot\exp\left(\frac{-E_g}{kT}\right), \tag{5}$$

where σ_{0g} is the pre-exponential factor, k is the Boltzmann constant, and T is absolute temperature. Values of activation energy for bulk ionic conductivity, E_g, for all the samples determined by fitting the data in Fig. 7 to Eq. (5) are given in Table 2. Activation energy for bulk conductivity of co-doped samples is lower than that of $Ce_{0.85}La_{0.15}O_{1.925}$. It can be noted from Table 2 that activation energy is more at low temperature and less at higher temperatures. Value of association energy ($E_A = E_a - E_M$) has been found to be minimum for the composition with x=0.025 which is 0.29 eV. It increases with increasing Sr content.

Arrhenius plots for the specific grain boundary conductivity of all the samples are shown in Fig. 8. These plots are linear having single slope. Specific grain boundary conductivity, σ^*_{gb}, was calculated using the following equation:

$$\sigma^*_{gb} = \frac{C_g}{C_{gb}}\sigma_{gb} \tag{6}$$

where C_g and C_{gb} are the bulk and grain boundary capacitance. σ_{gb} is the macroscopic grain boundary conductivity calculated from R_{gb} and the macroscopic dimensions of the sample [32]. It can be seen that grain boundary conductivity of

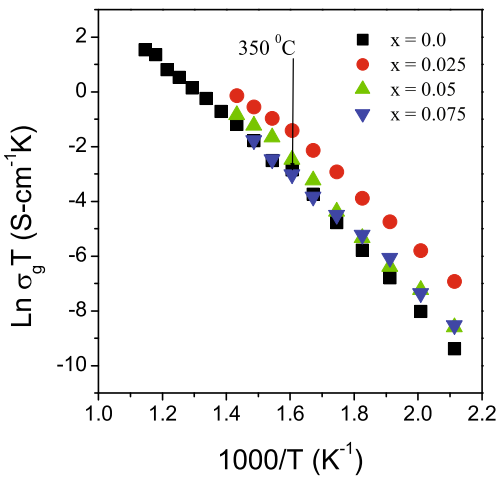

Fig. 7 Ln σ_g T versus 1,000/T plots of all the compositions of the system $Ce_{0.85}La_{0.15-x}Sr_xO_{\{2-(0.075+x/2)\}}$

Table 2 Total conductivity at 600 °C, activation energy of grains (E_g), grain boundaries (E_{gb}), and total (E_t) conductivity of various compositions in the system $Ce_{0.85}La_{0.15-x}Sr_xO_{\{2-(0.075+x/2)\}}$

S. No.	Compositions	σ_t at 600 °C (S/cm)	Eg (eV) (200–350 °C)	Eg (eV) (350–600 °C)	Egb (eV)	E_t (eV)
1.	$Ce_{0.85}La_{0.15}O_{1.925}$	9.40×10^{-4}	1.01 (200–600 °C)	–	1.30	1.06
2.	$Ce_{0.85}La_{0.125}Sr_{0.025}O_{1.9125}$	1.50×10^{-2}	0.94	0.65	1.07	0.91
3.	$Ce_{0.85}La_{0.10}Sr_{0.05}O_{1.9000}$	8.19×10^{-3}	1.03	0.70	0.99	0.98
4.	$Ce_{0.85}La_{0.075}Sr_{0.075}O_{1.8875}$	5.37×10^{-3}	1.04	0.64	0.80	0.95

co-doped samples is more than that of $Ce_{0.85}La_{0.15}O_{1.925}$. This clearly shows that doping with Sr has a significant influence on the conductivity of grain boundaries. This may be due to scavenging effect of strontium which removes siliceous impurities present at grain boundaries. Silicon increases the grain boundary resistance due to formation of resistive silicate phases. Sr^{2+} reacts with silicon present at the grain boundaries to form a second phase. This phase segregates at grain triple point junction rather than being present at the entire grain boundaries. Therefore, majority of grain boundaries become free from the resistive silicate phases. This increases the conductivity of grain boundaries substantially. This mechanism has been reported earlier [8, 33–35]. It has been reported by Gerhardt et al. [36] that grain boundary scavenging effect depends on the concentration and size of dopant. Concentration and size of the dopants control how much Si goes into solid solution and how much is segregated. On the basis of scanning transmission electron microscopy (STEM) combined with energy dispersive X-ray microanalysis (EDXM) and electron energy loss spectroscopy (EELS), Gerhardt et al. [37] reported that in yttrium-doped ceria, there exists an amorphous silica thick layer surrounding the grains. This layer blocks the charge carriers leading to increase in the resistivity of the grain boundaries. They also observed the formation of some silicate phases of yttrium. These phases pocket at the triple point junction leaving clean grain to grain contact area. Therefore, the amount of Si decreases as the concentration of dopants increases, i.e., less amount of Si is available for the formation of thick boundary layer. Similar silicate phases might have formed in the materials under present investigation. The exact compositions, morphology, and distribution of these phases require analytical studies as mentioned above.

To confirm the scavenging effect of strontium for grain boundaries, the influence of the grain boundary conductivity on the total conductivity is evaluated through the blocking factor (α_R) proposed by Gerhardt et al. [36]:

$$\propto_R = R_{gb}/R_g + R_{gb} \tag{7}$$

where R_g and R_{gb} are the resistance of the grains and grain boundaries. α_R gives the fraction of charge carriers being blocked at the impermeable internal surface under measuring conditions with respect to total number of charge carriers in the samples. The lowest blocking factor, 0.29, has been observed in the sample with x=0.025 at 375 °C which is much less than the value 0.90 [25] obtained for singly La-doped ceria. Therefore, it is concluded that strontium is an effective grain boundary scavenger.

It can also be observed that grain boundary conductivity increases with decreasing average grain size of the co-doped samples. This is because for small grain size, i.e., larger grain boundary area, the finite amount of impurity contained in the

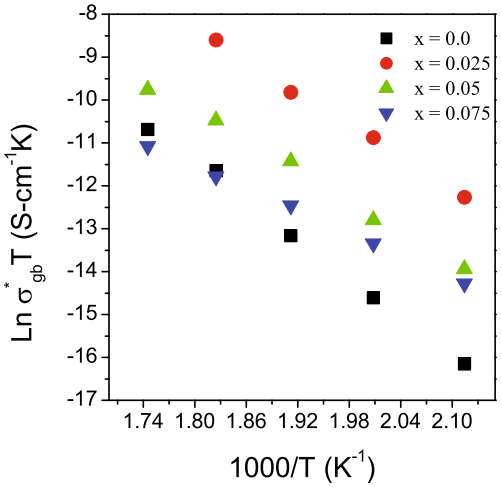

Fig. 8 Ln σ^*_{gb} T versus 1,000/T plots of all the compositions of the system $Ce_{0.85}La_{0.15-x}Sr_xO_{\{2-(0.075+x/2)\}}$

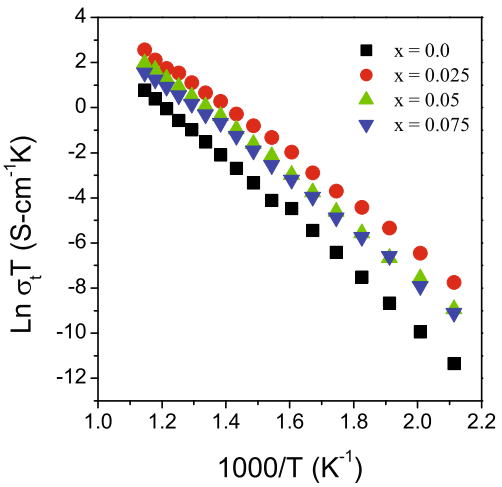

Fig. 9 Ln σ_t T versus 1,000/T plots of all the compositions of the system $Ce_{0.85}La_{0.15-x}Sr_xO_{\{2-(0.075+x/2)\}}$

sample is not sufficient to form a continuous and uniform glassy phase layer along grain boundaries. This leaves the remaining grain boundary area for clean grain to grain contact [38]. Therefore, the transport of O^{2-} ions becomes faster across the grains through clean grain boundaries.

Activation energy of the conduction for the grain boundaries, E_{gb}, was determined by fitting the data in Fig. 8 to Arrhenius relationship (Table 2):

$$\sigma^{*}_{gb} = \frac{\sigma^{*}_{0gb}}{T} exp\left(-\frac{5gb}{kT}\right) \quad (8)$$

Values of activation energy for the grain boundary conduction are given in Table 2.

Plots of Ln σ_t·T versus 1,000/T for all the compositions along with $Ce_{0.85}La_{0.15}O_{1.925}$ are shown in Fig. 9. Total conductivity of co-doped samples increases for the composition with x=0.025 as compared to the sample with x=0.00. On further increasing concentration of Sr, total conductivity decreases. Values of activation energy of total ionic conductivity, E_t, determined by fitting the data points in Fig. 9 to Eq. (9) are given in Table 2.

$$\sigma_t = \frac{\sigma_{0t}}{T} exp\left(-\frac{E_t}{KT}\right) \quad (9)$$

Values of total conductivity at 600 °C for all the compositions are given in Table 2. Composition with x=0.025 exhibits the highest conductivity among all the compositions. Its conductivity at 600 °C is higher than the highest values of conductivity reported for the compositions $Ce_{0.8}La_{0.14}Y_{0.06}O_{1.9}$ (6.1×10^{-3} S/cm) [39] $Ce_{0.8}Sm_{0.2}O_{1.9}$ (SDC) (1.20×10^{-2} S/cm) [40], and $Ce_{0.8}Gd_{0.2}O_{1.9}$ (GDC) (1.29×10^{-2} S/cm) [41] at 600 °C. This may make it a potential candidate as a solid electrolyte for IT-SOFCs. Its cost is definitely much less than the cost of CeO_2 singly doped with Sm and Gd as mentioned above. This is because La_2O_3 is cheaper than Sm_2O_3 and Gd_2O_3. Its compatibility with other cell components, however, is necessary for its application in IT-SOFC, and this needs to be checked.

Partial replacement of La with Sr in CeO_2 has some opposite effects. It leads to increase in number of oxygen vacancies. Ordering of oxygen vacancies is also suppressed due to co-doping [31]. This leads to decrease in the activation energy for conduction and increases the ionic conductivity. Sr^{2+} also acts as a grain boundary scavenger. This decreases the grain boundary resistance and hence increases the grain boundary conductivity as well as total conductivity. Number of associated defect pairs and their association energy increase with increasing Sr^{2+} substitution. This leads to decrease in the ionic conductivity. Deviation of lattice parameter on substituting La^{3+} and Sr^{2+} from that of undoped ceria increases the strain in the lattice because ionic radius increases in the order Ce^{4+} < La^{3+} < Sr^{2+} [42]. This increases the activation energy for diffusion of O^{2-} ions. Due to complex interplay of these opposite competing effects, conductivity increases for x= 0.025 followed by a decrease at higher concentration, i.e., x>0.025.

Conclusions

Co-doped ceria samples with nominal compositions $Ce_{0.85}La_{0.15-x}Sr_xO_{\{2-(0.075+x/2)\}}$ where x=0.025, 0.050, and 0.075 have been synthesized and studied to compare the conductivity with singly doped ceria. Single-phase solid solution has formed in all the compositions. For x=0.025 by sintering at 1,350 °C, 98 % theoretical density has been achieved. Composition with x=0.025 exhibits higher ionic conductivity than that of ceria-doped singly with La and almost equal to the best reported values for $Ce_{0.8}Sm_{0.2}O_{1.9}$ and $Ce_{0.8}Gd_{0.2}O_{1.9}$ at 600 °C. This makes it a potential candidate as a solid electrolyte for IT-SOFCs being much cheaper.

Acknowledgments Thanks to the Department of Science and Technology, New Delhi, for financial support. We are very much thankful to the Department of Anatomy IMS, BHU, Varanasi, for providing us the TEM facility.

References

1. Stimming U, Singhal SC, Tagawa H, Lehnert W (2002) Electrochem Soc, eds. Proc. of SOFC VIII
2. Kharton VV, Marques FMB, Atkinson A (2004) Transport properties of solid oxide electrolyte ceramics: a brief review. Solid State Ionics 174:135–149
3. Ishihara T, Tabuchi J, Ishikawa S, Yan J, Enoki M, Matsumoto H (2006) Recent progress in LaGaO3 based solid electrolyte for intermediate temperature SOFCs. Solid State Ionics 177:1949–1953
4. Sammes NM, Tompsett GA, Nafe H, Aldinger F (1999) Bismuth based oxide electrolytes—structure and ionic conductivity. J Eur Ceram Soc 19:1801–1826
5. Minh NQ, Takahashi T (1995) Science technology of ceramic fuel cells. Elsevier, Amsterdam
6. Goodenough JB (2003) Oxide ion electrolytes. Annu Rev Mater Res 33:91–128
7. Inba H, Tagawa H (1996) Ceria based electrolytes. Solid State Ionics 83:1–16
8. Steele BCH (2000) Appraisal of $Ce_{1-y}GdyO_{2-y/2}$ electrolytes for IT-SOFC operation at 500 °C. Solid State Ionics 129:95–110
9. Zha SW, Xia CR, Meng GY (2003) Effect of Gd (Sm) doping on properties of ceria electrolyte for solid oxide fuel cells. J Power Sources 115:44–48

10. Mogensen M, Sammes NM, Tompsett GA (2000) Physical chemical and electrochemical properties of pure and doped ceria. Solid State Ionics 129:63–94
11. Yahiro H, Eguchi K, Arai H (1989) Electrical properties and reducibilities of ceria-rare earth oxide systems and their application to solid oxide fuel cell. Solid State Ionics 36:71–75
12. Eguchi K, Setoguchi T, Inoue T, Arai H (1992) Electrical properties of ceria-based oxides and their application to solid oxide fuel cells. Solid State Ionics 52:165–172
13. Herle JV, Seneviratne D, McEvoy AJ (1999) Lanthanide co-doping of solid electrolytes: ac conductivity behaviors. J Eur Ceram Soc 19: 837–841
14. Mori T, Drennan J, Lee JH, Li JG, Ikegami T (2002) Oxide ionic conductivity and microstructures of Sm- or La-doped CeO_2-based systems. Solid State Ionics 154–155:461–466
15. Sha XQ, Lu Z, Huang XQ, Miao JP, Jia L (2006) Preparation and properties of rare earth co-doped $Ce_{0.8}Sm_{0.2-x}Yx O_{1.9}$ electrolyte materials for SOFC. J Alloys Compd 424:315–321
16. Singh NK, Singh P, Kumar D, Parkash O (2012) Electrical conductivity of undoped, singly doped and co-doped ceria. Ionics 18:127–134
17. Wang FY, Chen SY, Wang Q, Yu SX, Cheng SF (2004) Study on Gd and Mg co-doped ceria electrolyte for intermediate temperature solid oxide fuel cells. Catel Today 97:189–194
18. Lubke S, Wiemhofer HD (1999) Electronic conductivity of Gd-doped ceria with additional Pr-doping. Solid State Ionics 117:229–243
19. Zheng Y et al (2009) Effect of Sm and Mg co-doping on the properties of ceria-based electrolyte materials for IT-SOFCs. Mater Res Bull 44:775–779
20. Zheng Y, Shi Y, Gu H, Gao L, Chen H, Guo L (2009) La and Ca co-doped ceria-based electrolyte materials for IT-SOFCs. Mater Res Bull 44:1717–1721
21. Cioatera N, Parvulescu V, Rolle A, Vannier RN (2009) Effect of strontium addition on europium-doped ceria properties. Solid State Ionics 180:681–687
22. Yeh T-H, Chou C-C (2007) Ionic conductivity investigation in samarium and strontium co-doped ceria system. Phys Scr T129:303–307
23. Ramesh S, Vishnuvardhan Reddy C (2009) Electrical properties of co-doped ceria electrolyte $Ce_{0.8-x}Gd_{0.2}Sr_xO_{2-x}$ ($0 < x < 0.1$). Acta Phys Polon A115:909–913
24. Zheng Y, Wu L, Gu H, Gao L, Chen H, Guo L (2009) The effect of Sr on the properties of Y-doped ceria electrolyte for IT-SOFCs. J Alloys Compd 486:586–589
25. Jaiswal N, Upadhyay S, Kumar D, Parkash O (2013) Ionic conductivity investigation in lanthanum (La) and strontium (Sr) co-doped ceria system. J Power Sources 222:230–236
26. Basu S, Sujatha Devi P, Maiti HS (2004) Synthesis and properties of nano-crystalline ceria powders. J Mater Res 19:3162–3171
27. Holland TJB, Redfern SAT (1997) Unit cell refinement from powder diffraction data; the use of regression diagnostics. Mineral Mag 61: 65–77
28. Shannon RD (1976) Revised effective ionic radii and systematic studies of interatomic distances in halides and chalcogenides. Acta Crystallogr A 32:751–767
29. Vegard L, Dale H (1928) Untersuchungen über Mischkristalle und Legierungen, Zeitschrift Fur. Kristallographie 67:148–162
30. Christie GM, Berkel FPF (1996) Microstructure-ionic conductivity relationships in ceria-gadolinia electrolytes. Solid State Ionics 83:17–27
31. Yamamura H, Katoh E, Ichikawa M, Kakinuma K, Mori T, Haneda H (2000) Multiple doping effect on the electrical conductivity in the $(Ce_{1-x-y}La_xM_y)O_{2-.DELTA}$ (M=Ca, Sr) system. Electrochemistry 68: 455–459
32. Buchi SM, Roy J (2012) The effect of strontium doping on densification and electrical properties of $Ce_{0.8}Gd_{0.2}O_{2-\delta}$ electrolyte for IT-SOFC application. Ionics 18:291–297
33. Ralph JM, Kilner JA (1997) In: Stimming U, Singhal SC, Tagawa H, Lehnert W (eds) Proceedings of the fifth International Symposium on solid oxide fuel cells (SOFC-V), PV 97-40. The Electrochemical Society, Inc., Pennington, p 1021
34. Badwal SPS, Ciacchi FT, Rajendran S, Drennan J (1998) An investigation of conductivity, microstructure and stability of electrolyte compositions in the system 9 mol% (Sc_2O_3-Y_2O_3)-ZrO_2 (Al_2O_3). Solid State Ionics 109:167–186
35. Drennan J, Auchterlonie G (2000) Microstructural aspects of oxygen ion conduction in solids. Solid State Ionics 134:75–87
36. Gerhardt R, Nowick AS (1986) Grain boundary effect in ceria doped with trivalent cations: electrical measurements. J Am Ceram Soc 69: 641–646
37. Gerhardt R, Nowick AS, Mochel ME, Dumler I (1986) Grain boundary effect in ceria doped with trivalent cations: II, microstructure and microanalysis. J Am Ceram Soc 69:647–651
38. Tian C, Chan SW (2000) Ionic conductivities, sintering temperatures and microstructures of bulk ceramics CeO_2 doped with Y_2O_3. Solid State Ionics 134:89–102
39. Sha X, Lü Z, Huang X, Miao J, Ding Z, Xin X, Su W (2007) Study on La and Y co-doped ceria-based electrolyte materials. J Alloys Compd 428:59–64
40. Bryan Balazas G, Robert Glass S (1995) AC impedance studies of rare earth oxide doped ceria. Solid State Ionics 76:155–162
41. Fu Y-P, Chen SH, Huang JJ (2010) Preparation and characterization of $Ce_{0.8}$ $M_{0.2}O_{2-\delta}$ (M=Y, Gd, Sm, Nd, La) solid electrolyte materials for solid oxide fuel cells. Int J Hydrogen Energy 35:745–752
42. Kim DJ (1989) Lattice parameter, ionic conductivities, and solubility limits in fluorite structure MO_2 oxides (M=Hf^{4+}, Zr^{4+}, Ce^{4+}, Th^{4+}, U^{4+}). J Am Ceram Soc 72:1415–1421

Int. J. Appl. Ceram. Technol., 1–8 (2014)
DOI:10.1111/ijac.12327

Ceria (La^{3+}, Sr^{2+})/Carbonates Nanocomposite Electrolytes with High Electrical Conductivity for Low-temperature SOFCs

Nandini Jaiswal, Devendra Kumar, and Om Parkash*

Department of Ceramic Engineering, Indian Institute of Technology, Banaras Hindu University, Varanasi 221005, India

Shail Upadhyay

Department of Physics, Indian Institute of Technology, Banaras Hindu University, Varanasi 221005, India

A series of ceria-based nanocomposites consisting of lanthanum and strontium codoped ceria with composition $Ce_{0.89}La_{0.07}Sr_{0.04}O_{1.925}$ (CL7S4) and eutectic mixture of carbonates Li_2CO_3-Na_2CO_3 (LNCO) have been prepared by mixing nanosize powders of CL7S4 and LNCO. Samples have been characterized using differential thermal analysis, X-ray diffraction, scanning electron microscopy combined with energy-dispersive spectroscopy, thermal expansion, and impedance spectroscopy. A sharp increase in ionic conductivity is observed in all the composite specimens corresponding to superionic transition. Sample containing 35 wt% of carbonate shows the maximum conductivity (2.56×10^{-1} S/cm at 500°C) with activation energy of conduction, E_a 0.23 eV.

Introduction

During the last few decades, advanced energy conversion technologies have attracted considerable interest owing to the increase in energy demand and environmental pollution. Solid oxide fuel cells (SOFCs) are electrochemical energy devices, which convert chemical energy into electrical energy with high efficiency. SOFC contains three main components: an anode, a cathode, and a solid electrolyte. The solid electrolyte plays an important role in the operation of the cell. The electrolyte should be dense, electronically insulating and providing pathways for ionic conduction. To achieve a good performance and high efficiency of the cell, an electrolyte of high ionic conductivity in the intermediate temperatures (500–700°C) is desirable.

Enormous amount of efforts have been taken on the improvement of ionic conductivity for electrolytes including zirconia-based oxides, bismuth-based oxides, lanthanum gallate-based oxides, and ceria-based oxides.[1–5] Among these electrolytes, yttria-stabilized zirconia (YSZ) exhibits high ionic conductivity. But it operates at high temperature ~1000°C. This puts lot of constraints on using expensive materials for various components of the cell. Gadolinium (GDC)- and samarium (SDC)-doped ceria show much higher ionic conductivity as compared to YSZ in the intermediate-temperature range. But Gd and Sm are very costly. Doped ceria electrolytes show mixed ionic and electronic conductivity due to conversion of Ce^{4+} to Ce^{3+} in reducing atmosphere. This leads to a significant decrease in power output and efficiency of the cells.[6,7] To remove these problems, codoping approach has been introduced. Herle, *et al.*[8] found that ceria doped with two or more cations showed significantly higher ionic conductivity than the best singly doped ceria. Codoping suppresses ordering of oxygen vacancies leading to decrease in activation energy of conduction and hence increasing the conductivity.[9,10] $Ce_{1-x-y}Sm_xCa_yO_{2-\delta}$[11] and $Ce_{0.85}Gd_{0.10}Mg_{0.05}O_{2-\delta}$[12] are well-known examples. Alkaline earth oxides are more cost-effective than the rare earth oxides. The most distinguished feature of using alkaline earth ions as codopants is their potential as scavengers of siliceous impurities present at the grain boundaries. This increases the conductivity of grain boundaries. Kim *et al.*[13] studied the scavenging effect of SrO. It reacts with SiO_2 and the resultant material segregates at the triple point junctions of grain boundaries. This reduces the grain boundary resistance. An increase in the configurational entropy[3,14,15], modifications in the lattice strain,[16,17] and changing the grain boundary composition [3,9] may be a good approach for further enhancement in the ionic conductivity.

Recent work by Hui *et al.*[18] suggested that introducing a liquid phase at the grain boundaries/interfaces forming the composite electrolyte may improve the ionic conductivity. Composite electrolyte contains two phases:

*oprakash.cer@itbhu.ac.in

One is based on crystalline ceria oxide and other is of amorphous salts. Salts exist in a molten state, for example eutectic mixture of Li_2CO_3 and Na_2CO_3 above 500°C. It has been demonstrated that the interfaces provide more conducting channels for ions transport. The interface regions have no structural limit for creation of mobile ions.[19] This implies that interface regions have larger concentrations of mobile ions than that in the bulk. Electric field distribution in the interfaces between two phases is a key to realize the interface ionic conduction. This allows ions to move on surfaces or interfaces through high conducting pathways. It has been reported by Huang *et al.*[20] that O^{2-} ions could conduct through the bulk and interface region formed between ceria and the carbonate phases. H^+ ion conduction also occurs via HCO_3^- in H_2/O_2 fuel environment during cell operation. M^+ cations (e.g., Li^+, Na^+) and CO_3^{2-} ions also contribute to the conductivity above the melting temperature.[21] In molten carbonate fuel cells (MCFCs), the electrolyte is the eutectic mixture of Li_2CO_3 and Na_2CO_3 retained by $LiAlO_2$ insulating solid phase. The electrolyte must contain above 40 wt% of carbonates and operate at 650°C.[22] In ceria/carbonate composite, the carbonate content was used up to 40 wt% to avoid deformation of the pellets.[23] In ceria/carbonate composites, therefore, conduction of CO_3^{2-} ions is considered to be negligible.

Among the series of composite electrolytes, doped ceria–carbonate composites show a better performance than the other ceria–salt composite electrolytes.[24–30] According to previous researches, it was found that codoping enhances the electrical conductivity of ceria-based composite electrolytes.[21] Therefore, using codoped ceria/carbonate composites, conductivity may further improve at lower temperatures.

In our previous work, La^{3+} and Sr^{2+} codoped ceria nanopowders were prepared by citrate–nitrate auto-combustion method.[31] It was observed that the composition $Ce_{0.89}La_{0.07}Sr_{0.04}O_{1.925}$ (CL7S4) shows the highest ionic conductivity of all the compositions (4.75×10^{-3} S/cm at 500°C).[31] In the present work, a few compositions of CL7S4/$(Li\text{-}Na)_2CO_3$ composite electrolytes have been prepared and investigated.

Experimental

Lanthanum and strontium codoped ceria, $Ce_{0.89}La_{0.07}Sr_{0.04}O_{1.925}$ (CL7S4) powder was prepared by citrate–nitrate auto-combustion method as described in our previous paper.[30] Nanosized CL7S4 powder was mixed thoroughly with binary mixture of $(Li\text{-}Na)_2CO_3$ (52 mol% Li_2CO_3:48 mol% Na_2CO_3) (LNCO). The weight ratios of CL7S4:LNCO were 80:20, 70:30, and 65:35 designated as CL7S4/20LNCO, CL7S4/30LNCO, and CL7S4/35LNCO, respectively. The mixtures were ground for 5 h in acetone employing Fritsch Pulverisette ball mill in zirconia jars making use of zirconia balls as grinding media. Milled powders were drying in an oven at 60°C for 24 h. Dried powders were calcined at 600°C for 2 h in air. The resultant powder was pressed uniaxially into cylindrical pellets (diameter ~15-mm, thickness ~2-mm) under a load of 5 tons using a hydraulic press. Pellets were sintered at 700°C for one and half an hour.

Thermal behavior of the composites was studied using a NETZSCH Gerate Bau DTA at a heating rate of 10°C/min over the temperature range 100–800°C in N_2 atmosphere. X-ray powder diffraction (XRD) patterns were recorded with Rigaku X-ray diffractometer using CuKα radiation and Ni filter. Average crystallite size was calculated using Scherrer's formula:

$$D = 0.9\lambda/\beta\cos\theta \quad (1)$$

where β is the full width at half maxima (FWHM) excluding instrumental broadening, λ is the wavelength of X-rays, and θ is Bragg angle. β is taken for the strongest Bragg's peak corresponding to (111) reflection for all the samples. Experimental density of the sintered pellets was determined by Archimedes principle. Theoretical density was calculated using mixture rule.

Micrographs and energy-dispersive spectra of all the samples were taken using FEI Nova NanoSEM. Bars of dimension 50 mm × 10 mm × 4 mm were prepared for measuring thermal expansion from room temperature to 700°C in the air with a heating rate of 5°C/min. Sintered pellets were polished on both the sides using emery paper of grade 1/0, 2/0, 3/0, and 4/0 Sia Switzerland. High-temperature silver paste in an epoxy was applied on both the surfaces of polished pellets and pellets were heated at 700°C for 15 min to form a smooth conducting silver layer on both the surfaces. Two probe impedance measurements were taken using Novocontrol Alpha-A high-performance frequency analyzer in air in the temperature range 200–700°C and frequency range 1 Hz–1 MHz with an ac signal of 20 mV. Data were collected using "Win data" program and fitted to equivalent circuits using "ZView" software. Impedance measurement of carbonate mixture was also taken by same procedure. The error in conductivity measurement at temperature above melting point may be caused due to disturbance of molten carbonate phase.

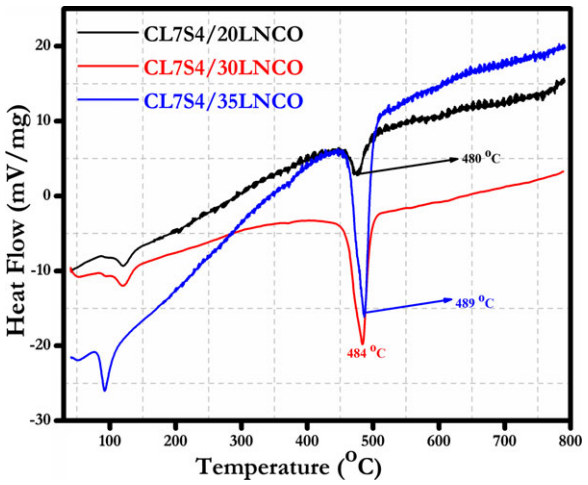

Fig. 1. DTA plots of all the composite samples.

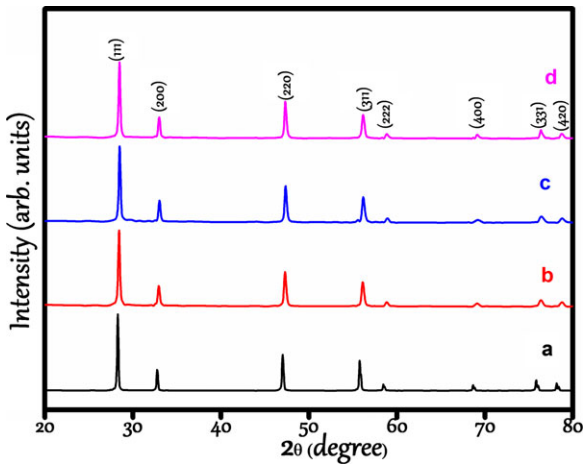

Fig. 2. Powder X-ray diffraction patterns of various compositions (a) CL7S4/35 LNCO (b) CL7S4/30 LNCO (c) CL7S4/20 LNCO, and (d) CL7S4 sintered powders.

Result and Discussion

DTA plots of all the composites are shown in Fig. 1. Two endothermic peaks have been observed in the DTA plot for all the composites. One is observed in the temperature range 100–150°C. This is due to evaporation of adsorbed moisture. Second endothermic peaks observed at 480, 484, and 489°C in CL7S4/20LNCO, CL7S4/30LNCO, and CL7S4/35LNCO, respectively, correspond to melting of eutectic carbonate mixture. These curves show that there is no chemical reaction between ceria and carbonates phases. Molten $(Li\text{-}Na)_2CO_3$ fills in the interspaces between the ceria particles and increases the density at working temperature. No endothermic or exothermic peaks are present above 500°C. Based on DTA results, composite samples were calcined at 600°C for 2 h.

Figure 2 shows XRD patterns of CL7S4/LNCO composites sintered at 700°C along with CL7S4 (sintered at 1350°C). XRD patterns have been indexed based on fluorite structure similar to ceria. No peak due to any secondary phase has been observed in the powder XRD pattern of CL7S4.[31] Absence of diffraction peaks due to carbonates in the patterns shows that these exist in an amorphous state. The density of the sintered composite pellets is found to be in the range 82–85% of the theoretical density. This is because sintering was carried out at low temperature of 700°C. Composites, however, can still be used as an electrolyte because carbonates melt at working temperature and serve as seals to avoid crossover of gases.[26] Average crystallite size of synthesized composites has been found in the range of 15–20 nm. Nanosized particles lead to more interaction among the two phases particles due to large surface area which tends to create large interface region.

Micrographs of CL7S4 and all the composite samples are shown in Figs. 3(a–d). It can be seen from Figs. 3(b–d) that CL7S4 grains are surrounded by the amorphous carbonate phase. As carbonate content increases, a continuous carbonate layer is formed. It can also be observed from these micrographs that percolated islands of ceria and carbonate phases having dimensions of the order of few micrometers have been formed. Due to the presence of large pores between ceramic grains, percolation of the carbonate phase is obvious. It can be seen from micrographs that average grain size of composites is less than 100 nm. These micrographs show that the interface between ceria and carbonates phase provides more paths for ionic conduction. Figure. 4 shows EDS spectrum of CL7S4/35LNCO composite. Higher-contrast regions represent crystalline phase and the light gray regions correspond to the amorphous phase.[21] It should be noted that Li cannot be detected by EDS.

Dilatometric curves of all the composites are shown in Fig. 5. It can be seen that thermal expansion behavior of all the samples is nonlinear with temperature having an inflection point in the temperature range 450–500°C. Inflection point around 450°C is attributed to the phase transition of carbonate from the solid to softening phase. Around 500°C, remaining carbonates melt and fill in the interspaces forming a continuous path. Above 500°C, thermal expansion curve is again linear. It can also be seen from Fig. 5 that below 450°C, thermal expansion of composites increases with increase in carbonates content. Values of thermal expansion coefficient are given in Table I.

Impedance measurements have been taken in air in the temperature range 200–700°C. Figures. 6 (a–f) show

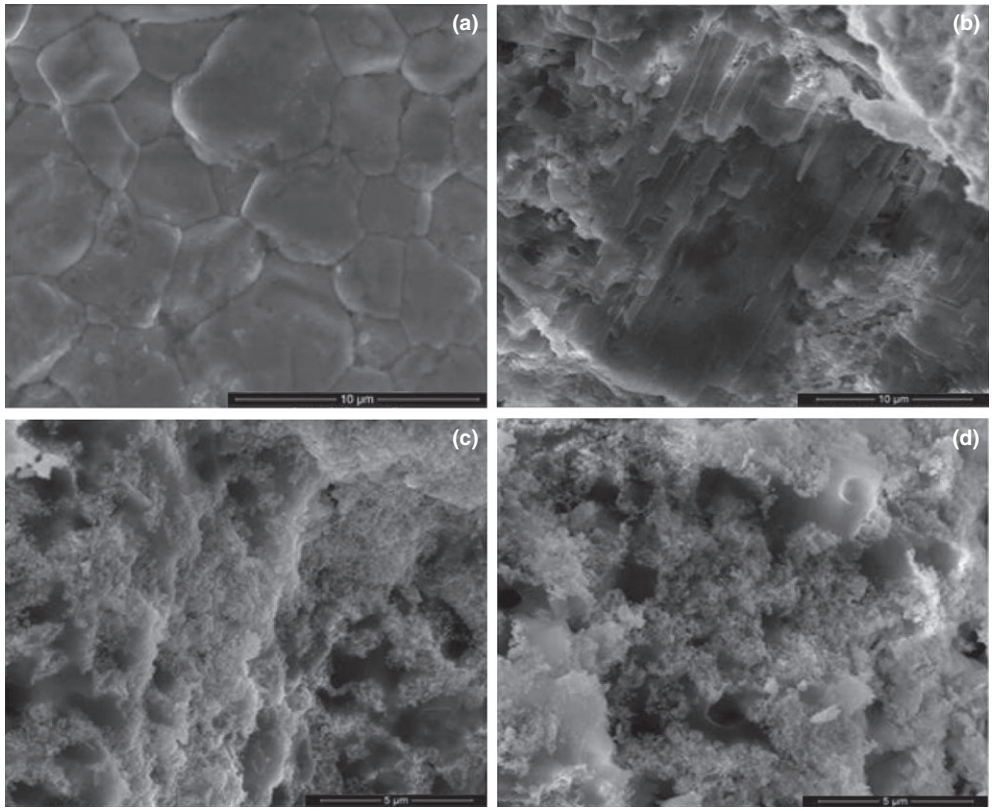

Fig. 3. Scanning electron micrograph of all the compositions (a) CL7S4: after polishing and thermal etching (b) CL7S4/20 LNCO: fractured sample (c) CL7S4/30 LNCO: fractured sample, and (d) CL7S4/35 LNCO: fractured sample.

typical Nyquist plots of the CL7S4/35LNCO composite at different temperatures. At 200°C, two depressed high-frequency arcs and a low-frequency tail have been observed. The high-frequency arcs correspond to grains and grain boundaries contribution and the tail in the low-frequency region corresponds to electrode/electrolyte interface to the total resistance. The unique feature of the impedance spectra is that the arcs due to grains and grain boundaries are not distinct. This provides an evidence for the major role of the carbonates in the composite electrolyte. As temperature increases, relaxation frequency of various polarization processes increases leading to shifting of the arcs toward higher frequency. Arcs due to grains and grain boundaries disappear above 350°C. At higher temperature, only the arc due to electrode polarization is observed. The arc shown in Fig. 6(c) is the low-frequency electrode arc. This arc is large because of the barrier between the ionic conduction in the electrolyte and electronic conduction in the electrode.[25] In Figs. 6 (d–f), the electrode arc is associated with tail which is ascribed to mass transfer process.[26] It has been cleared from this distinct phenomenon that the conduction mechanism in the composite electrolytes is different from the ceria-based ceramic electrolyte. Impedance spectra have been fitted to equivalent circuits. Below 250°C, the equivalent circuit consists of two parallel (R–CPE) circuits connected in series. One is due to grains and other is due to grain boundaries. Above 250°C, equivalent circuit consists of $(R_1)_{Grain}$ and $(R_2\text{–}CPE2)_{Grain\ boundary}$ connected in series. Use of a simple capacitor is not sufficient to model the electrical response of the materials due to the presence of microstructural inhomogeneities. A constant-phase element (CPE) is, therefore, used to fit the data.[32] CPE is equivalent to a distribution of relaxation times. Above 350°C, the total resistance is determined from the intercept on the real axis (Z') in the complex plane impedance plots on the higher-frequency side. Total conductivity of the samples is calculated using the following relation:

$$\sigma_t = \frac{L}{S \times R_t} \tag{2}$$

where σ_t is the total conductivity, R_t is the total resistance, L is the thickness, and S is the area of the sample.

Figure. 7 shows Arrhenius plots of total conductivity for CL7S4/LNCO composites along with those of

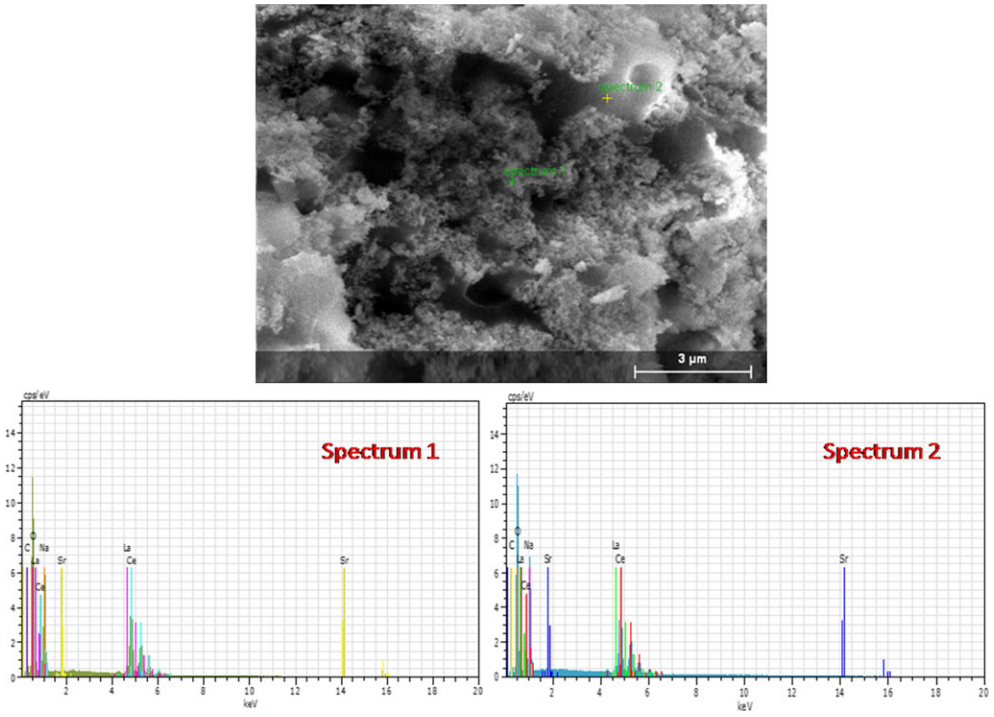

Fig. 4. SEM image of CL7S4/35 LNCO composite with EDS points: Spectrum 1 and Spectrum 2.

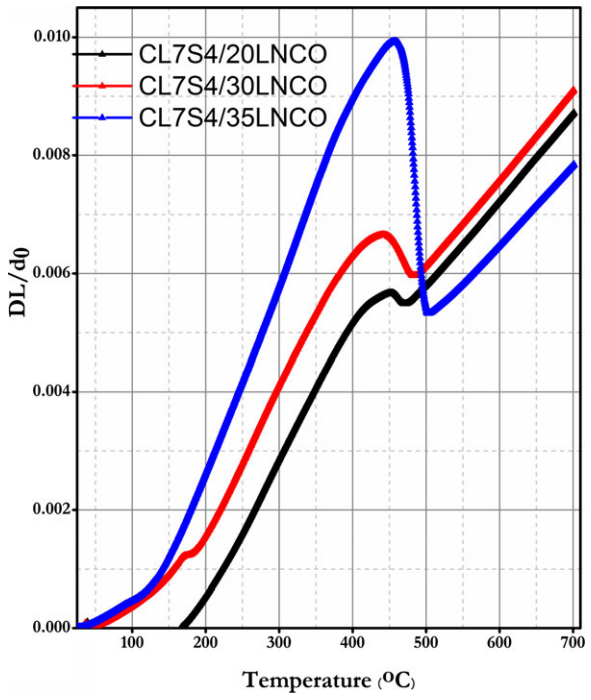

Fig. 5. Thermal expansion curves for CL7S4/LNCO composites.

CL7S4 and LNCO eutectic mixture. It is noted from Fig. 6 that a sharp increase in conductivity is observed at 400°C. It is referred to as superionic phase transition at

Table I. Coefficient of Thermal Expansion of All the Composites

S. No.	Compositions	CTE (K^{-1})
1.	CL7S4/20LNCO	4.8×10^{-6}
2.	CL7S4/30LNCO	5.0×10^{-6}
3.	CL7S4/35LNCO	5.6×10^{-6}

the interfaces.[33] Similar behavior has also been reported on mixed lanthanum, cerium, and praseodymium carbonates (LCP)/(Li-Na)$_2$CO$_3$ composites by Zhu *et al.*[34] The transition temperature is lower than the melting temperature of carbonate mixture due to interaction between ceria and carbonate phases. This leads to the threshold percolation to form a highly conducting continuous path at the interfaces below the melting temperature.[23] The interfaces formed between ceria and carbonate phases in the composites have no structural limits and have large number of cationic defects than that in the bulk.

Below the transition point, conductivity of the composites is less than that of CL7S4. Because, migration of ions has been blocked by solid dispersed amorphous carbonate phase. Conductivity of composites is higher than that of CL7S4 and LNCO above the melting temperature and increases with increasing carbonate content.

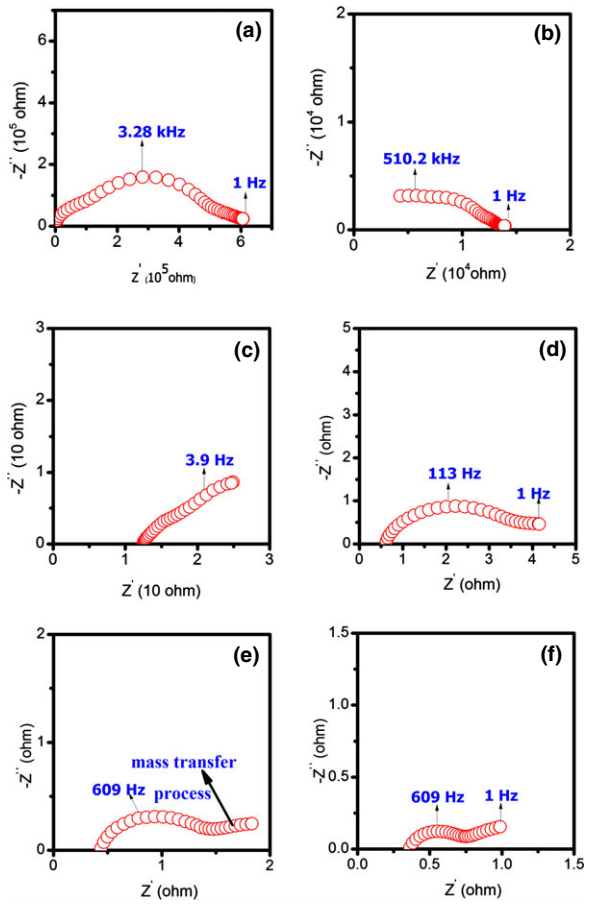

Fig. 6. Impedance plots of CL7S4/35LNCO at temperatures (a) 225 (b) 300 (c) 375 (d) 475 (e) 575, and (f) 675°C.

This is attributed to conduction of O^{2-} ions at the interfaces rather than in the bulk due to interaction between CL7S4 and LNCO phases[25,26,34]. Conductivity of the composite for higher content of carbonates >35 wt% is not investigated because these contain a large volume of liquid. This may be deleterious for the measurements.

Above the transition point, concentration of ionic defects in the interfaces and constituent phases increases due to melting from sublattice to bulk.[23] At elevated temperatures, M^+ (Li^+, Na^+) and CO_3^{2-} ions in carbonates are highly mobile together with O^{2-} ions, resulting in higher conductivity than that of the codoped ceria. In the molten carbonate phase, O^{2-} conduction occurs due to equilibrium between CO_3^{2-} and O^{2-} ions as given below:[28,35]

$$CO_3^{2-} \leftrightarrow CO_2 + O^{2-} \tag{3}$$

Therefore, the carbonate phase also provides a conducting path for O^{2-} ions in addition to ceria phase.

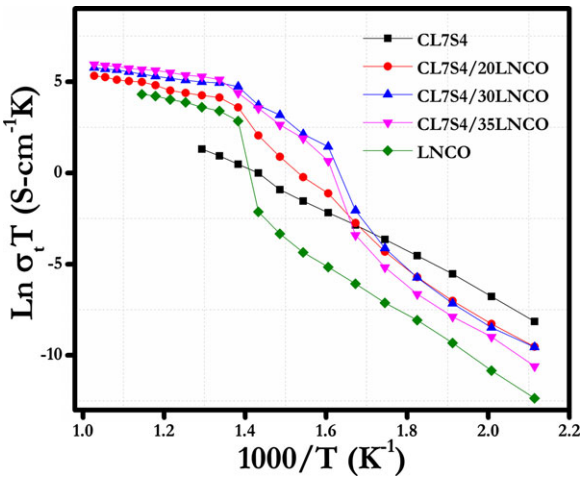

Fig. 7. Arrhenius plots of total conductivity for all the compositions in air.

After melting, carbonates fill in the interspaces. This generates more interfaces for transport of ions.

Conduction mechanism in composite electrolytes can be explained using the theory of defect chemistry.[36,37] O^{2-} ion conduction in doped ceria occurs by migration of oxygen ions through vacancies of oxygen ion generated by doping of La_2O_3 and SrO in CeO_2 as follows:

$$La_2O_3 \overset{2CeO_2}{\rightarrow} 2La'_{Ce} + 3O_O^{\times} + V_{\ddot{O}} \tag{4}$$

$$SrO \overset{CeO_2}{\rightarrow} Sr''_{Ce} + 2O_O^{\times} + V_{\ddot{O}} \tag{5}$$

where the symbols are used in accordance with Kroger–Vink notation of defects. In the presence of carbonates, oxygen ions may accumulate on the surface of the CL7S4 bulk resulting in higher concentration of oxygen vacancies in the bulk of CL7S4 due to interfacial interaction.

$$O_O^X + V_S \leftrightarrow V_{\dot{O}} + O''_S \tag{6}$$

In case of alkali carbonate (M_2CO_3, M = Li, Na, and K) phase, a reaction occurs on the surface of the bulk as follows:

$$M_M^X + V_S \leftrightarrow M_{\dot{S}} + V'_M \tag{7}$$

$$M_{\dot{S}} + V_i \leftrightarrow M_i + V'_M \tag{8}$$

subscripts M, S, and i represent the regular M lattice site, surface site, and interstitial site, respectively. This reaction increases M^+ ion concentration on the surface of one grain and equivalent number vacancies of M^+ on the surface of adjacent grain.[37] This may form a space charge layer on the surface of ceria/carbonate phases which

enhances the rate of cation disorder reaction [given by Eqs. (6) and (7)] leading to enrichment of cations at the interfaces. Huang *et al.*[23] argued that cationic defect concentration is much higher in the space charge zones near phase boundaries than in the bulk. Mobility of defects in the space charge zone is higher due to melting from sublattice to bulk. Therefore, concentration of cation vacancies increases in the bulk and carbonate phase. Certainly, this enhances the conductivity below the melting temperature of the carbonates.

$$M_M^{\cdot} V_A \leftrightarrow M_A + V_M' \tag{9}$$

$$M_A^{\cdot} + V_i \leftrightarrow M_i + V_A' \tag{10}$$

where "A" denotes the interface site. Conductivity of CL7S4/35LNCO composite is 2.56×10^{-1} S/cm at 500°C, which is much higher than the value of 4.75×10^{-3} S/cm found in CL7S4 at the same temperature.[31] This value is also higher than 0.01 S/cm reported for $Ce_{0.8}Sm_{0.1}Nd_{0.1}O_{1.9}/(Li/Na)_2CO_3$ by Liu *et al.* at 481°C.[21] Enhancement in the conductivity with the carbonate concentration can be explained using percolation model. According to this model, electrical conductivity of the composites varies linearly with the volume fraction of the molten carbonate phase. The relation between the conductivity of composite electrolyte and molten carbonate content can be given by Archie equation as given below[38]:

$$\frac{\sigma}{\sigma_0} a\varphi^m \tag{11}$$

where σ, σ_0, a, ϕ, and m are the total measured conductivity, conductivity of the carbonates, a constant, molten salt content, and cementation index, respectively. Cementation index represents the solid packing circumstance and depends on the interaction between solid and molten carbonate phase. Archie plot of the CL7S4/LNCO composites is shown in Fig. 8. It is observed that logarithm of total conductivity of CL7S4/LNCO composites normalized by the conductivity of carbonates varies linearly with the logarithm of volume fraction of molten carbonate phase.

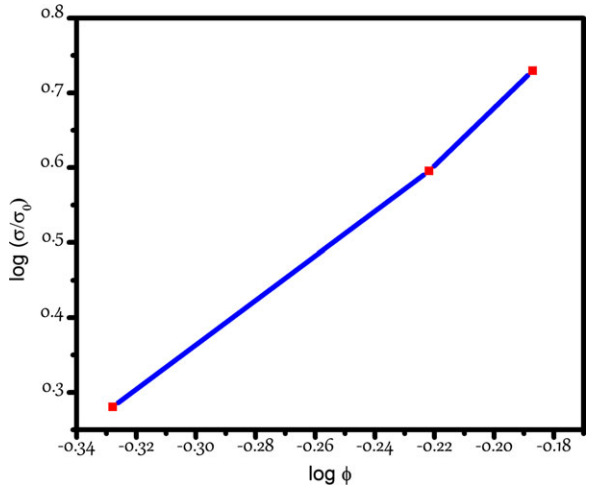

Fig. 8. Archie plot for CL7S4/LNCO composites.

Activation energy of conduction, E_a, has been determined using Arrhenius relationship:

$$\sigma = \sigma_0 \exp\left(\frac{-E_a}{kT}\right) \tag{12}$$

where σ_0 is the preexponential factor, k is the Boltzmann constant, and T is the absolute temperature. It can be clearly seen from Eq.(12) that conductivity, σ, can be enhanced either by increasing σ_0 or by decreasing E_a. Below the transition point, the activation energy is higher in all the composites as compared to that of CL7S4. This may be due to inhibition of oxide ions by solid carbonate phase at lower temperatures. Activation energy for CL7S4/35LNCO above the transition point is 0.23 eV. This is much smaller than the value 0.89 eV obtained by Wang *et al.*[39] It again provides the role of molten carbonate phase. This may be due to easier migration of O^{2-} ion in the molten carbonate phase than that in the bulk ceria phase. It can also be observed from Table II that activation energy decreases with increasing

Table II. Total Conductivity at 500°C and Activation Energy at Temperature >400°C for All the Samples

S. No.	Compositions	σ_t at 500°C S/cm	E_a > 400°C (eV)
1.	CL7S4	4.75×10^{-3}*	0.91 (200–500 °C)*
2.	LNCO	4.73×10^{-2}	0.30
3.	CL7S4/20LNCO	9.13×10^{-2}	0.35
4.	CL7S4/30LNCO	1.88×10^{-1}	0.25
5.	CL7S4/35LNCO	2.56×10^{-1}	0.23

*Data taken from previous work.[27]

volume fraction of the carbonate content. Therefore, it is concluded that above the melting point, conductivity of the composite electrolytes is predominantly due to interfacial oxygen ion migration. This results in low-activation energy and high ionic conductivity.

Conclusions

Composites of $Ce_{0.89}La_{0.07}Sr_{0.04}O_{1.925}$ with various amounts of $(Li\text{-}Na)_2CO_3$ have been prepared by mixing $Ce_{0.89}La_{0.07}Sr_{0.04}O_{1.925}$ nanosized powder prepared by citrate–nitrate auto-combustion method with $(Li\text{-}Na)_2CO_3$ and sintered at 700°C for one and half an hour. Single phase formation has been observed in all the composites. Micrographs show homogeneous distribution of both the phases with ceria grains surrounded by amorphous carbonate phase. Impedance spectroscopy provides evidence that the charge transport in the composites is different from that in ceria-based electrolytes. A sharp increase in the conductivity occurs at 400°C. This is attributed to superionic conduction at the interfaces. Composite CL7S4/35LNCO shows the maximum conductivity of 2.56×10^{-1} S/cm at 500°C. Activation energy of conduction in CL7S4/35LNCO composite is found to be 0.23 eV. This may make this composite useful for application in LT-SOFCs (500°C).

Acknowledgments

We are thankful to Department of Science and Technology, New Delhi and MHRD for financial support. We are also very much thankful to Prof. S. K. Pratihar, Department of Ceramic Engineering, NIT Rourkela for providing SEM/EDX facility.

References

1. V. V. Kharton, F. M. B. Marques, and A. Atkinson, *Solid State Ionics.*, 174 [1–4] 135–149 (2004).
2. T. Ishihara, J. Tabuchi, S. Ishikawa, J. Yan, M. Enoki, and H. Matsumoto, *Solid State Ionics*, 177 [19–25] 1949–1953 (2006).
3. N. M. Sammes, G. A. Tompsett, H. Näfe, and F. Aldinger, *J. Eur. Ceram. Soc.*, 19 [10] 1801–1826 (1999).
4. N. Q. Minh, *Science and Technology of Ceramic Fuel Cells*, Elsevier, Amsterdam, 1995.
5. J. B. Goodenough Annu, *Annu. Rev. Mater. Res.*, 33 91–128 (2003).
6. M. Dudek, *J. Eur. Ceram. Soc.*, 28 [5] 965–971 (2008).
7. S. K. Tadokoro and E. N. S. Muccillo, *J. Eur. Ceram. Soc.*, 27 [13–15] 4261–4264 (2007).
8. V. J. Herle, D. Senevirante, and A. J. McEvoy, *J. Eur. Ceram. Soc.*, 19 [6–7] 837–841 (1999).
9. A. Boden, J. Di, C. Lagergren, G. Lindbergh, and C. Y. Wang, *J. Power Sources*, 172 [2] 520–529 (2007).
10. W. Zajac and J. Molenda, *Solid State Ionics*, 179 [1–6] 154–158 (2008).
11. T. Mori, J. Drennan, J. H. Lee, J. G. Li, and T. Ikegami, *Solid State Ionics*, 154–155 461-66 (2002).
12. F. Y. Wang, S. Y. Chen, Q. Wang, S. X. Yu, and S. F. Cheng, *Catel. Today*, 97 189–194 (2004).
13. Y. H. Cho, P. S. Cho, G. Auchterlonie, D. K. Kim, J. H. Lee, and D. Y. Kim, *Acta Mater.*, 55 4807–4815 (2007).
14. S. Omar, E. D. Wachsman, and J. C. Nino, *Solid State Ionics*, 178 1890–1897 (2008).
15. H. Yamamura, E. Katoh, M. Ichikawa, K. Kakinuma, T. Mori, and H. Haneda, *Electrochem. Commun.*, 68, 455–459 (2000).
16. B. C. H. Steele, *Solid State Ionics*, 129 95–110 (2000).
17. D. J. Kim, *J. Am. Ceram. Soc.*, 72 1415–1421 (1989).
18. H. Shiqiang, *et al.*, *J. Power Sources*, 172 493–502 (2007).
19. B. Zhu, S. Li, and B. E. Mellander, *Electrochem. Commun.*, 10 [2] 302–305 (2008).
20. J. Huang, L. Yang, R. Gao, Z. Mao, and C. Wang, *Electrochem. Commun.*, 8 [5] 785–789 (2006).
21. W. Liu, Y. Liu, B. Li, D. T. Sparks, X. Wei, and W. Pan, *Compos. Sci. Technol.*, 70 [1] 181–185 (2010).
22. B. Zhu and M. D. Mat, *Electrochem. Sci.*, 1, 383–402 (2006).
23. J. B. Huang, Z. Q. Mao, Z. X. Liu, and C. Wang, *Electrochem. Commun.*, 9 [10] 2601–2605 (2007).
24. B. Zhu, *J. Power Sources*, 114 [1] 1–9 (2003).
25. X. Wang, Y. Ma, R. Raza, M. Muhammed, and B. Zhu, *Electrochem. Commun.*, 10 [10] 1617–1620 (2008).
26. J. Di, M. Chen, C. Wang, J. Zheng, L. Fan, and B. Zhu, *J. Power Sources*, 195 [15] 4695–4699 (2010).
27. L. Fan, C. Wang, M. Chen, J. Di, J. Zheng, and B. Zhu, *Int. J. Hydrogen Energy*, 36 9987–9993 (2011).
28. X. Wang, Y. Ma, S. Li, A. H. Kashyout, B. Zhu, and M. Muhammed, *J. Power Sources*, 196 [5] 2754–2758 (2011).
29. J. Huang, Z. Mao, L. Yang, and R. Peng, *Electrochem. Solid-State Lett.*, 8 A437–A440 (2005).
30. C. M. Lapa, F. M. L. Figueiredo, D. P. F. de Souza, L. Song, B. Zhu, and F. M. B. Marques, *Int. J. Hydrogen Energy*, 35 2953–2957 (2010).
31. N. Jaiswal, S. Upadhyay, D. Kumar, and O. Parkash, *J. Power Sources*, 222 230–236 (2013).
32. G. M. Christie and F. P. F. Berkel, *Solid State Ionics*, 83 [1–2] 17–27 (1996).
33. T. Schober, *Electrochem. Solid State Lett.*, 8 [4] A199–A200 (2005).
34. B. Zhu, X. R. Liu, Z. G. Zhu, and R. Ljungberg, *Int. J. Hydrogen Energy*, 33 3385–3392 (2008).
35. J. Huang, Z. Gao, and Z. Mao, *Int. J. Hydrogen Energy*, 35 4270–4275 (2010).
36. S. S. Bhoga and K. Singh, *Solid State Ionics*, 111 [1–2] 85–92 (1998).
37. Y. C. Zhao, C. Xia, Y. J. Wang, Z. R. Xu, and Y. D. Li, *Int. J. Hydrogen Energy*, 37 8556–8561 (2012).
38. M. Mizuhata, A. B. Bleke, H. Watanabe, Y. Harada, and S. Deki, *Electrochim. Acta*, 53 [1] 71–78 (2007).
39. S. Li, X. D. Wang, and B. Zhu, *Electrochem. Commun.*, 9 2861–2866 (2007).

Available online at www.sciencedirect.com

ScienceDirect

journal homepage: www.elsevier.com/locate/he

Ionic conduction in Mg^{2+} and Sr^{2+} co-doped ceria/carbonates nanocomposite electrolytes

Nandini Jaiswal [a], *Shail Upadhyay* [b], *Devendra Kumar* [a], *Om Parkash* [a,*]

[a] *Department of Ceramic Engineering, Indian Institute of Technology, Banaras Hindu University, Varanasi- 221005, India*

[b] *Department of Physics, Indian Institute of Technology, Banaras Hindu University, Varanasi- 221005, India*

ARTICLE INFO

Article history:
Received 13 September 2014
Received in revised form
17 December 2014
Accepted 1 January 2015
Available online 28 January 2015

Keywords:
Co-doped ceria
Nanocomposite
Electrical conductivity
LT-SOFC

ABSTRACT

Nanocomposite electrolytes consisting of Mg^{2+} and Sr^{2+} co-doped ceria (CM6S4) and eutectic mixture of $(Li–Na)_2CO_3$ (LNCO) have been synthesized and characterized using XRD and SEM. Thermal expansion and electrical conductivity have been studied as a function of temperature. All the samples have fluorite structure similar to ceria and carbonates are present as an amorphous phase surrounding the ceria phase. Impedance measurements have been made in air in the temperature range 200–650 °C. Conductivity of the composites increases very rapidly around the softening temperature of the carbonates. After melting, carbonates fill in the interspaces of the ceria phase and form a percolated network. This leads to the formation of high conducting pathways at the interfaces. Composition CM6S4/35LNCO shows the highest conductivity, 0.4 S/cm at 500 °C which is two orders of magnitude higher than that of CM6S4 (2.4×10^{-3} S/cm). This improvement in the conductivity has been ascribed to the interfacial ionic conduction.

Introduction

Intermediate temperature solid oxide fuel cells (IT-SOFCs) have been investigated extensively in the last few years being highly efficient, environment friendly with very low emission of pollutant gases [1]. Solid electrolyte having adequate high oxygen ions conductivity in the intermediate temperature range (500–700 °C) is a key component of IT-SOFCs [1]. Lower temperature operation of these cells as compared to the currently used SOFCs based on yttria stabilized zirconia (YSZ) facilitates the use of cheaper materials for various components of the cells/cells stack. Some doped and co-doped ceria based solid electrolytes e.g. $Ce_{0.80}Sm_{0.20}O_{1.90}$ (SDC) [2], $Ce_{0.80}Gd_{0.20}O_{1.90}$ (GDC) [3], and $Ce_{0.80}Gd_{0.2-x}Sm_xO_{1.9}$ [4] etc has been reported to possess ionic conductivity of ~10^{-2} S/cm at 500–700 °C. One problem associated with the use of ceria based electrolytes in this temperature range is the tendency of Ce^{4+} to get reduced to Ce^{3+} in the reducing atmosphere at the anode. This gives rise to electronic conductivity leading to short circuiting of the cell. The research has been focused to decrease the operating temperature of SOFCs below 600 °C abbreviated as low temperature SOFC (LT-SOFC) [5–7].

Ceria/salt based composites especially ceria/carbonates show much higher ionic conductivity in the range 0.01–1 S/cm and a performance of 300–1100 mW/cm^2 at 400–600 °C [8]. Ceria/carbonate composites contain two phases at the

* *Corresponding author*. Tel.: +91 542 6701791; fax: +91 542 2368428.
E-mail address: oprakash.cer@itbhu.ac.in (O. Parkash).
http://dx.doi.org/10.1016/j.ijhydene.2015.01.002

working temperature of SOFCs viz the ceria phase and the molten carbonate phase. H^+ and CO_3^{2-} ions also contribute to the conductivity above the melting point of the carbonates in addition to O^{2-} ions [9]. O^{2-} ions conduct via bulk ceria and the interfaces between ceria and carbonate phases. H^+ ions transport via CO_3^{2-} (HCO_3^-) through the interfaces [10]. Multi-ions conduction, therefore, improves the performance of the SOFCs.

Zhu et al. [11–17] suggested the idea of nanocomposite to further improve the performance of the composites. Nano-sized powders provide large surface area for interaction between the two phases. This leads to superionic conduction at very low temperatures (300–600 °C). This is due to an enhancement in the area of the interfacial region leads to increase the density of mobile defects in the space charge region [18]. Gao et al. [19] studied the performance of SDC/Na_2CO_3 composite based fuel cells using SDC particles of size less than 100 nm. They reported that SDC/Na_2CO_3 nanocomposite shows conductivity several times higher than that of SDC/Na_2CO_3 microcomposite.

In our previous work, nanocrystalline Mg and Sr co-doped ceria powders were synthesized successfully via citrate-nitrate auto-combustion method [20]. It was found that conductivity of the composition $Ce_{0.90}Mg_{0.06}Sr_{0.04}O_{1.90}$ (CM6S4) shows the highest conductivity of 2.0×10^{-2} S/cm at 700 °C with an activation energy of conduction 0.85 eV. In the present work, CM6S4/(Li–Na)$_2CO_3$ nanocomposites have been prepared to further enhance the ionic conductivity at lower temperatures. In addition, effect of the carbonate content on the phase, microstructure and electrical conductivity of CM6S4/(Li–Na)$_2CO_3$ have been investigated. It is worth mention that use of both the alkaline earth element as dopants in this composition in place of one or two rare earth ions will reduce the cost of the electrolyte considerably.

Experimental

Mg^{2+} and Sr^{2+} co-doped nanocrystalline ceria powders were synthesized via citrate-nitrate auto-combustion method [20]. These powders were mixed with binary mixture of Li_2CO_3 and Na_2CO_3 having a molar ratio 52:48. The weight ratios of the co-doped ceria powder and carbonate mixture were 80:20, 70:30 and 65:35 and the corresponding compositions are designated as CM6S4/20LNCO, CM6S4/30LNCO and CM6S4/35LNCO respectively. The mixed powders were milled thoroughly using acetone for 5 h in Fritsch Pulverisette Ball Mill and dried at 60 °C for 24 h in an electrical oven. Dried powders were calcined at 600 °C for 2 h and pressed uniaxially into cylindrical pellets (diameter ~15 mm, thickness ~2 mm) under a load of 50 kN using a hydraulic press. Sintering was carried out at 700 °C for $1\frac{1}{2}$ h in air.

Thermal behavior of the milled composites powders was studied using a NETZSCH Gerate Bau DTA in the temperature range 30–800 °C in N_2 atmosphere. Powder X-ray diffraction technique was used to study the phases and crystal structure using Rigaku X-ray diffractometer employing CuKα radiation with a Ni filter. Average crystallite size, D was determined using Scherrer's formula:

$$D = \frac{0.9\lambda}{\beta\cos\theta} \quad (1)$$

where, $\beta = \sqrt{\beta_m^2 - \beta_s^2}$, is the full width at half maxima (FWHM) excluding instrumental broadening, λ is the wave length of X-rays and θ is Bragg angle. β is taken for the strongest Bragg's peak corresponding to (111) reflection for all the samples. Density was determined using Archimedes principle. Theoretical density, ρ, of the composites was determined using mixture rule as follows:

$$\rho = \rho_a V_a + \rho_b V_b \quad (2)$$

where, ρ_a, ρ_b, V_a and V_b are the density of ceria phase, carbonate phase, volume of ceria and carbonate phase respectively.

Micrographs of the sintered fractured samples were recorded with the help of a scanning electron microscope, INSPECT 50 FEI. For the measurement of thermal expansion, bars of dimensions 50 mm × 10 mm × 4 mm of the calcined composite powders were prepared by applying a load of 50 kN using a rectangular die of stainless steel. Measurements were made using Dilatometer (V. B. Ceramics, Chennai, India) in the temperature range 30–650 °C at a heating rate of 10 °C/min.

Silver paste was brushed on both the surfaces of a polished pellet followed by heating at 700 °C for 15 min to get conducting surfaces for electrical measurements. Impedance measurements were made using Novocontrol Alpha-A High

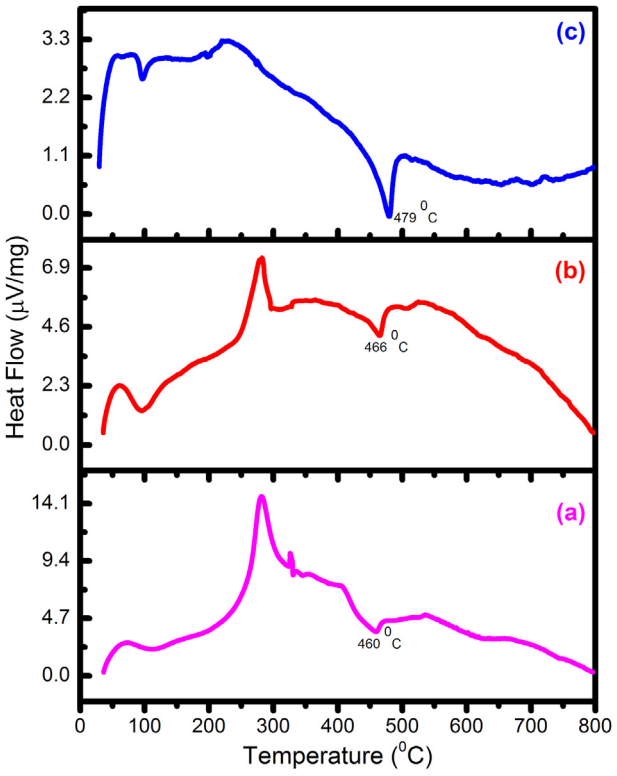

Fig. 1 – DTA plots of all the composite samples (a) CM6S4/20LNCO (b) CM6S4/30LNCO and (c) CM6S4/35LNCO.

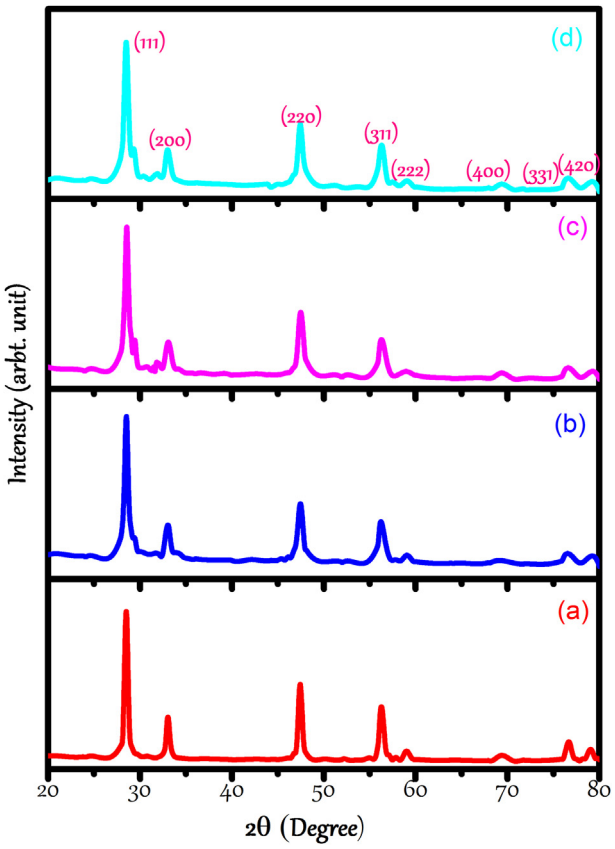

Fig. 2 – Powder X-ray diffraction patterns of calcined powders of all the compositions (a) CM6S4 (b) CM6S4/20 LNCO (c) CM6S4/30 LNCO and (d) CM6S4/35LNCO.

Performance Frequency Analyzer in air in the frequency range 1 Hz–1 MHz between 200–650 °C. Data were collected using 'Win data' program and fitted to equivalent circuits using 'ZView' software.

Results and discussion

Thermogravimetric analysis (TGA) and differential thermal analysis (DTA)

Plots of DTA of all the composite samples are shown in Fig. 1(a)–(c). One endothermic and one exothermic peak have been observed in the DTA plots corresponding to loss of adsorbed moisture and burning of organic residues respectively. One broad endothermic peak is observed around 460, 466 and 479 °C for the samples CM6S4/20LNCO, CM6S4/30LNCO and CM6S4/35LNCO respectively. This is ascribed to melting of the carbonates. Based on DTA results, samples were calcined at 600 °C for 2 h.

Phase analysis

Powder X-ray diffraction (XRD) patterns of all the samples are shown in Fig. 2. XRD peaks have been indexed on the basis of fluorite structure similar to CeO_2 using JCPDS file no. 43-1002. XRD patterns do not contain any diffraction line characteristic of carbonates. This confirms that carbonates exist as an amorphous phase in the composites. Composites CM6S4/20LNCO, CM6S4/30LNCO and CM6S4/35LNCO have density 85%, 85% and 78% of the theoretical value. This low density is due to low temperature of sintering (700 °C). These composites, however, can still be used as electrolytes because the carbonates melt at the working temperature and serve as a seal to avoid the gas crossover and also leads to increase in the

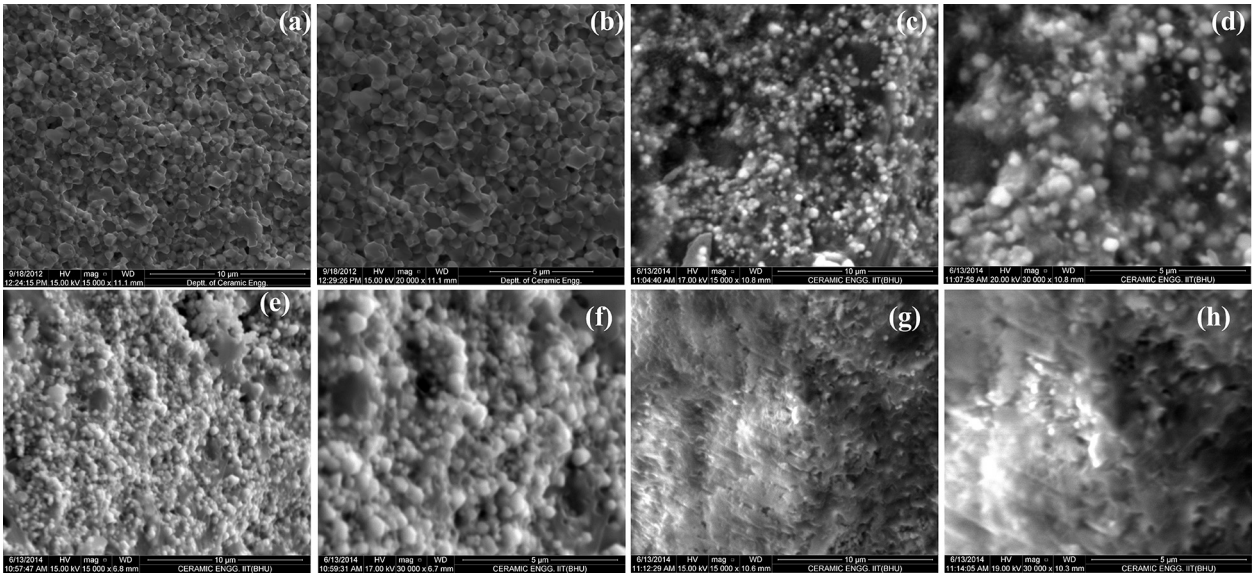

Fig. 3 – Scanning electron micrograph of all the sintered fractured samples (a) CM6S4 (b) CM6S4/20 LNCO (c) CM6S4/30 LNCO and (d) CM6S4/35 LNCO.

mechanical strength [21]. Average crystallite size, D, of the milled powders determined by Scherrer's formula is in the range 17–19 nm. Nanosized particles have large surface area which enhances the area of interface region.

Microstructure

Micrographs of the freshly fractured surfaces of all the sintered samples are shown in Fig. 3(a)–(d). Micrograph of CM6S4 is very dense. Grains are of hexagonal shape having an average grain size of 1 μm. Composite samples have porous microstructure due to low sintering temperature. The grains are fully covered by amorphous carbonate phase. Percolation of molten carbonate is obvious due to this morphology of the composites. Above the melting temperature of the carbonates, the liquid fills in the interspaces among the ceria particles and serves as a gas tight for the electrolyte. As the carbonate content increases, these form a continuous path around the ceria phase creating large interfacial region. Average grain size of the sintered composites samples determined using 'ImageJ' software is in the range of 180–200 nm because the grain growth is inhibited by the amorphous carbonate phase.

Thermal expansion coefficient (TEC)

Thermal expansion plots of all the composites are given in Fig. 4(a) and (b). Thermal expansion behavior of CM6S4/20LNCO is non linear. Two inflection points have been observed around 400 and 500 °C. Former is due to softening of the carbonate phase. At 500 °C, carbonates melt completely and fill in the interspaces between the ceria particles causing expansion again. This shows that a solid network persists in this composition even after 500 °C due to insufficient amount of the liquid formed to fill the interspaces. In the case of CM6S4/30LNCO and CM6S4/35LNCO the thermal expansion behavior is almost linear upto 450 °C and then decreases sharply beyond this. The decrease in the thermal expansion in both compositions seems to be due to formation of enough liquid on melting of the carbonates which fills the interspaces leading to contraction. It is observed from Fig. 4 that thermal expansion increases with increasing carbonate content. Compositions, CM6S4/30LNCO and CM6S4/35LNCO show nearly the same expansion behavior. Coefficient of thermal expansion of all the composites is given in Table 1.

Electrical conductivity

Impedance measurements have been made to separate the contributions of grains, grain boundaries and electrode/electrolyte interface to the total observed resistance of the composites. Fig. 5(a)–(f) show the complex plane impedance plots of the sample CM6S4/35LNCO. Two depressed arcs have been observed below 350 °C. The arc passing through the origin in the high frequency region corresponds to the contribution of the grains to the total resistance. A tail in the low frequency range observed is ascribed to the electrode/electrolyte interface. As the temperature increases, the relaxation frequency of the polarization processes increases leading to shifting of the arcs towards higher frequency. There are two arcs present

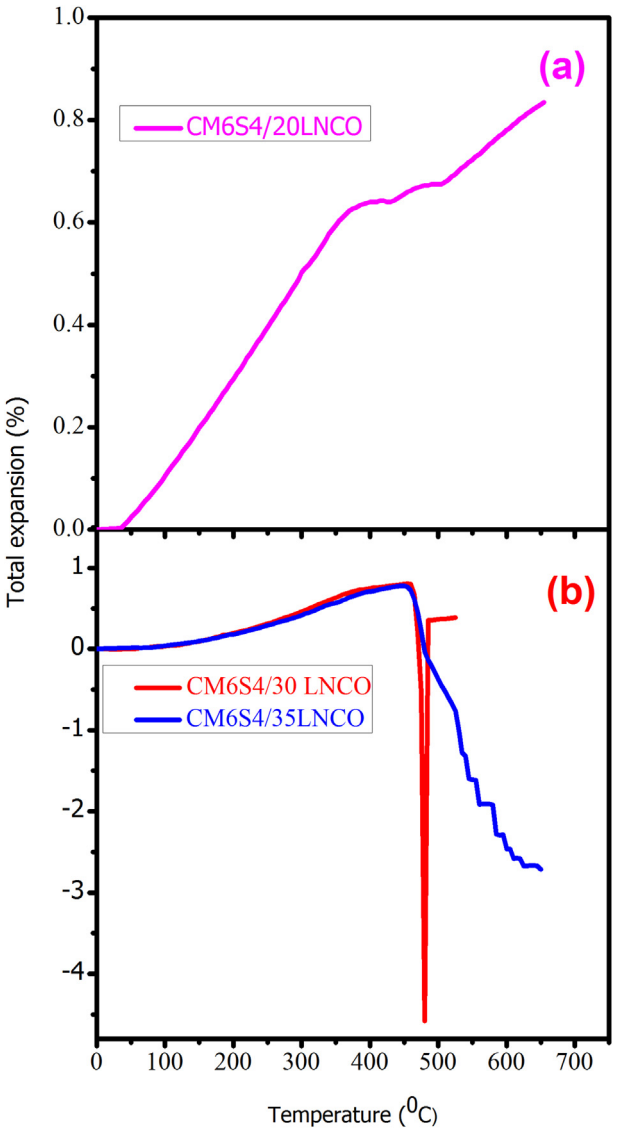

Fig. 4 – Thermal expansion curves for CM6S4/LNCO composites.

in the Fig. 5(e) corresponds to the electrode/electrolyte interface and a mass transfer process [21]. It is noted from the impedance plots that a distinct arc due to grain boundaries is absent. This may be due to existence of different ionic species and conduction mechanism involved in the dual phase ceria based nanocomposites [22]. It can be concluded from these impedance plots that there are several processes with different relaxation times in contrast to the co-doped ceria

Table 1 – Coefficient of thermal expansion of all the composites.

S. No.	Compositions	CTE (/°C)
1.	CM6S4/20LNCO	16.0×10^{-6}
2.	CM6S4/30LNCO	11.4×10^{-6}
3.	CM6S4/35LNCO	3.0×10^{-6}

based electrolytes. Relaxation frequencies of the polarization processes observed from these arcs are close to those of the alkaline carbonate mixtures but lower than those of the bulk polarization of ceria based electrolytes. This has also been reported by other researchers [23]. Impedance spectra were fitted to equivalent circuit containing a resistance and a constant phase element connected in parallel. At higher temperatures, intercept on the high frequency side was taken as equal to the total resistance of the electrolyte. Total conductivity of the samples was determined using the following formula:

$$\sigma = \frac{L}{S \times R} \tag{3}$$

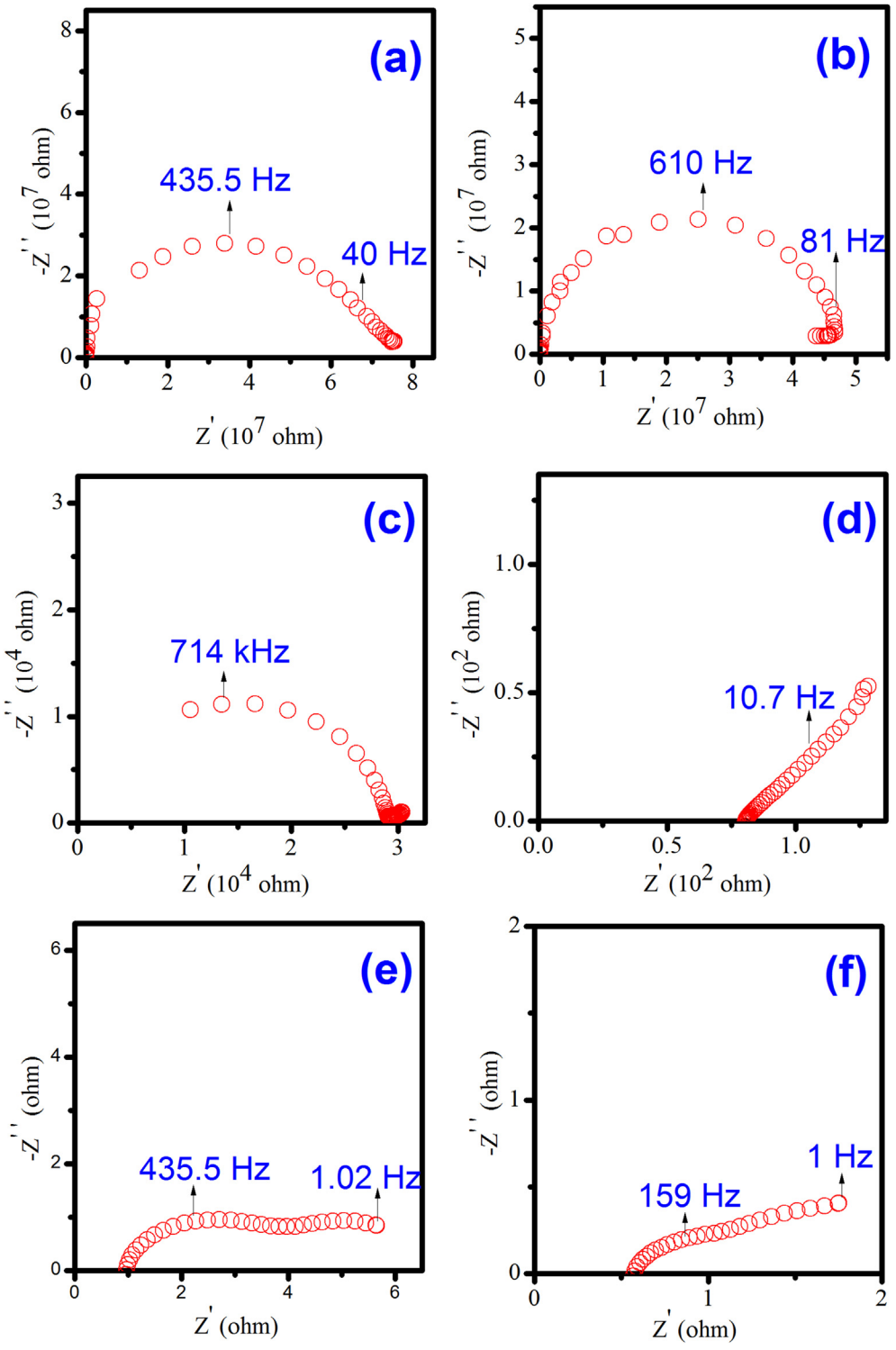

Fig. 5 – Impedance plots of CM6S4/35LNCO at temperatures (a) 200 (b) 250 (c) 325 (d) 375 (e) 500 and (f) 650 °C.

where, L, S and R are the thickness, area and resistance of the electrolyte respectively. The conductivity data were fitted to an Arrhenius equation,

$$\sigma = \sigma_0 exp\left(-\frac{E_a}{kT}\right) \quad (4)$$

where, σ_0, E_a, K and T are the pre-exponential factor, activation energy, Boltzmann constant and absolute temperature respectively.

Arrhenius plots for all the composites along with CM6S4 [20] and LNCO are given in Fig. 6. These plots show prolonged Z-shape curve with a sharp increase in conductivity around 350 °C. This temperature is certainly below the melting point of the carbonates, 460 °C and is called superionic transition. The possible reason for lowering of the transition temperature is the interfacial interaction between the two phases. This leads to the threshold percolation to form a highly conducting continuous path through the interfaces below the melting temperature [24]. Above the transition temperature, conductivity of the composites is higher than that of CM6S4 and LNCO. CM6S4/35LNCO shows the highest conductivity 0.4 S/cm at 500 °C. Conductivity of the composites increases with increasing the carbonate content. In the present investigation, measurements were not made for the samples having carbonate content >35 wt% as the samples containing higher concentration of carbonate de-shaped after sintering due to large volume of the liquid formed. This has been reported earlier also [8]. Interfacial interaction in the composites can be explained using the theory of defect chemistry [25,26]. In doped or co-doped ceria, conduction is due to migration of oxide ions through oxygen ion vacancies formed due to charge compensation as given below:

$$MgO \xrightarrow{CeO_2} Mg''_{Ce} + 2O^{\times}_{O} + V^{\bullet\bullet}_{O} \quad (5)$$

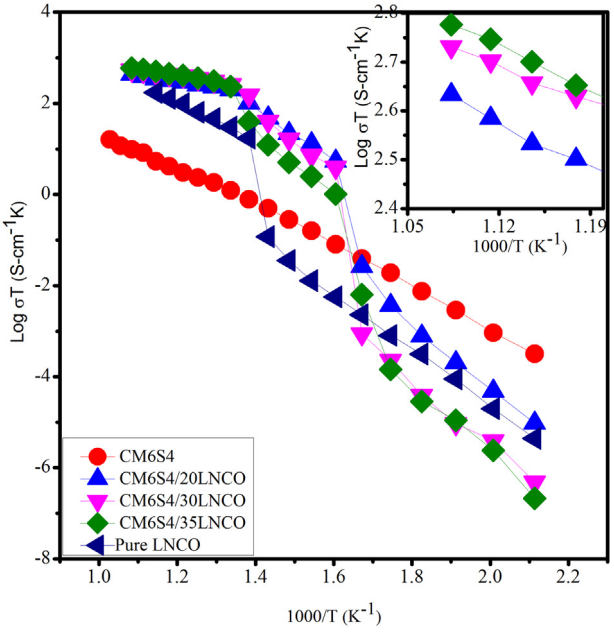

Fig. 6 – Arrhenius plots of total conductivity for all the compositions.

$$SrO \xrightarrow{CeO_2} Sr''_{Ce} + 2O^{\times}_{O} + V^{\bullet\bullet}_{O} \quad (6)$$

where, all the symbols are in accordance with Kroger Vink notation of defects. Due to presence of carbonates in the composites, oxygen ions may accumulate on the surface of ceria particles due to interfacial interaction and creates more oxygen vacancies in the bulk.

$$O^{\times}_{O} + V_S \rightarrow V^{\bullet\bullet}_{O} + O''_{S} \quad (7)$$

At the surface of carbonates some reactions occur [Eqs. (8) and (9)] which cause an increase in concentration of M^+ vacancies at the surface of one grain and an equivalent number of interstitials M^+ concentration at the surface of adjacent grain [26]. Therefore, concentration of the cation vacancies increases in the bulk and the carbonate phases. Certainly, this enhances the conductivity below the melting temperature of the carbonates.

$$M^{\times}_{M} + V_S \rightarrow M^{\bullet}_{S} + V'_{M} \quad (8)$$

$$M^{\bullet}_{S} + V_i \rightarrow M^{\bullet}_{i} + V_S \quad (9)$$

where, M = Li^+, Na, subscripts M, S, and i represent regular M lattice site, surface site and interstitial site respectively. A space charge zone is, therefore, formed at the interfaces containing much higher concentration of mobile defects than that in the bulk [27].

Below the transition temperature, conductivity of the composites is lower than that of CM6S4 due to blocking of diffusion of O^{2-} ions by dispersed solid carbonate phase. After melting, carbonates fills in the pores and interspaces among the ceria particles creating more interfacial region for diffusion of ions. Conductivity at higher temperatures has contribution from all the mobile ions such as Na^+, Li^+, H^+, O^{2-} and CO_3^{2-} leading to superionic conduction [28]. Activation energy has been calculated from the slope of Arrhenius plots at lower and higher temperatures both. Activation energy is high at low temperature and low at higher temperature. At low temperature, diffusion of ions is hampered by the solid amorphous carbonate phase leading to high activation energy. Values of activation energy are given in Table 2. Values of the pre-exponential factor, σ_0 determined from the intercept of Arrhenius plots are given in Table 2.

It can be concluded that conductivity of Mg^{2+} and Sr^{2+} co-doped ceria/carbonate composite electrolytes increases due to two reasons: (i) co-doping of Sr^{2+} and Mg^{2+} in ceria

Table 2 – Total conductivity at 500 °C, activation energy and pre-exponential factor for all the compositions.

Compositions	σ at 500 °C (S/cm)	E_g < 350 °C (eV)	E_g > 350 °C (eV)	σ_0
CM6S4	2.39×10^{-3}[a]	1.12	0.73	5.49×10^{3}
LNCO	4.73×10^{-2}	1.26 (<500 °C)	0.30 (>500 °C)	3.05×10^{6}
CM6S4/20LNCO	2.95×10^{-1}	1.50	0.26	1.05×10^{4}
CM6S4/30LNCO	3.93×10^{-1}	1.61	0.24	1.20×10^{4}
CM6S4/35LNCO	3.98×10^{-1}	1.60	0.23	3.00×10^{4}

[a] Data taken from Ref. [20].

enhances the total conductivity as discussed in detail in our previous work [20] and (ii) molten carbonates form a uniform continuous path enveloping the ceria phase. This creates highways for the conduction of ions. In nanocomposites conduction of O^{2-} via the interfaces dominates over the bulk conduction. As discussed above, conductivity can be enhanced by increasing the value of σ_0 which depends on the concentration of mobile ions and the ion jump distance [28]. Therefore, large number of mobile ions in the space charge zone and long jump distance at the interfaces formed between CM6S4 and LNCO results in higher ionic conductivity and low activation energy.

In the present work, the compostion CM6S4/35LNCO shows conductivity of 0.4 S/cm at 500 °C which is two orders of magnitude higher than the value 2.40×10^{-3} S/cm observed for CM6S4 [20]. At 450 °C this composition shows a conductivity 0.05 S/cm which is five times higher than the value 0.01 S/cm at 481 °C reported for SNDC/$(Li–Na)_2CO_3$ by Liu et al. [28].

Conclusion

Nanocomposites based on CM6S4/$(Li–Na)_2CO_3$ have been successfully synthesized by mixing nanosize co-doped ceria powder with the binary carbonate mixture. Single phase formation has been confirmed by powder XRD. Carbonates are present as an amorphous phase throughout the ceria matrix. SEM micrographs show percolated islands of ceria and carbonate phases. Conductivity increases abruptly above the melting temperature of the carbonates due to increase in the number of pathways for oxygen ion conduction. Activation energy is very low at high temperatures. This is suggested that O^{2-} ions conduct via the interfaces formed between two phase particles rather than the bulk where the activation energy is around 1 eV. The composition CM6S4/35LNCO shows the highest conductivity of 0.4 S/cm at 500 °C with an activation energy of conduction 0.30 eV.

Acknowledgement

Thanks to Department of Science and Technology, New Delhi and Ministry of Human Resources & Development for financial support.

REFERENCES

[1] Steele B, Heinzel A. Materials for fuel-cell technologies. Nature 2001;414:345–52.
[2] Omar S, Wachsman E, Nino J. A co-doping approach towards enhanced ionic conductivity in fluorite based electrolytes. Solid State Ionics 2006;177:3199–203.
[3] Sha X, Huang Z, Miao X, Ding J, Xin Z, Su X. Study on La and Y co-doped ceria-based electrolyte materials. J Alloys Compd 2007;428:59–64.
[4] Tsung H, Chou C. Ionic conductivity investigation in samarium and strontium co-doped ceria system. Phys Scr 2007;T129:303–7.
[5] Goodenough J. Ceramic technology: oxide ion conductors by design. Nature 2000;404:821–3.
[6] Li S, Wang X, Zhu B. Novel ceramic fuel cell using non ceria based composites as electrolytes. Electrochem Commun 2007;9:2863–6.
[7] Huang J, Mao Z, Liu Z, Wang C. Performance of fuel cell with proton conducting ceria based composite electrolyte and nickel metal based electrodes. J Power Sources 2008;175:238–43.
[8] Huang J, Mao Z, Liu Z, Wang C. Development of novel low temperature SOFCs with co-ionic conducting SDC-carbonate composite electrolytes. Electrochem Commun 2007;92:2601–5.
[9] Huang J, Mao Z, Yang L, Peng R. SDC/carbonate electrolytes for low temperature SOFCS. Electrochem Solid State Lett 2005;8:A437–40.
[10] Zhu B, Mahmut D. Studies on dual phase ceria based composites in electrochemistry. Int J Electrochem Sci 2006;1:383–402.
[11] Zhu B, Mellander B. In: Singhal SC, Dokiya M, editors. Solid oxide fuel cells-VI. Pennington, NJ: The Electrochemical Society, Inc; 1999. p. 244.
[12] Zhu B. Advantages of intermediate temperature solid oxide fuel cells for tractionary applications. J Power Sources 2001;93:82–6.
[13] Zhu B, Yang X, Xu J, Zhu Z, Ji S, Sun M, et al. Innovative low temperature SOFCs and advanced materials. J Power Sources 2003;118:47–53.
[14] Fu Q, Meng G, Zhu B. Intermediate temperature fuel cells based on doped ceria- LiCl-$SrCl_2$ composite electrolyte. J Power Sources 2002;104:73–8.
[15] Zhu B, Liu X, Sun M, Ji S, Sun J. Calcium doped ceria based materials for cost effective intermediate temperature solid oxide fuel cells. Solid State Sci 2003;5:1127–34.
[16] Liu X, Zhu B, Xu J, Sun J, Mao Z. Sulphate ceria composite ceramics for energy environmental co-generation technology. Key Eng Mater 2004;280–283:425–30.
[17] Hu J, Tosto S, Guo Z, Wang Y. Dual phase electrolytes for advanced fuel cells. J Power Sources 2006;154:106–14.
[18] Arico A, Bruce P, Scrosati B, Tarascon J. Nanostructured materials for advanced energy conversion and storage devices. Nat Mater 2005;4:366–77.
[19] Gao Z, Raza R, Zhu B, Mao Z, Wang C, Liu Z. Preparation and characterization of $Sm_{0.2}Ce_{0.8}O_{1.9}/Na_2CO_3$ nanocomposite electrolyte for low temperature solid oxide fuel cells. Int J Hydrogen Energy 2011;36:3984–8.
[20] Jaiswal N, Kumar D, Uppadhyay S, Parkash O. Effect of Mg and Sr co-doping on the electrical properties of ceria-based electrolyte materials for intermediate temperature solid oxide fuel cells. J Alloys Compd 2013;577:456–62.
[21] Chen J, Wang C, Zhang J. Samarium doped ceria-$(Li/Na)_2CO_3$ composite electrolyte and its electrochemical properties in low temperature solid oxide fuel cell. J Power Sources 2010;195:4695–9.
[22] Lapa C, Figueiredo F, Souza D, Song L, Zhu B, Marques F. Synthesis and characterization of composite electrolytes based on samaria doped ceria and Na/Li carbonates. Int J Hydrogen Energy 2010;35:2953–7.
[23] Ferreira S, Cátia C, Filipe Figueiredo M, Fernando B. Intrinsic and extrinsic compositional effects in ceria/carbonate composite electrolytes for fuel cells. Int J Hydrogen Energy 2011;36:3704–11.
[24] Mizuhata M, Bleke A, Watanabe H, Harada Y, Deki S. Effect of Υ-$LiAlO_2$ powder on ionic conductivity of co-existing single alkali carbonates. Electrochim Acta 2007;53:71–8.
[25] Huang J, Gao Z, Mao Z. Effects of salt composition on the electrical properties of samarium-doped ceria/carbonate

composite electrolytes for low-temperature SOFCs. Int J Hydrogen Energy 2010;35:4270–5.

[26] Bhoga S, Singh K. Li_2CO_3–ABO_3 (A = Li, K, Ba and B = Nb, Ti) composite solid electrolyte systems. Solid State Ionics 1998;111:85–92.

[27] Zhang L, Lan R, Xu X, Tao S, Jiang Y, Kraft A. A high performance intermediate temperature fuel cell based on a thick oxide carbonate electrolyte. J Power Sources 2009;194:967–71.

[28] Liu W, Liu Y, Li B, Sparks D, Wei X, Pan W. Ceria (Sm, Nd) carbonate composite electrolytes with high electrical conductivity at low temperature. Compos Sci Technol 2010;70:181–5.

Ionics
DOI 10.1007/s11581-015-1386-2

ORIGINAL PAPER

Enhanced ionic conductivity in La^{3+} and Sr^{2+} co-doped ceria: carbonate nanocomposite

Nandini Jaiswal · Shail Upadhyay · Devendra Kumar · Om Parkash

Received: 27 October 2014 / Revised: 18 January 2015 / Accepted: 4 February 2015

Abstract A series of ceria-based nanocomposites consisting of $Ce_{0.85}La_{0.125}Sr_{0.025}O_{1.9125}$ (LSCO) and binary carbonate mixture Li_2CO_3–Na_2CO_3 (LNCO) have been prepared as functional electrolytes for low-temperature solid oxide fuel cells (LT-SOFCs). These have been characterized using powder X-ray diffraction, scanning electron microscope, differential thermal analysis, and measurement of conductivity as a function of temperature using complex plane impedance analysis. Crystalline ceria-based single phase formation has been found in all the composites. Carbonates are present as an amorphous phase in the composites. Impedance analysis has been used to study the electrical behavior of the composites. A jump in the conductivity vs temperature plots has been observed in all the composites containing different carbonate contents. This is related to superionic transition at the interfaces. Conductivity of the composites increases with increasing amount of carbonate. This is due to the increase in the interfacial area between the two phases, which promotes interfacial interaction between them. Composition, LSCO/35LNCO, shows conductivity of 0.203 S cm^{-1} at 500 °C with an activation energy of conduction of 0.19 eV.

Keywords Co-doped ceria · Nanocomposites · Impedance analysis · Electrical conductivity · LT-SOFCs

N. Jaiswal · D. Kumar · O. Parkash (✉)
Department of Ceramic Engineering, Indian Institute of Technology, Banaras Hindu University, Varanasi 221005, India
e-mail: oprakash.cer@itbhu.ac.in

S. Upadhyay
Department of Physics, Indian Institute of Technology, Banaras Hindu University, Varanasi 221005, India

Introduction

Solid oxide fuel cell (SOFC) is an electrochemical device that converts chemical energy of the fuels into electrical energy by exploiting natural tendency of hydrogen to react with oxygen. SOFCs have received much attention due to their environmental friendliness, fuel flexibility, and high efficiency [1]. SOFCs consist of three parts: an anode, a solid electrolyte, and a cathode. Electrolyte is the main component of a SOFC through which oxide ions migrate from cathode to anode constituting an electric current. At present, SOFCs use yttria stabilized zirconia (YSZ) as a solid electrolyte, which operates at 1000 °C. Due to high working temperature, these SOFCs cannot be commercially acceptable. Some singly doped ceria-based electrolytes such as $Ce_{1-x}Gd_xO_{2-\delta}$ (GDC), $Ce_{1-x}Sm_xO_{2-\delta}$ (SDC), and $Ce_{1-x}Y_xO_{2-\delta}$ (YDC) show high ionic conductivity [2, 3]. Park et al. [4] observed a power density of 594 mW/cm^2 at 600 °C in a cell containing $Ce_{0.90}Gd_{0.10}O_{1.95}$ sintered at 1400 °C as an electrolyte. However, Sm_2O_3 and Gd_2O_3 are very costly. The research has been going on to produce cost-effective SOFCs by reducing the operating temperature of the cells between 300 and 600 °C [5–7]. These are called as low-temperature SOFCs (LT-SOFCs).

Recently, ceria/salt-based nanocomposite solid electrolytes have been proved to be a promising candidate for LT-SOFCs [8–11]. Ceria/salt composites consist of two phases: one is nanocrystalline doped or co-doped ceria, and another is an amorphous salt. Salts exist either as a molten phase, e.g., a mixture of Li_2CO_3–Na_2CO_3 above 500 °C or a solid phase such as Na_2CO_3 [12]. The interfaces formed between two phases provide highway channels for transport of the ions. This leads to enhancement in the conductivity of the electrolytes. Transport efficiency depends on the two parameters: one is the interface density, and second is the contact area between the two phases [12]. In the nanocomposite electrolytes, the larger the interfacial area or grain boundaries area, the higher

Published online: 17 February 2015

the concentration of mobile defects in the space charge region [13].

Ceria/carbonate-based composites showed dual ion (O^{2-}/H^+) conduction with an overall value of conductivity, 0.1 S cm^{-1} in H_2/O_2 at 600 °C [14]. O^{2-} ions diffuse through the ceria bulk phase and the interfaces between the ceria and carbonate phase. H^+ ions diffuse via CO_3^{2-} ions (HCO_3^-) [12]. Conduction due to CO_3^{2-} ions may be present, but it is not significant [15]. In the case of molten carbonate fuel cells (MCFCs), the electrolyte is molten carbonate retained by the insulating $LiAlO_2$ phase operated at 650 °C. The electrolyte contains 60–70 vol.% of carbonate [15]. In ceria carbonate composites, however, carbonate content is below 40 wt%. Xia et al. [16] found that the cell performance can be further enhanced using a mixture of CO_2/O_2 at the cathode. Single cell based on $Ce_{0.80}Sm_{0.20}O_{1.90}$/($Li_2CO_3$–$Na_2CO_3$) composite electrolyte showed a power density of 1700 mW cm^{-2} at a current density of 3000 mA cm^{-2} at 650 °C when CO_2/O_2 atm was used at cathode [16].

In our previous work, La^{3+} and Sr^{2+} co-doped ceria nanopowders were prepared by citrate–nitrate auto-combustion method [17]. It was found that the composition $Ce_{0.85}La_{0.125}Sr_{0.025}O_{1.9125}$ (LSCO) shows the highest ionic conductivity (1.50×10^{-2} S cm^{-1} at 600 °C) of all the compositions [17]. This value is higher than the highest values of the conductivity reported for the compositions $Ce_{0.80}Sm_{0.20}O_{1.90}$ (SDC) (1.20×10^{-2} S cm^{-1}) [18] and $Ce_{0.80}Gd_{0.20}O_{1.90}$ (GDC) (1.29×10^{-2} S cm^{-1}) [19] at 600 °C. Use of both La_2O_3 and SrO in LSCO reduces the cost of the electrolyte significantly because both are cheaper than Sm_2O_3 and Gd_2O_3. In the present work, nanocomposite electrolytes based on LSCO/(Li–Na)$_2CO_3$ have been prepared and characterized by thermal analysis, crystal structure, microstructure, and impedance analysis.

Experimental

$Ce_{0.85}La_{0.125}Sr_{0.025}O_{1.9125}$ was synthesized using citrate–nitrate gel auto-combustion method as reported in our previous work [17]. The carbonate mixture was prepared by mixing 52 mol.% Li_2CO_3 and 48 mol.% Na_2CO_3 (LNCO) for 2 h employing a Fritsch pulverisette ball mill in zirconia jars making use of zirconia balls as grinding media. The ground carbonate mixture was then mixed with calcined LSCO powder in different weight ratios. The weight ratios of LSCO/LNCO were 80:20, 70:30, and 65:35 designated as LSCO/20LNCO, LSCO/30LNCO, and LSCO/35LNCO, respectively. The carbonate content was not used above 35 wt% to prevent deshaping of the sample during sintering. The mixtures were ground for 5 h in acetone using the Fritsch pulverisette ball mill. Milled powders were dried in an oven at 60 °C for 24 h. Dried powders were calcined at 600 °C for 2 h in air. The resulting powder was pressed uniaxially into cylindrical pellets (diameter, ~15 mm; thickness, ~2 mm) under a load of 5 t using a hydraulic press. Pellets were sintered at 700 °C for 1 1/2 h.

Differential thermal analysis (DTA) of the composites was carried out using a NETZSCH Gerate Bau DTA at a heating rate of 10 °C/min over the temperature range of 100–800 °C in N_2 atm. X-ray powder diffraction (XRD) patterns were recorded with a Rigaku X-ray diffractometer using CuKα radiation and Ni filter. Average crystallite size was calculated using Scherrer's formula:

$$D = 0.9\lambda/\beta\cos\theta \quad (1)$$

where β is the full width at half maxima (FWHM) excluding instrumental broadening, λ is the wavelength of X-rays, and θ is Bragg's angle. β is taken for the strongest Bragg's peak corresponding to (111) reflection for all the samples. Experimental density of the sintered pellets was determined by the Archimedes principle. Theoretical density was calculated using mixture rule as follows:

$$\rho = \rho_a V_a + \rho_b V_b \quad (2)$$

where ρ_a, ρ_b, V_a, and V_b are the density of ceria phase, density of carbonate phase and volume fractions of the ceria and carbonate phases, respectively.

Micrographs of all the samples were recorded using an INSPECT 50 FEI scanning electron microscope (SEM). Bars of dimension, 50×10×4 mm were prepared and sintered at 700 °C for 1 1/2 h for measuring thermal expansion from room temperature to 650 °C in air with a heating rate of 5 °C/min.

Sintered pellets were polished on both the sides using emery papers of grade 1/0, 2/0, 3/0, and 4/0 Sia Switezerland. High-temperature silver paste in an epoxy was applied on both the surfaces of the polished pellets, and pellets were heated at 700 °C for 15 min to form a smooth conducting silver layer on both the surfaces. Two probe impedance measurements were made using a Novocontrol Alpha-A high performance frequency analyzer in air in the temperature range of 200–650 °C and frequency range of 1 Hz–1 MHz with an ac signal of 20 mV. The data were collected using "Win data" program and fitted to equivalent circuits using "ZView" software.

Results and discussion

Differential thermal analysis

Figure 1 shows DTA plots of all the composite samples. In the DTA plots, two endothermic peaks have been observed. One is around 100 °C, which is due to evaporation of adsorbed moisture in the sample. Second, a broad endothermic peak has been observed in the temperature range of 486–490 °C.

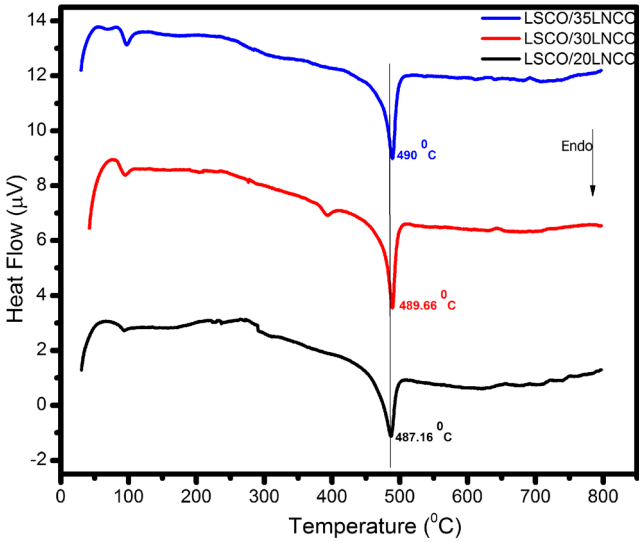

Fig. 1 DTA plots of all the composite samples

This is ascribed to melting of the binary carbonate mixture. As the carbonate content increases, the second endothermic peak slightly shifts towards higher temperature. There is no exo- or endothermic peak beyond 490 °C. Based on the DTA results, all the composite powders were calcined at 600 °C for 2 h.

X-ray powder diffraction

Powder X-ray diffraction patterns of all the sintered powders are shown in Fig. 2. Diffraction peaks have been indexed on the basis of JCPDS file no. 43-1002 for ceria. There is no peak of Li_2CO_3 and Na_2CO_3. This shows that carbonates are present in the amorphous state throughout the ceria matrix. Density of the composites has been found to be in the range of 82–85 % of the theoretical value. This low value of density

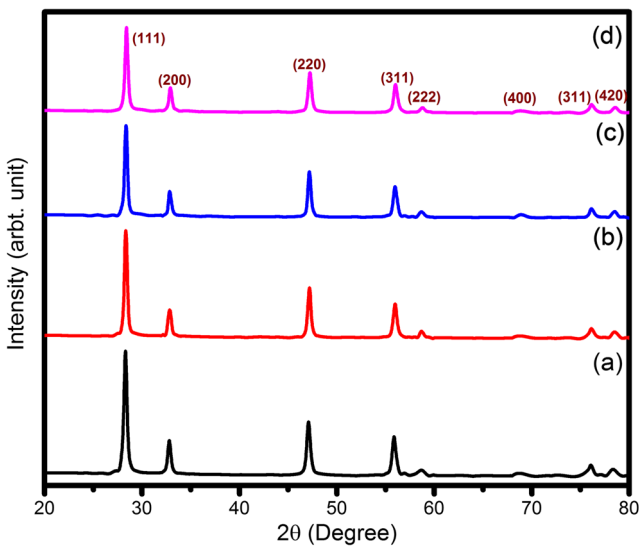

Fig. 2 Powder X-ray diffraction patterns of various compositions: **a** LSCO, **b** LSCO/20 LNCO, **c** LSCO/30 LNCO, and **d** LSCO/35LNCO sintered powders

is due to very low sintering temperature of 700 °C. Carbonates melt at working temperature, which fills in the interspaces between the ceria particles and consequently enhance the density and work as a seal to avoid crossover of the gases [1]. Average particle size has been found to be in the range of 19–23 nm. Nanosize particles will produce large interfacial region for the conduction of ions.

Thermal expansion

Thermal expansion curves of the composites are shown in Fig. 3. It is noted that these curves are linear. Coefficient of thermal expansion (CTE), $\alpha_{T_2-T_1}$, is determined using the following formula:

$$\alpha_{T_2-T_1} = \frac{\mathrm{d}L}{Lo(T_2-T_1)} \tag{3}$$

where dL and L_0 are the change in the length and initial length of the sample, respectively. T_2 and T_1 are the final and initial temperature, respectively. Values of CTE of all the samples are given in Table 1. Compositions, LSCO/20LNCO and LSCO/30LNCO, have nearly the same values of CTE, and LSCO/35LNCO has the highest CTE.

Microstructure

Figure 4 shows the micrographs of all the samples. It can be observed from Fig. 4a that LSCO shows very dense structure with distinct grains and grain boundaries. It can be seen from Fig. 4b–d that LSCO particles are surrounded by molten carbonate amorphous phase. SEM micrographs of nanocomposites reveal that the size of LSCO particles is <100 nm. Due to presence of the large pores between the ceria grains,

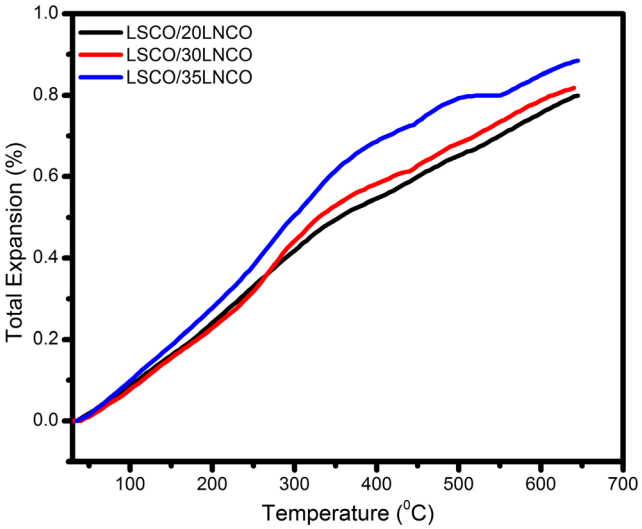

Fig. 3 Thermal expansion curves for LSCO/LNCO composites

Table 1 Coefficient of thermal expansion of all the composites

Sample no.	Compositions	CTE (K^{-1})
1	LSCO/20LNCO	14.30×10^{-6}
2	LSCO/30LNCO	14.40×10^{-6}
3	LSCO/35LNCO	16.70×10^{-6}

percolation of the carbonate phase is obvious. This microstructure may create large interfacial region for conduction of ions.

Electrical conductivity

Impedance measurements have been made to study the conduction mechanism in the composites. Complex plane impedance plots of LSCO/35LNCO at different temperatures are shown in Fig. 5. At 200 °C, three arcs have been observed. One in the highest frequency range corresponds to contribution of the grains (bulk), second in the intermediate frequency range is ascribed to grain boundaries, and a tail in the lowest frequency range corresponds to electrode/electrolyte interface polarization. However, it can be seen that grains and grain boundaries arcs are not very distinct. This behavior is different from that of doped or co-doped ceria where distinct grains and grain boundaries arcs have been observed. This emphasizes a different conduction mechanism in the composite electrolytes. As the temperature increases, the relaxation frequency increases. Therefore, the arcs shift towards higher frequency. The arcs due to grains and grain boundaries disappear above 350 °C. At higher temperatures, only the arc due to the electrode/specimen interface polarization has been observed. In Fig. 5d–f, the electrode arc is associated with a tail, which is ascribed to mass transfer process [1]. The grains and grain boundaries arcs are associated with capacitance in the pF (10^{-10}–10^{-12}) and nF (10^{-7}–10^{-9}) range, respectively [20, 21]. These are determined from the relation $2\pi f_{max}RC=1$, where f_{max} is the applied frequency at the arc maximum, R is the resistance, and C is the capacitance of a particular contribution. Relaxation frequencies of these arcs are close to those of alkaline earth carbonate mixtures and lower than the relaxation frequencies observed in the case of single-phase ceria [22]. Impedance spectra were fitted to equivalent circuits as shown in Fig. 5. In the circuits, R and CPE are the resistance and constant phase element, respectively. CPE has been used in place of ideal capacitor due to presence of inhomogenities in the sample [23]. CPE is equivalent to the distribution of capacitors in parallel. At higher temperatures, intercept on

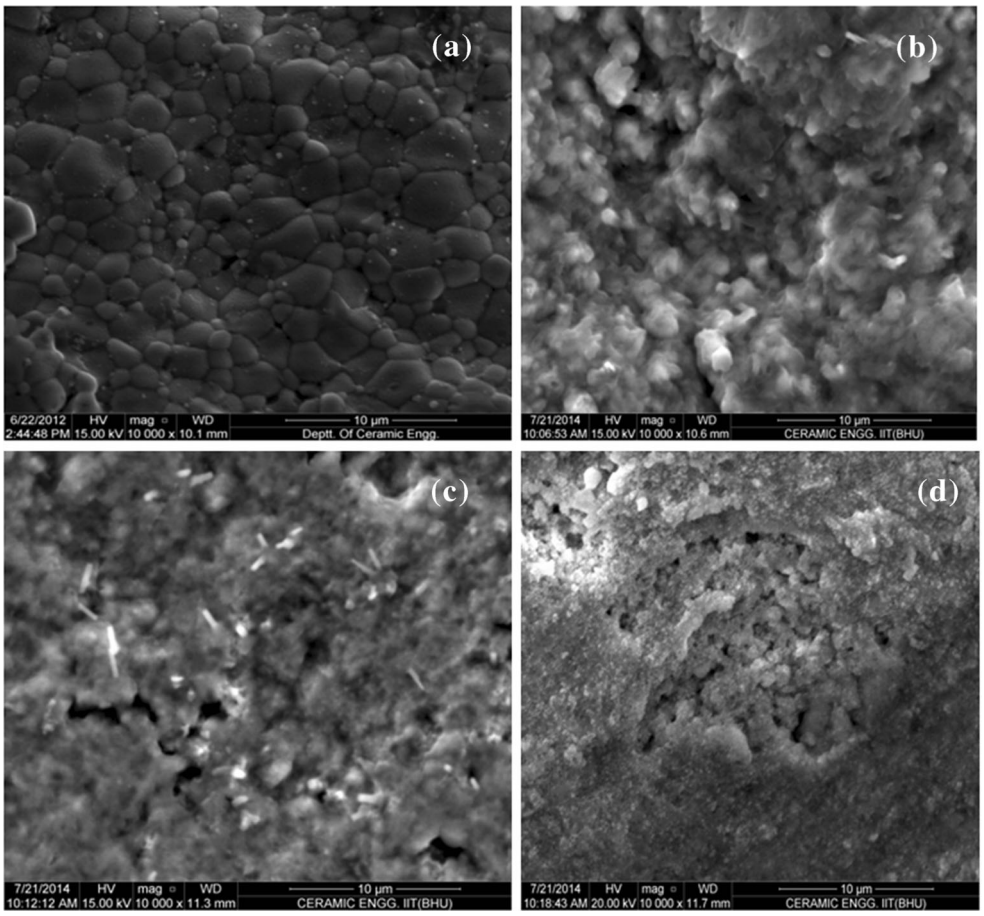

Fig. 4 Scanning electron micrograph of all the fractured samples: **a** LSCO, **b** LSCO/20 LNCO, **c** LSCO/30 LNCO, and **d** LSCO/35 LNCO

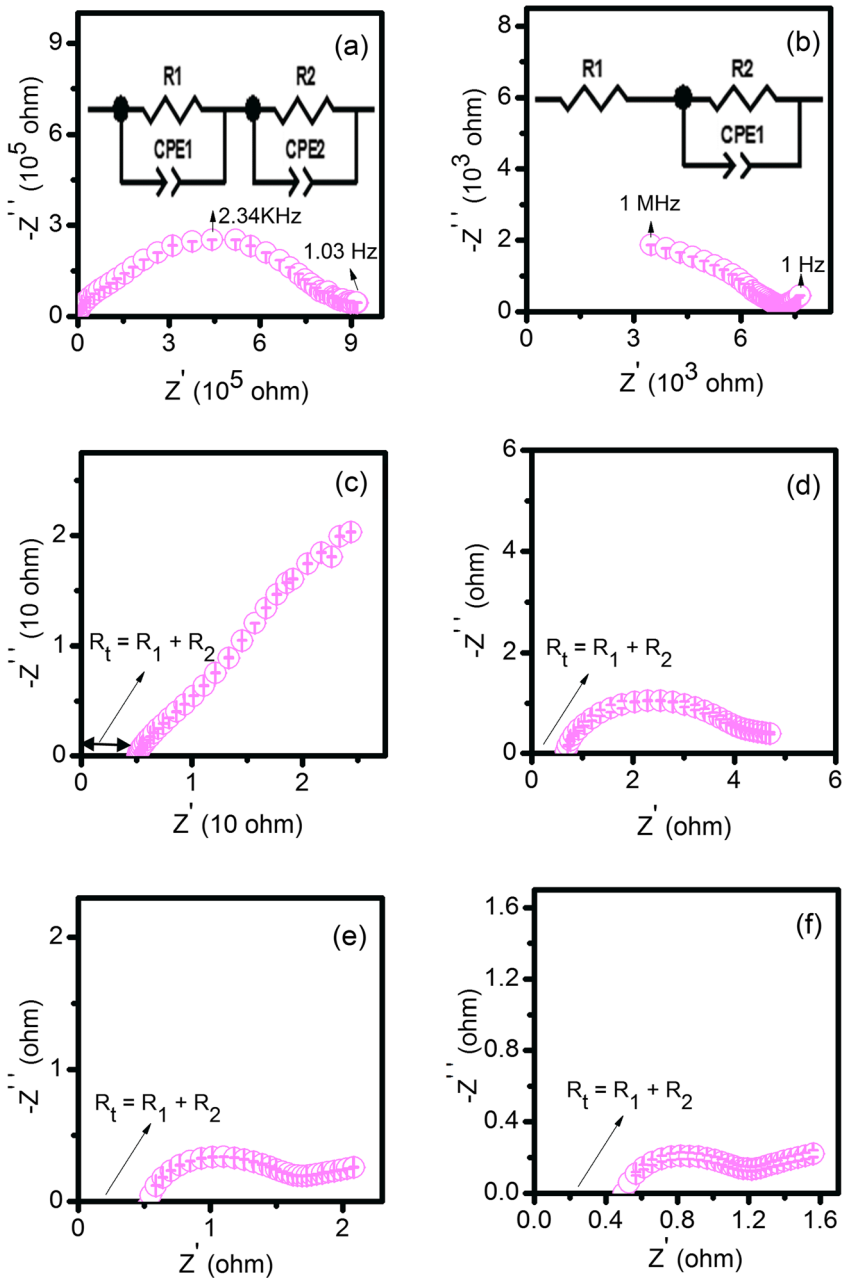

Fig. 5 Impedance plots of LSCO/35LNCO at temperatures: **a** 200, **b** 275, **c** 400, **d** 500, **e** 600, and **f** 650 °C

the high frequency side of the tail was taken as equal to the total resistance of the electrolyte. Total conductivity, σ, is determined using the following formula:

$$\sigma = \frac{L}{S \times R} \tag{4}$$

where L, S, and R are the thickness, area, and resistance of the electrolyte, respectively.

Figure 6 shows Arrhenius plots for the total ionic conductivity of the composites as well as LSCO [17] and pure LNCO. Enhancement in conductivity with the carbonate content (at higher temperatures) is evidenced by the plots in the insets. A jump in the conductivity plots has been observed for the composites around 350 °C. This corresponds to superionic transition at the interfaces [1]. It is a consequence of the capillary forces due to surface tension, which comes into play because of the presence of smaller pores among the ceria particles throughout the matrix [24]. In the space charge zone, concentration of cationic defects is higher than that in the bulk. Mobility of these defects increases due to melting from the sublattice to bulk [25]. Above the transition temperature, mobility of various ions Na^+, Li^+, H^+, and CO_3^{2-} leads to superionic conduction. The transition temperature is lower than the melting temperature of carbonates. This is due to threshold percolation, which leads to formation of highly

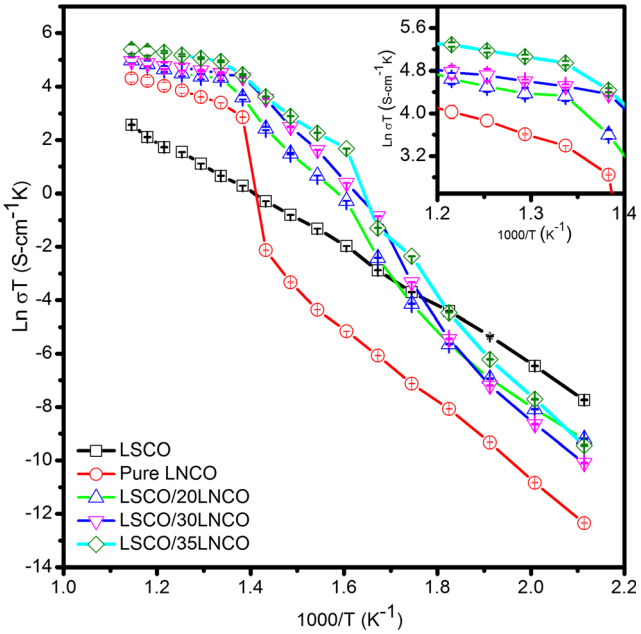

Fig. 6 Arrhenius plots of total conductivity for all the compositions in air

conducting continuous pathways throughout the ceria matrix. Conductivity of the composites increases with increasing the carbonate content, and it is higher than that of LSCO and LNCO above the transition temperature. This is due to interfacial interaction between the two phases. Conduction mechanism in the carbonate composite electrolytes has been explained by theory of defect chemistry [26, 27]. O^{2-} ion conduction in doped ceria occurs by migration of oxygen ions through oxygen ion vacancies generated from incorporation of La_2O_3 and SrO into CeO_2 as follows:

$$La_2O_3 \xrightarrow{2CeO_2} 2La'_{Ce} + 3O^X_O + V^{\bullet\bullet}_O \tag{5}$$

$$Sro \xrightarrow{CeO_2} Sr''_{Ce} + 2O^X_O + V^{\bullet\bullet}_O \tag{6}$$

where symbols are in accordance with the Kröger–Vink notation of defects. In the case of the composites, O^{2-} ions may accumulate at the surface of ceria particles due to interfacial interaction. This results in the formation of more oxygen vacancies in the bulk of LSCO as follows:

$$O^X_O + V_S = V^{\bullet\bullet}_O + O''_S \tag{7}$$

At the surface of alkaline earth carbonates, a reaction occurs as given below:

$$M^X_M + V_S \leftrightarrow V'_M + M^{\bullet}_S \tag{8}$$

$$M^{\bullet}_S + V_i = V_S + M^{\bullet}_i \tag{9}$$

where M=Li^+ and Na, and subscripts M, S, and i represent regular M lattice site, surface site, and interstitial site, respectively. This causes an increase in the interstitial M^+ concentration at the surface of one grain and an equivalent M^+ vacancy concentration adjacent on the surface of another grain in contact [27]. Therefore, concentration of cation vacancies increases in the bulk and carbonate phase. Certainly, this enhances the conductivity below the melting temperature of the carbonates. The interface reactions are given below:

$$M^{\bullet}_M + V_A \leftrightarrow M^{\bullet}_A + V'_M \tag{10}$$

$$M^{\bullet}_A + V_i \leftrightarrow M^{\bullet}_i + V'_A \tag{11}$$

where "A" denotes an interface site.

Composite with 35 wt% of carbonate shows conductivity of 0.203 S cm^{-1} at 500 °C. This value is two orders of magnitude higher than that of 3.91×10^{-3} S cm^{-1} observed for LSCO at the same temperature [17]. At 475 °C, LSCO/35LNCO has conductivity of 0.186 S cm^{-1}, which is one order of magnitude more than 0.01 S cm^{-1} observed in $Ce_{0.8}Sm_{0.1}Nd_{0.1}O_{1.9}/(Li/Na)_2CO_3$ by Liu et al. [28] at 481 °C. Activation energy of conduction, E_a, has been determined by fitting the data points to the Arrhenius equation:

$$\sigma = \sigma_0 \exp\left(\frac{-E_a}{kT}\right) \tag{12}$$

where σ_0, k, and T are the pre-exponential factor, Boltzmann's constant, and absolute temperature, respectively. It can be noted from Eq. (11) that conductivity can be enhanced either by increasing σ_0 or decreasing E_a. Values of E_a at higher and lower temperatures are given in Table 2. In the case of the composites, E_a is higher at lower temperature and vice versa. This is due to blocking of the mobile ions by the solid carbonate phase in the low temperature region. Above the transition temperature, mobility increases due to melting from sublattice

Table 2 Total conductivity at 500 °C, activation energy, and pre-exponential factor for all the compositions

Sample no.	Compositions	σ_t at 500 °C (S cm^{-1})	E_a (200–450 °C) (eV)	E_a (500–650 °C) (eV)	Pre-exponential factor, σ_0
1.	LSCO	3.91×10^{-3}	–	0.91 (200–600 °C)	2.36×10^{6}
2	LSCO/20LNCO	1.03×10^{-1}	1.50	0.31	1.82×10^{10}
3.	LSCO/30LNCO	1.20×10^{-1}	1.56	0.22	2.75×10^{10}
4.	LSCO/35LNCO	2.03×10^{-1}	1.63	0.19	3.47×10^{10}

to the bulk causing low activation energy. Values of E_a decreases with increasing carbonate content above the transition temperature. Pre-exponential factors of all the samples are given in Table 2. LSCO/LNCO samples have higher values of σ_0 than that of LSCO i.e., concentration of mobile defects is higher in the composites than that in the LSCO. Therefore, it can be concluded that interfacial conduction of O^{2-} ions in composites dominates over the bulk conduction.

Conclusion

Composites in the system, $Ce_{0.85}La_{0.125}Sr_{0.025}O_{1.9125}$ with varying amounts of $(Li\text{-}Na)_2CO_3$, have been prepared by mixing nanosized $Ce_{0.85}La_{0.125}Sr_{0.025}O_{1.9125}$ powder with $(Li–Na)_2CO_3$ and sintering at 700 °C for 1 1/2 h. Ceria-based single-phase formation has been observed in all the composites. Micrographs show continuous distribution of both the phases with ceria grains surrounded by the carbonate amorphous phase. Impedance analysis shows that the charge transport in the composites is different from that in the ceria-based electrolytes. A sharp increase in the conductivity occurs around 350 °C. This is attributed to superionic conduction at the interfaces. The composition, LSCO/35LNCO, shows the maximum conductivity of 2.03×10^{-1} S cm^{-1} at 500 °C. Activation energy of conduction in LSCO/35LNCO composite is found to be 0.19 eV. These features may make this composite useful for application in LT-SOFCs (500 °C).

Acknowledgments We are thankful to the Department of Science and Technology, New Delhi, and MHRD for financial support.

References

1. Di J, Chen M, Wang C, Zheng J, Fan L, Zhu B (2010) Samarium doped ceria–$(Li/Na)_2CO_3$ composite electrolyte and its electrochemical properties in low temperature solid oxide fuel cell. J Power Sources 195:4695–4699
2. Yahiro H, Eguchi K, Arai H (1989) Electrical properties and reducibilities of ceria–rare earth oxide systems and their application to solid oxide fuel cell. Solid State Ion 36:71–75
3. Eguchi K, Setoguchi T, Inoue T, Arai H (1992) Electrical properties of ceria-based oxides and their application to solid oxide fuel cells. Solid State Ion 52:165–172
4. Park SY, Na CW, Ahn JH, Yun UJ, Lim TH, Song RH, Shin DR, Lee JH (2012) Intermediate temperature nickel yttria stabilized zirconia supported tubular solid oxide fuel cells using gadolinia doped ceria electrolyte. J Power Sources 218:119–127
5. Goodenough JB (2000) Ceramic technology: oxide-ion conductors by design. Nature 404:821–823
6. Li S, Wang X, Zhu B (2007) Novel ceramic fuel cell using non ceria based composites as electrolyte. Electrochem Commun 9:2863–2866
7. Huang J, Mao Z, Liu Z, Wang C (2008) Performance of fuel cell with proton conducting ceria based composite electrolyte and nickel based electrodes. J Power Sources 175:238–243
8. Zhu B, Liu X, Zhou P, Yang X, Zhu Z, Zhu W (2001) Innovative solid carbonate–ceria composite electrolyte fuel cell. Electrochem Commun 3:566–571
9. Zhu B (2003) Functional ceria salt composite materials for advanced IT-SOFC applications. J Power Sources 114:1–9
10. Zhu B, Liu X, Schober T (2004) Novel hybrid conductors based on doped ceria and BCY20 for IT-SOFC applications. Electrochem Commun 6:378–383
11. Zhu B, Albinsson I, Andersson C, Borsand K, Nilsson M, Mellander B (2006) Electrolysis studied based on ceria based composites. Electrochem Commun 8:495–498
12. Fan L, Wang C, Chen M, Zhu B (2013) Recent development of ceria based (nano) composite materials for low temperature ceramic fuel cells and electrolyte free fuel cells. J Power Sources 234:154–174
13. Arico AS, Bruce P, Scrosati B, Tarascon JM, Schalkwijk WV (2005) Nanostructured materials for advanced energy conversion storage devices. Nat Mater 4:366–377
14. Zhu B, Mat MD (2006) Studies on ceria based dual phase composites in electrochemistry. Int J Electrochem Sci 1:383–402
15. Huang J, Yang L, Gao R, Mao Z, Wang C (2006) A high performance ceramic fuel cell with samarium doped ceria-carbonate composite electrolyte at low temperature. Electrochem Commun 8:785–789
16. Xia C, Lib Y, Tian Y, Liu Q, Wang Z, Jia L, Zhao Y, Li Y (2010) Intermediate temperature fuel cell with a doped ceria carbonate composite electrolyte. J Power Sources 195:3149–3154
17. Jaiswal N, Kumar D, Upadhyay S, Parkash O (2014) Preparation and characterization of $Ce_{0.85}La_{0.15-x}Sr_xO_{\{2-(0.075+x/2)\}}$ solid electrolytes for intermediate temperature solid oxide fuel cells. Ionics. doi:10.1007/s11581-014-1190-4
18. Bryan Balazas G, Robert Glass S (1995) ac impedance studies of rare earth oxide doped ceria. Solid State Ion 76:155–162
19. Fu Y-P, Chen SH, Huang JJ (2010) Preparation and characterization of $Ce_{0.8}M_{0.2}O_{2-\delta}$ (M=Y, Gd, Sm, Nd, La) solid electrolyte materials for solid oxide fuel cells. Int J Hydrog Energy 35:745–752
20. Jaiswal N, Kumar D, Upadhyay S, Parkash O (2014) Ceria co-doped with calcium (Ca) and strontium (Sr): a potential candidate as a solid electrolyte for intermediate temperature solid oxide fuel cells. Ionics 20:45–54
21. Hodge IM, Ingram MD, West AR (1976) Impedance and modulus spectroscopy of polycrystalline solid electrolytes. J Electroanal Chem 74:125–143
22. Ana Ferreira SV, Cátia Soares MC, Filipe Figueiredo MHLR, Fernando Marques MB (2011) Intrinsic and extrinsic compositional effects in ceria/carbonate composite electrolytes for fuel cells. Int J Hydrog Energy 36:3704–3711
23. Christie GM, Berkel FPF (1996) Microstructure–ionic conductivity relationships in ceria gadolinia electrolytes. Solid State Ion 83:17–27
24. Nafe H (2014) Conductivity of alkali carbonates, carbonate based composite electrolytes and IT-SOFC. ECS J Solid State Sci Technol 3:N7–N14
25. Chockalingam R, Basu S (2011) Impedance spectroscopy studies of $Gd–CeO_2–(Li–Na)_2CO_3$ nanocomposite electrolytes for low temperature SOFC applications. Int J Hydrog Energy 36:14977–14983
26. Huang J, Gao Z, Mao Z (2010) Effects of salt composition on the electrical properties of samarium-doped ceria/carbonate composite electrolytes for low-temperature SOFCs. Int J Hydrog Energy 35:4270–4275
27. Bhoga SS, Singh K (1998) $Li_2CO_3–ABO_3$ (A=Li, K, Ba and B=Nb, Ti) composite solid electrolyte systems. Solid State Ion 111:85–92
28. Liu W, Liu Y, Li B, Sparks TD, Wei X, Pan W (2010) Ceria (Sm, Nd) carbonate composite electrolytes with high electrical conductivity at low temperature. Compos Sci Technol 70:181–185